

ÉCOLE DE TECHNOLOGIE SUPÉRIEURE
UNIVERSITÉ DU QUÉBEC

A THESIS PRESENTED TO THE
ÉCOLE DE TECHNOLOGIE SUPÉRIEURE

IN PARTIAL FULFILLMENT OF THE THESIS
REQUIREMENT FOR THE DEGREE OF
PHILOSOPHY DOCTOR IN ENGINEERING
Ph.D.

BY
EL MOSTAFA SEKOURI

MODELING AND SHAPE ESTIMATION OF SMART STRUCTURES FOR
ACTIVE CONTROL

MONTREAL, 1 APRIL 2004

©copyright reserved by El Mostafa Sekouri

THIS THESIS WAS EVALUATED
BY THE COMMITTEE COMPOSED OF:

Dr. Anh Dung Ngo, Thesis Supervisor
Department of Mechanical Engineering, École de technologie supérieure

Dr. Yan-Ru Hu, Thesis Co-Supervisor
Department of Space Technology, Canadian Space Agency

Dr. Van Ngan Lê, President
Department of Mechanical Engineering, École de technologie supérieure

Dr. Suong Van Hoa, External Examiner
Department of Mechanical Engineering, Concordia University

Dr. Patrick Terriault, Examiner
Department of Mechanical Engineering, École de technologie supérieure

THIS THESIS WAS DEFENDED IN FRONT OF THE EXAMINATION
COMMITTEE AND THE PUBLIC
ON 5TH FEBRUARY 2004
AT THE ÉCOLE DE TECHNOLOGIE SUPÉRIEURE

MODELING AND SHAPE ESTIMATION OF SMART STRUCTURES FOR ACTIVE CONTROL

El Mostafa Sekouri

ABSTRACT

Piezoelectric materials allow the transformation of electric constraints into mechanical constraints and vice versa. They are used as controllers or sensors in the industrial field. The analysis of the behavior of piezoelectric materials lays within the use of these materials in structures whose form or modes of vibration are to be controlled.

The need for these studies is crucial. From a general point of view, the need for stability of structures has become increasingly important with the development of technologies related to telecommunications and microtechniques. Adaptive structures are the only means to achieve the requisite stability in the face of diverse situations. The objective of this research is to model the effect of electro-mechanical coupling and to estimate the shape of the adaptive structures for active control.

Ideal models were developed for various adaptive structures. These models make it possible to determine the static and dynamic behavior of these structures. The model behavior was compared with experimental results and the, numerical, finite elements and the Rayleigh-Ritz methods. Results obtained from all of the above approaches reveal good agreements among them. For a possible application of active control, the analysis of substructures in commercial FEA software ANSYS is used to extract the mass, the rigidity and input matrices.

In order to evaluate at real time the shape of the flexible or composite structures, an algorithm was developed to determine the forms of the structures under arbitrary loads and different boundary conditions. The results obtained by this method were compared with those obtained from numerical, the finite elements and experimental methods. The results also, show that the developed algorithm makes it possible to correctly estimate the structures.

MODÉLISATION ET ESTIMATION DE LA FORME DES STRUCTURES INTELLIGENTES POUR LE CONTRÔLE ACTIF

El Mostafa Sekouri

SOMMAIRE

Les matériaux piézo-électriques permettent la transformation de contraintes électriques en contraintes mécaniques et vice-versa. Ils sont utilisés comme contrôleurs ou capteurs dans l'industrie. L'analyse du comportement des matériaux piézo-électriques, en plus de son intérêt propre réside dans l'utilisation de ces matériaux dans des structures dont on veut contrôler, soit la forme, soit les modes de vibration.

L'intérêt de ces études est multiple. D'un point de vue plus général, le besoin de stabilité des structures devient de plus en plus important avec le développement des technologies liées aux télécommunications et micro - techniques. Les structures adaptatives sont la seule solution d'un point de vue théorique en mesure d'assurer la stabilité. L'objectif de cette recherche consiste à modéliser l'effet de couplage mécanique - électrique et à estimer la forme des structures adaptatives pour le contrôle actif.

Des modèles théoriques ont été développés pour différentes structures adaptatives. Ces modèles permettent de déterminer le comportement statique et dynamique de ces structures. Les résultats de ces modèles ont été comparés avec les résultats expérimentaux et numériques : élément finis ou/et la méthode de Rayleigh Ritz. Les résultats obtenus montrent de bonnes concordances avec les trois approches. Pour une application éventuelle du contrôle l'analyse de sous-structure dans le logiciel commercial d'élément fini ANSYS est employée pour extraire les matrices de masse, de rigidité et d'entrée.

Afin d'évaluer en temps réel la forme des structures flexibles ou composites, un algorithme a été développé pour déterminer la forme des structures dans des conditions de chargement arbitraires et différentes conditions aux limites. Les résultats obtenus par cette méthode sont comparés à ceux obtenus par les méthodes numériques, les éléments finis et les résultats expérimentaux. Les résultats obtenus montrent que l'algorithme développé permet d'estimer les structures correctement.

MODÉLISATION ET ESTIMATION DE LA FORME DES STRUCTURES INTELLIGENTES POUR LE CONTRÔLE ACTIF

El Mostafa Sekouri

RÉSUMÉ

Les matériaux piézo-électriques permettent la transformation des contraintes électriques en contraintes mécaniques et vice-versa. Ils sont utilisés comme contrôleurs ou capteurs dans l'industrie. L'analyse du comportement des matériaux piézo-électriques réside en plus de son intérêt propre, dans l'utilisation de ces matériaux dans des structures dont on veut contrôler soit la forme, soit les modes de vibrations. Le contrôle actif des structures ou micro - structures constitue un sujet d'un intérêt capital pour les laboratoires de l'Agence Spatiale Canadienne (ASC).

Les intérêts de ces études sont multiples. D'un point de vue plus général, le besoin de stabilité des structures joue, de plus en plus, un rôle majeur dans le développement des technologies liées aux domaines des télécommunications et de la micro - technique. Sur le plan théorique, les structures adaptatives forment la seule solution en mesure d'assurer la stabilité recherchée.

Pour mieux adapter et rendre en quelque sorte intelligents les matériaux composites et surtout les structures composites résultant de la conception d'un objet à diverses fonctions, la communauté scientifique internationale a déployé, depuis quelques années, des efforts considérables. En effet, ces efforts ont permis d'introduire en surface ou à l'intérieur d'une structure composite ou flexible des éléments piézo-électriques pouvant jouer le rôle d'actionneur ou de capteur. Les résultats obtenus ont permis donc de corriger le comportement de la structure afin d'éviter par exemple une instabilité statique ou dynamique, de limiter l'amplitude des vibrations et en fait de prévenir sa destruction ou bien un impact sur l'environnement. Ces structures possèdent les caractéristiques de structures intelligentes ou adaptatives.

Le sujet de cette thèse de doctorat se propose de répondre à cette problématique. En effet, cette étude concerne la modélisation et l'estimation de la forme des structures adaptatives pour le contrôle actif. Les méthodes utilisées sont théoriques, numériques et expérimentales applicables aux structures adaptatives de types poutres, plaques et membranes qui représentent la grande majorité des structures spatiales et en particulier dans les satellites et de leur environnement.

L'intérêt majeur de ces structures composites réside dans leur capacité d'engendrer des déformations contrôlables par application de champs électriques appropriés ou de capter,

de façon sensible, des sollicitations mécaniques. Ce résultat ne pourrait être obtenu qu'avec des matériaux non structurés.

Le contrôle actif de vibrations consiste à analyser (amplitudes, modes, fréquences) les vibrations mécaniques des structures mécaniques à l'aide de la fonction capteur d'éléments piézo-électriques. Il permet, via des processeurs, d'injecter suivant une loi de contrôle (en déplacement, en vitesse retardée, par exemple) un potentiel électrique approprié à des éléments piézo-électriques (servant d'actionneurs) judicieusement placés pour annihiler certains modes de vibrations indésirables.

Le concept de base du contrôle passif de vibration est de modifier les propriétés dynamiques (masse, rigidité, etc.) de la structure mécanique à contrôler par l'adjonction d'éléments tels que des ressorts ou raidisseurs, de masses localisées, d'amortisseurs, de couches viscoélastiques, etc. L'utilisation d'actionneurs électromécaniques apporte alors de nouvelles opportunités de contrôle. Parmi les matériaux présentant un couplage électromécanique, ce sont ceux basés sur l'effet piézo-électrique qui s'avèrent les plus intéressants. Cela est dû essentiellement à leur bonne réponse fréquentielle, à l'efficacité du couplage, et à leur miniaturisation favorisant leur intégration dans les structures élastiques.

Le système le plus simple de contrôle consiste en un élément piézo-électrique attaché à la structure élastique à contrôler connecté à un circuit électrique extérieur incluant la capacitance de l'élément piézo-électrique lui-même. Le principe est basé sur la conversion d'une portion de l'énergie mécanique en énergie électrique via l'effet piézo-électrique. L'efficacité du contrôle est fonction du circuit extérieur et de la modélisation de l'élément piézo-électrique.

La présente recherche s'intéresse, plus particulièrement, à des poutres, membranes et plaques intégrant des couches électro-actives du type piézo-électrique. Notre objectif est la modélisation et l'estimation de forme de ces structures.

La modélisation de l'effet de couplage mécanique - électrique permet d'estimer la forme des structures adaptatives par le contrôle actif. Elle concerne le développement des modèles à posteriori correspondant à différents types de structures. Cependant, les structures spatiales utilisées pour les satellites (structures flexibles rectangulaire et circulaire, composite ou métallique) ont bénéficié d'un intérêt particulier.

La modélisation prend en compte les points originaux suivants :

- Les conditions d'interface.
- Les conditions aux limites mécaniques et électriques.

- Les effets directs et inverses piézo-électriques.
- La possibilité d'appliquer un large éventail de sollicitations électromécaniques (forces, contraintes, potentiel électrique, charges électriques).

Dans la première partie de cette thèse:

Nous avons développé des modèles pour les structures de type poutre en aluminium et en composite avec des piézoélectriques collés sur la surface ou intégrés dans les structures. Nous avons réalisé un banc d'essai pour faire les tests statique et dynamique. Nous avons aussi appliqué des méthodes numériques telles que la méthode des éléments finis et la méthode de Ritz. Les résultats obtenus par les modèles sont vérifiés avec ceux obtenus par des tests expérimentaux et par des simulations numériques. Les résultats expérimentaux confirment les estimations fournies par les modèles pour l'analyse statique (déflexion, contraintes, charges électriques, etc.) et l'analyse dynamique (fréquences naturelles et les modes propres de vibration).

Pour l'analyse statique, nous avons considéré différents types de sollicitations:

- Pression ou force ponctuelle appliquée sur la face supérieure de la plaque.
- Différence de potentiel électrique appliqué aux faces des couches piézo-électriques.

Pour assurer un bon contrôle des perturbations par l'environnement de ces structures, nous avons réalisé un placement optimal d'éléments actionneurs et capteurs.

Pour les structures axisymétriques, nous avons développé des modèles théoriques pour différentes structures adaptatives. Ces modèles développés permettent de déterminer les comportements statique et dynamique de ces structures. Nous avons aussi appliqué les méthodes numériques à ces structures. Enfin, nous avons développé un banc d'essai pour faire les tests statique et dynamique de ces structures. La comparaison des résultats de ces modèles avec les résultats expérimentaux et numériques (élément finis ou la méthode de Rayleigh Ritz) montrent qu'il y a de bonnes concordances avec les trois approches. Pour une application éventuelle du contrôle actif, nous avons besoin des matrices de masse, de rigidité et d'entrée. De ce fait, nous avons utilisé l'analyse de sous-structure à l'aide du logiciel commercial d'élément fini ANSYS afin d'extraire ces matrices.

La deuxième partie de cette thèse est consacrée à l'estimation de la forme des structures. Nous avons particulièrement utilisé des structures en résonance, en aluminium et en composite utilisés dans l'industrie spatiale. Afin d'évaluer en temps réel la forme de ces structures flexibles ou composites, un algorithme a été développé pour déterminer la forme des structures dans des conditions de chargement arbitraires et des conditions aux

limites différentes. Le modèle utilise seulement l'information de la déformation mesurée par des capteurs de déformation. Ces capteurs sont collés sur la surface des structures. Les capteurs (Jauge de contraintes) sont installés sur un nombre limité d'emplacements de la structure étudiée. L'emplacement optimal des capteurs a été choisi après plusieurs tests par simulations numériques (la méthode des éléments finis). Les études impliquent non seulement les emplacements optimaux, mais aussi le nombre optimum pour les capteurs.

Pour les plaques rectangulaires, le champ de déformation est représenté par une fonction polynomiale à deux dimensions. Pour les plaques circulaires, le champ de déformation est calculé en utilisant les coordonnées polaires et la fonction de contraintes d'Airy. Les coefficients de chaque fonction sont déterminés en se basant sur la relation de déformation - déplacement, relation de compatibilité et conditions aux limites. Enfin, Le champ de déformation est construit par la procédure de la méthode moindres carrés. Les résultats obtenus par cette méthode sont comparés à ceux obtenus par la méthode numérique (les éléments finis) et les résultats expérimentaux. Les résultats obtenus montrent que l'algorithme développé dans le cadre de cette recherche permet d'estimer et de déterminer de manière correcte et précise la forme des structures.

ACKNOWLEDGEMENTS

There are many people I would like to thank for their help and support. Without them, I would not have been able to accomplish this milestone so quickly and with such satisfying results. I would like to thank my supervisors Dr. Anh Dung NGO and Dr. Yan-Ru HU, for their comments and suggestions. They have always believed in my abilities and provided whatever advice and resources were necessary for me to reach my goals. Their invaluable suggestions and generous support through the course of this research at École de technologie supérieure, University of Quebec and the Canadian Space Agency (CSA) are highly appreciated. I would like to express my appreciation to my friends, especially Sylvain Mondor and the staff of CSA for providing a pleasant, friendly, and supportive environment during the pursuit of my research.

Lastly, I need to thank all my family members who have always supported me.

TABLE OF CONTENTS

	Page
ABSTRACT	I
SOMMAIRE	II
RÉSUMÉ	III
ACKNOWLEDGEMENTS	VII
TABLE OF CONTENTS.....	VIII
LIST OF TABLES	XI
LIST OF FIGURES	XII
INTRODUCTION	1
CHAPTER 1 BACKGROUND	7
1.1 History of piezoelectricity.....	7
1.2 Review of literature.....	8
1.2.1 Smart materials and structures	8
1.2.2 Actuators	12
1.2.3 Sensors	14
1.2.4 Vibration control	15
1.2.5 Modeling	18
1.2.6 Polarization	21
1.2.7 Piezoelectricity.....	22
1.2.8 Shape estimation	23
CHAPTER 2 MODELING OF ALUMINIUM BEAM WITH PIEZOELECTRIC.....	25
2.1 Introduction.....	25
2.2 Piezoelectric finite element formulation	26
2.2.1 Equilibrium Equations	26
2.2.2 Constitutive Relationships	27
2.3 Analytical model	30
2.3.1 Analytical procedures	30
2.3.2 Simple beam theory	30
2.3.3 Modal Analysis	40
2.3.4 Static Analysis.....	42
2.4 Experimental approach	43
2.5 Results and comparison	45

2.5.1	Example 1	46
2.5.2	Example 2	50
2.6	Summary	53
CHAPTER 3 MODELING OF LAMINATED BEAM WITH PIEZOELECTRIC		54
3.1	Introduction	54
3.2	Problem statement	55
3.3	Transverse vibration of laminate beam	55
3.3.1	Static analysis	61
3.3.2	Modal analysis	63
3.4	Numerical approach	64
3.4.1	Assumed – modes method	64
3.4.2	Finite element method	67
3.5	Results and comparisons	67
3.6	Summary	75
CHAPTER 4 MODELING OF CIRCULAR PLATE WITH PIEZOELECTRIC		76
4.1	Introduction	76
4.2	Plate model	77
4.2.1	Modal Analysis	84
4.2.2	Boundary and joint conditions	86
4.3	Energy method	87
4.3.1	Strain energy	87
4.3.2	Kinetic Energy	88
4.3.3	Electric energy	88
4.4	Lagrange's equation	89
4.4.1	Equation of Motion	90
4.5	Model for vibration control	91
4.5.1	Assumed-modes method	91
4.5.2	Plate	92
4.3.3	Actuator	93
4.5.4	Mass, stiffness and load vector extraction	96
4.6	Experimentation	97
4.7	Results and comparisons	99
4.7.1	Obtaining matrices using assume mode model	103
4.7.2	Obtaining matrices using super-element	109
4.8	Summary	113
CHAPTER 5 SHAPE ESTIMATION OF STRUCTURES		114
5.1	Introduction	114
5.2	Model for rectangular plate	115
5.2.1	Assumptions	115
5.2.2	Method	116
5.2.3	Least Squares Method	117

5.3	Model for circular plate.....	124
5.3.1	Description.....	124
5.3.2	Method.....	124
5.3.3	Application.....	126
5.3.3.1	Axisymmetric problem.....	126
5.3.3.2	Quasi axisymmetric problem.....	128
5.3.3.3	General case.....	130
5.5	Experimentation.....	132
5.5	Results and comparison.....	135
5.5.1	Rectangular plate.....	135
5.5.2	Circular plate.....	146
5.6	Summary.....	149
CONCLUSION.....		151
APPENDIX 1.....		155
CONTRIBUTIONS TO RESEARCH AND DEVELOPMENT.....		155
BIBLIOGRAPHY.....		158

LIST OF TABLES

	Page
Table I	Variables in the Euler-Bernoulli beam equation..... 35
Table II	Properties of various piezoelectric materials 44
Table III	Beam A- Geometrical and material properties of test specimen 47
Table IV	Natural frequencies (Hz) for beam A without any piezo-elements..... 48
Table V	Natural frequencies (Hz) for beam A with bonded piezo-ceramics..... 48
Table VI	Geometrical and material properties of test specimen 51
Table VII	Natural frequencies (Hz) for beam B without any piezo-ceramics..... 52
Table VIII	Natural frequencies (Hz) for beam B with piezoelectric 52
Table IX	Material properties 69
Table X	Natural frequencies (Hz) of the beam without piezoelectric 74
Table XI	Natural frequencies (Hz) of the beam with 6 piezoelectric..... 74
Table XII	Dimension and material properties of plate and piezoelectric 98
Table XIII	Natural frequencies for circular plate with eight actuators 100
Table XIV	Material properties of plate structure (2) and piezoelectric 103
Table XV	Natural frequencies (Hz) of the plate with 8 piezoelectric 107
Table XVI	Natural frequencies ω for annular plate without actuators 108
Table XVII	Natural frequencies ω for annular plate with actuators..... 108
Table XVIII	Natural frequencies (Hz) for circular plate with actuators..... 111
Table XIX	Dimension and material properties of plate and piezoelectric 123

LIST OF FIGURES

	Page
Figure 1	Actuator versus sensor 15
Figure 2	Schematic for active vibration control 17
Figure 3	Schematic of a cantilever beam with double-sided piezo-actuators 31
Figure 4	Beam element in bending..... 32
Figure 5	The activation of piezoelectric bonded to beam 37
Figure 6	Experimental set up..... 44
Figure 7	Schematic of experimental set up 45
Figure 8	Deflection of the beam A under static piezoelectric actuation 49
Figure 9	Tip amplitude of the beam A versus voltage 49
Figure 10	Beam B model with sensor and actuators 52
Figure 11	Deflection of the beam B under static piezoelectric actuation..... 53
Figure 12	Laminate beam with piezoceramics 69
Figure 13	Effect of actuator voltage on transverse deflection..... 70
Figure 14	One pair of actuators located at the left of the beam 70
Figure 15	Two pairs of actuators located at the left and the middle of the beam .. 71
Figure 16	Two pairs of actuators: located at the left end and at the right end 71
Figure 17	Three pairs of actuators located at: left end, $L/4$ and $3L/4$ 72
Figure 18	One pair of actuators at different positions (220V) 72
Figure 19	Finite element mesh of the laminate beam..... 73
Figure 20	Mode shape 1 73
Figure 21	Mode shape 2 73
Figure 22	Circular plate with piezoelectric patches 78
Figure 23	Geometry of piezoelectric sheet actuator 94
Figure 24	Geometry of piezoelectric sheet actuator 94
Figure 25	Experimental set up..... 98

Figure 26	Tip deflection on the circular plate in terms of the input voltage	100
Figure 27	Experimental modal analysis	101
Figure 28	Response of the modal displacement at nodes 988 and 909	101
Figure 29	Frequency of the nodal displacement at point A.....	102
Figure 30	Mode 1	104
Figure 31	Mode 2	105
Figure 32	Mode 3	105
Figure 33	Mode 4	106
Figure 34	Mode 5	106
Figure 35	Frequency response at the free end and the centre of the actuator	107
Figure 36	Location of master nodes	112
Figure 37	Geometry of flat plate subjected force in z-direction	115
Figure 38	Geometry of Laminate plate with strain gages	116
Figure 39	Set-up of Laminate plate with strain gages.....	133
Figure 40	Experimental set up.....	134
Figure 41	Experimental set up of simply supported circular plate.....	134
Figure 42	Placement of strain gages.....	135
Figure 43	Optimization of the number of strain gages (linear estimation)	139
Figure 44	Optimization of the number of strain gages (quadratic estimation).....	139
Figure 45	Optimization of the number of strain gages (cubic estimation).....	140
Figure 46	Deformation at line $y = - 0.1$ for 12 strain gages	140
Figure 47	Deflection for a plate with piezoelectric	141
Figure 48	Deformation at line $y = 0.06$ and load at one of the free crones	141
Figure 49	Deformation at line $x = 0.266$ and load at one of the free corners.....	142
Figure 50	Deformation at line $y = 0.06$ and load at both of the free corners	142
Figure 51	Deformation at line $y = 0.266$ and load at both of the free corners	143
Figure 52	Deformation at line $y = 0.06$ and opposite load at the free corners	143
Figure 53	Deformation at line $x = 0.226$ and opposite load at the free corners ...	144
Figure 54	For 31 strain and opposite load at the free corners	144

Figure 55	Deformation for 5 strain gages along the line $y = - 0.1105$	145
Figure 56	Deformation for 5 strain gages along the line $x = 0.2473$	145
Figure 57	For applied voltage 100V at eight actuator and eight strain gages	147
Figure 58	Deformation for applied voltage in 3D	148
Figure 59	Deflection of simple supported circular plate	148
Figure 60	Deformation for applied voltage 150V at four actuator.....	149

INTRODUCTION

Physicists, mathematicians, and engineers from aerospace, chemical, civil, electrical, materials, and mechanical engineering fields are all involved in some part of the development of smart materials and structural systems. One reason for this activity is that it may be possible to create structures and systems that are capable of adapting or correcting in response to changing operating conditions without human intervention. The advantage of incorporating these special types of materials into a structure is that the sensing and actuating mechanisms become a part of the structure and can directly sense and actuate strains.

Smart materials are defined as materials that are capable of automatically and inherently sensing or detecting changes in their environment and responding to those changes with some kind of actuation or actions (Shahinpour, 1996). These characteristics provide several possible applications for these materials in aerospace, manufacturing, civil infrastructure systems, and biomechanics. Active vibration and acoustic transmission control, active shape control, and active damage control are some of the areas that have found innovative applications for smart materials and structures (Shakeri, Noori, and Hou, 1996). Examples of specific applications are micro positioning, vibration isolation, fast acting valves and nozzles, transducers, luxury car shock absorbers, and active engine mounts in aircraft. Some of the benefits of using smart materials are system integration, reduction of mass and energy requirements, elimination of moving parts in actuators, and collocation between actuator and sensor.

There are five types of smart materials that have been widely reported in the literature: piezoelectric, shape memory alloys, electrostrictors, magnetostrictors and electro-rheological fluids. In this thesis, piezoelectric is used as the adaptive material.

Piezoelectric materials are now available as piezoceramics and piezopolymers. Piezoceramics are polycrystalline ceramics. These materials are hard and dense and can

be manufactured in many shapes and tailored to various applications. The most common type is made of Lead-Zirconate-Titanate (PZT). The piezoelectric effect occurs when a pressure is applied to a material, creating an electric charge on the surface and, as a result, a change in the dimensions of the material is observed with an applied electric field. Piezopolymers (e.g. Polyvinylidene fluoride, PVDF) are clear plastic films and can be readily cut and shaped into complex patterns.

Problem statement

In satellite design, providing precision surfaces for antenna reflectors has been a challenging problem. Surface errors are introduced during manufacture, by thermal distortion in orbit, moisture, loose joints, material degradation, and creep. Significant time and money is invested during fabrication, analysis and ground testing to minimize and predict surface errors. Even with this effort, serial current spacecraft antenna have experienced degraded performance due to surface errors higher than predicted. Smart structures with the ability to correct surface errors in orbit have great potential for use in these microwave devices. Therefore, smart structure technology has the potential of not only improving the performance of these structures, but also to reduce the cost of analysis and ground tests.

Piezoelectric materials are already used as controllers or sensors in industry. Analysis of the behavior of piezoelectric materials is based on the use of these materials in structures whose form or modes of vibration need to be controlled. Modeling of smart materials and structures is often an overlooked step in the development process. In many cases, computational modeling is addressed only after the design has been completed and initial prototypes have been fabricated and performance problems encountered. This approach is in contrast to the use of computational methods in the design of many conventional material applications. Smart materials and structures provide unique challenges to the analyst. Multiple scales and several materials are included in the "typical" smart structure adding complexity to any representation. Material constitutive

response for both passive and active materials must be addressed. Analytical and computational models that may provide accurate results for an isolated actuator do not always provide similar results for actuators embedded in a structure. While diverse geometries and materials comprise smart materials and structures, common to all problems are the needs for comparison with experimental results whenever possible and the need for multiple types of models and techniques. It is important to understand that computational modeling can be used to predict performance and performance trends. Modeling should be an integral part of the design and development process from initial planning to final deployment.

For a sensor, a new discipline has emerged concerning the development and integration of advanced sensor concepts. Strain sensors such as fiber optic sensors and rosette strain gauges can be embedded or bonded into long flexible structures. The readings from these sensors can be incorporated into shape estimation algorithms to predict structural displacement..

Goals

The primary goal of this research is the modeling of smart structures. Static and dynamic analytic models will be derived for segmented piezoelectric actuators that are either bonded to an elastic substructure or embedded in a laminated composite. These models lead to the ability to predict:

- The natural frequencies and mode shapes of these adaptive structures,
- The deflection and the response of a structure induced by external forces or piezoelectric actuators or both piezoelectric actuators and external forces,
- The effects of the number and location of the actuators on the control system.

The models include the inertia and stiffness of the actuator. In order to control vibration, a modeling approach based on the Rayleigh-Ritz assumed mode shape to predict the behavior of an adaptive structure will be presented. Moreover, the substructuring analysis in ANSYS was used to extract the mass, stiffness and the input matrices (load vector of the system). Two test specimens of cantilevered beams and the test of circular plate were constructed, using aluminum and laminated composite beams with distributed piezoceramics and circular plate with bonded piezoelectric actuators. The results of these models will be compared to numerical and experimental results.

The second goal of this thesis is the shape estimation of flexible structures. An analytical model will be developed to determine the deflection of flexible structures under arbitrary loads and boundary conditions. The model utilizes only strain information from a set number of strain sensors mounted on the structure. The numerical method, finite element analysis (FEA) and the experimental results will be used to verify this shape estimation method.

Thesis outline

This document consists of seven chapters (including the introduction and the conclusion) and one appendix. The introduction outlines the problem we are working with and lays the foundation for the rest of the thesis. A literature survey including a brief history of piezoelectricity, adaptive structures, piezoelectric sensors and actuators, vibration control, modeling and shape estimation is presented in chapter 1.

In chapter 2, general models are presented describing the structural dynamics when the piezoelectric as actuators and sensors are bonded to aluminum beams. Static as well as dynamic mechanical or electrical loading are investigated. The results of these models are compared to finite element analysis and to experimental results.

In chapter 3, an analytical model based on the first order shear deformation beam theory is introduced. The model includes the inertia and stiffness of the actuator, which has

been used to predict the frequency response of the composite beam. Also, a modeling approach based on the Rayleigh-Ritz assumed mode shapes method is presented. Experimental results obtained from Sung (1992) using T300/976 composite and PZT G1195 piezoelectric ceramics are used to verify the theory and the computer simulations. Finally, the effects of the number and location of the actuators on the control system are also investigated.

An analytical approach for modeling circular plate structures containing distributed piezoelectric under static as well as dynamic mechanical or electrical loading is presented in chapter 4. In addition, this chapter introduces a modeling approach based on the Rayleigh-Ritz assumed mode shape method to predict the behavior of a thin circular plate excited by a patch of piezoelectric material bonded to its surface. The model includes the added inertia and stiffness of the actuator and has been used to predict the natural frequencies and mode shape of the plate. The substructuring analysis in ANSYS is used to extract eigenmodes of the system. Experiments using a thin circular aluminum plate structure with distributed piezoelectric actuators are also presented to verify the analysis and the computer simulations.

Chapter 5 focuses on the shape estimation of flexible structures. An analytical model to determine deflection of structures under arbitrary loads and boundary conditions was developed. The model utilizes only strain information from a set number of strain gauge sensors mounted on the structures. The research encompasses not only finding the best locations for strain sensors, but also the optimum number of strain gauge sensors. For a rectangular plate, the strain field is represented by a two-dimensional bi-polynomial function, while for a circular plate, the strain field is calculated using polar components of stress in terms of Airy's stress function. The strain field is constructed by a least squares smoothing procedure. This shape estimation method is verified by the finite element method, and by experimental results.

Finally, the conclusions and suggestions for future work in the use of piezoelectric materials for smart structural systems are presented.

CHAPTER 1

BACKGROUND

In this chapter, the history of piezoelectricity is briefly reviewed. Then, the smart materials and adaptive structure are introduced and reviewed. Applications of piezoelements as actuators and sensor are extensively reviewed. The modeling of smart structures using piezoelectric sensors and actuators are studied. The basic theory and issues regarding the implementation of distributed actuators and sensors commonly encountered in active vibration control systems are briefly discussed. Finally, the shape estimation review was addressed.

1.1 History of piezoelectricity

The piezoelectric effect was first discovered in 1880 by Pierre and Jacques Curie who demonstrated that when a stress field is applied to certain crystalline materials, an electrical charge is produced on the material surface. Their experiments led them to elaborate the early theory of piezoelectricity. The first applications of the piezoelectricity appeared during the First World War with the sonar in which piezoelectric quartz was used to produce ultrasonic waves (P. Langevin) as sensors. W.G. Cady, an American physicist, proposed the use of quartz to control the resonance frequency of oscillators. It is during the period following the First World War that most of the piezoelectric applications we are now familiar with (microphones, accelerometers, ultrasonic transducers, benders...) were conceived. However, the materials available at that time often limited device performance, the development of electronics, especially during the Second World War, and the discovery of ferroelectric ceramics increased the use of piezoelectric materials. Piezoelectric materials belong to a class of dielectrics, which exhibit significant material deformations in response to an applied electric field and produce dielectric polarization in response to mechanical strains. In current

technology, poling an appropriate substrate through the application of a large electric field at high temperatures can create piezoelectric sensors and actuators. Substrates for the process are chosen to have a crystalline, ceramic or polymeric lattice structure in which the atomic structure along at least one axis differs from that in the remaining coordinates; hence the material is anisotropic and typically orthotropic. Poling has the effect of partially aligning the polar axes of the domains to yield a macroscopic polarization, which facilitates the electromechanical coupling. As a result of this coupling, the piezoelectric material will deform in response to an applied electric field. Therefore, it gives the material its actuating properties. The sensing capabilities come from the converse effect in which the mechanical stresses in the materials cause rotations of the partially aligned dipoles to generate an electric field.

The direct piezoelectric effect consists of the ability of certain crystalline materials (i.e. ceramics) to generate an electrical charge in proportion of an externally applied force. The direct piezoelectric effect has been widely used in transducers design (accelerometers, force and pressure transducers...). According to the inverse piezoelectric effect, an electric field induces a deformation of the piezoelectric material. The inverse piezoelectric effect, an electric field induces a deformation of the piezoelectric material (Figure 1). The inverse piezoelectric effect has been applied in actuator design.

1.2 Review of literature

1.2.1 Smart materials and structures

The application of adaptive structure technology at the present time is at the research and development stage, as depicted by this brief survey. However, when the technology reaches a mature stage, applications could span the aeronautical, aerospace and ground transportation fields. Aeronautical applications could include attenuation of dynamic

loads by means of an active wing fuselage interface or an active wing -engine pylon; flutter vibration suppression by means of adaptive wing camber and active internal cockpit noise cancellation.

In aerospace system, such as the proposed space station and other large truss space structures with high performance requirements using length adjustable active truss members can attain vibration control. Another potential application would be in the realization of space structures with precise shapes, such as space antennas of high frequency range and solar collectors.

Noise and vibration from the motor, road roughness and wind heavily affect ground vehicles. There are different options for noise and vibration reduction. The most conventional method is to integrate passive damping materials, which unfortunately entails additional weight. A more sophisticated way is the use of anti-noise loudspeakers in the passenger compartment or in the exhaust system and the use of additional rotating shafts integrated in the motor unit, compensating for the second-order harmonic loads particularly active as a vibration source in engines. Other possible applications include vibration and noise reduction by an active control of motor suspension systems, attenuation of noise radiation by actively controlling the vibrations of the roof sheets and the splash board, and noise and vibration control by means of an adaptively controlled suspension system.

Flexible structures are widely used in space applications such as potential solar power satellites, large antennas, and large space robots as well as terrestrial applications such as high-speed robots, large bridges, and others (Ashley (1995), Barrett (1994), Khorrami (1994), Preumont (1990), Umland (1990)). In recent years, there has been an increasing interest in the development of lightweight smart or intelligent structures for space applications to control distortions caused by the effects of out space.

Numerous applications for adaptive materials have been reported in the literature. For instance, Grawley and Anderson (1990) used piezoceramics bonded to the surface of cantilever beams as actuators to excite vibrations and to suppress the vibrations by introducing damping to the system. Palazollo et al. (1989) and Lin (1990) derived simulation models and demonstrated test results of active vibration control of rotor bearing systems utilizing piezoelectric pushers as actuators. Moreover, adaptive concepts have been used in vibration suppression of truss structures. Natori et al. (1989) has proposed a method for vibration control of truss structures using struts as active axial force actuators.

Smart composite materials and adaptive structures with sensory/active capabilities combine the superior mechanical properties of composite materials as well as incorporate the additional capability to sense and adapt their static and vibro-acoustic response. Such materials/structures appear promising in revolving current barrier problems in advanced propulsion systems. One such area is management of clearance between the casing and the tips of the blades in a particular turbo machinery stage (reference Saravanos, Lin, Choi, and Hopkins (1994)). In the same reference, the developed mechanics are integrated with a control scheme that uses feedback from the sensors to actively maintain the tip clearance within acceptable margins. In order to obtain real time response, the development of neural network controller architecture is addressed.

The idea of utilizing smart materials in adaptive control applications has been proposed in reference Wang, Lai, and Yu (1994). In structural vibration suppression via parametric control actions, the structural parameters are varied on-line according to feedback signals and control commands. These semi-active (also known as adaptive passive) structures have the advantages of both passive and active systems. They can adapt to system variations through feedback actions, and are thus more effective than passive structures. On the other hand, they normally require less power, are less sensitive to spillover, and more stable than structures under fully active actions. With the

recent development of smart materials, online parameter variations could be physically achievable. A comprehensive study on real time control of this class of adaptive structures has yet to be performed. While the concept of structural vibration control using semi-active piezoelectric circuits is promising, more research work is needed to realize this idea. Novel methodologies need to be developed to address the unique characteristics of such structures. Since the advent of composite materials, the development of delaminating cracks has presented one of the principal concerns to their engineering applications. Vibration methods based on the detection of frequency variations associated with the presence of a delaminating have recently gained popularity. A relative new area of non-destructive delaminating monitoring is associated with adaptive or smart structures and materials. Some researchers have recommenced the use of piezoelectric sensors to detect delaminating in composite beams. An analytical model for detection and control of delaminating growth using piezoelectric sensors and actuators has been proposed in reference Birman, Saravanos, and Hopkins (1994).

There are five types of adaptive materials that have been widely reported in the literature: piezoelectric, shape memory alloys, electrostrictors, magnetostrictors and electro-rheological fluids.

Shape memory alloys have the ability to recover a particular shape when activated by an external stimulus. One common type is Nitinol, which is a nickel and titanium alloy that undergoes a reversible phase transformation from austenite to martensite. The shape of the alloy, which is to be remembered, is formed at the high temperature in the martensitic phase. Once the alloy is heated above the transformation temperature, the originally formed shape is remembered, exerting stresses up to 100,000 psi if restrained, or creating strains up to 8 percent if unrestrained.

Like piezoelectric, electrostrictive ceramics also change in dimension when an electric field is applied. However, the strain induced is proportional to the square of the electric field, so positive displacements are always created, (i.e. the material cannot contract).

Magnetostrictive alloy (e.g. Terfenol-D) expands under the influence of a magnetic field. Electrorheological fluids consist of polarizable, high dielectric constant particles suspended in a dielectric fluid. When exposed to an electric field, the viscosity in these fluids increases.

The definition of piezoelectric was described before this chapter. This thesis focuses on models that use piezoelectric as actuators and sensors.

1.2.2 Actuators

Sensors and actuators are analogous to the nerve and muscle systems, respectively, of a human body that is itself an adaptive system. The signals that are sensed by the sensors and modified by the actuators must be processed in real time under very restrictive conditions. A number of actuator types are available:

Piezoelectric actuators in general, are best suited for high frequency and medium stroke with low to medium power requirements. Piezoelectric fibers are an attractive option due to the ease in incorporating them into the manufacturing process; however, they are difficult to produce in long enough lengths to be useful. Piezoelectric ceramics and polymers are both good candidates for adaptive structures. They can be machined to a wide variety of shapes, and have good strength, stiffness, stroke and bandwidth characteristics; however, the application of piezoceramic materials in actuator devices is limited by the material non-linearity and high density. Although the low modulus in piezopolymers often precludes their use as actuators, their high field tolerance and electro-mechanical coupling result in large actuation strains which make them effective actuators in applications where obtaining a good mechanical impedance match is possible.

Electrostrictive device appears to be especially suited for high frequency and low stroke applications, with lower power requirements. The advantage of constrictive ceramics

over piezoelectric is that they can potentially achieve a large displacement. Hysteresis appears less significant, and since they have a higher density charge, they can produce a greater force when activated.

Furthermore, electrostrictives do not exhibit hysteresis and creep at low frequencies and moderate temperatures, due to the absence of permanent polarization. This gives these materials excellent set point accuracy, which makes these actuators ideal choices for low frequency precision positioning.

Magnetostrictive materials are the magnetic analogy of electrostrictives. Ferro-magnetic materials, or magnetostrictors, strain as a result of the interaction between applied magnetic fields and magnetic dipoles in the materials. Magnetostrictive materials have a relatively high modulus; they exhibit fast responses and produce large actuation strains. However, mechanical resonance, magnetic eddy currents and high-energy requirements limit the bandwidth of these materials.

Shape Memory Alloys are ideal actuators for low frequency and high stroke applications, with lower power requirements. Actuator applications are generally in the form of fine wires, which are activated by resistive heating when an electric current is passed through the wire. This heating raises the metal to its austenite temperature including it to return to its original shape. The high force and large stroke capability exhibited by these materials make them excellent actuator materials. Fatigue may become a problem, especially if the alloy is deformed to a high strain configuration. Nickel-Titanium alloys (Nitinol) exhibit unique mechanical memory characteristics, which make them suitable candidates.

Electro-Rheological (ER) fluid has the property that its viscosity changes drastically upon application of a voltage. This effect has been used to demonstrate an increase-damping rate when the ER fluid is activated. ER fluid responds quickly enough to warrant their application in active control, however, they present weight penalties

associated with introducing fluid into the structure. There is also an uncertainty about whether they can be made to be stable for a long enough period of time. The most common ER fluids are composed of silicon oil and corn starch.

Mechanical actuators are not considered suitable in adaptive structures applications because they tend to be bulky in size, and embedding the devices in an automated manufacturing process would be difficult.

1.2.3 Sensors

Piezoelectric sensors use the same type of materials described for use as actuators. The operation of these transducers is essentially a reversible process. They can act as sensors by producing a voltage change in response to deformation. In particular, piezopolymers make excellent sensors due to their low modulus and weight, and they can easily be shaped into much geometry, which allow for flexible and unobtrusive use in many sensing applications.

Strain Gages are simple and inexpensive sensors, and represent a mature technology. Since they are discrete devices, they may be difficult to embed in a composite type structure. This problem can be overcome by producing a thin film with gages printed on it at regular intervals. And subsequently, bonding it to the wall of a structure during the manufacturing process.

Fiber Optics make excellent sensors because they are immune to the electromagnetic interference which eliminates costly and heavy shielding that is necessary to support electrical sensors. Additionally, they can be made extremely small and can be embedded into composite materials without structural degradation. The inherent high bandwidth of fiber optic sensors and the data links supporting them enable the potential of systems with a large number of sensors. Finally, because of the high melting point of these fibers

and the high inherent strength of glass, they are able to perform in extremely hostile environments at high temperatures, vibrations and shocks loading.

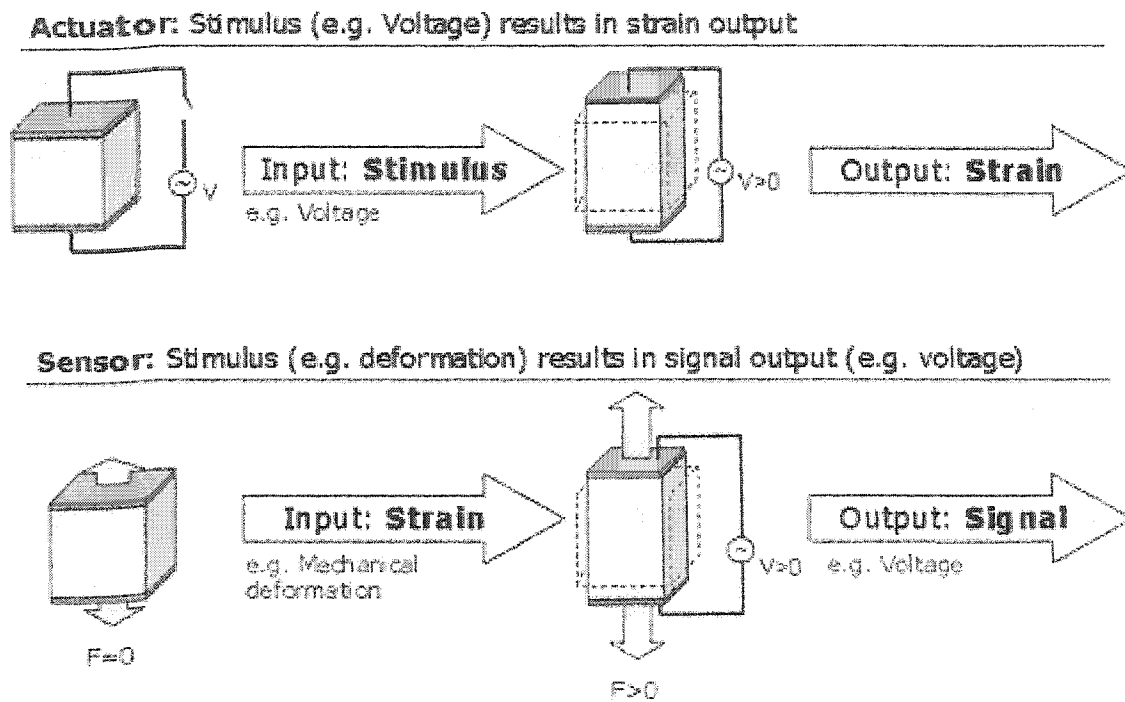


Figure 1 Actuator versus sensor

1.2.4 Vibration control

Three important approaches in vibration control can be identified as:

- Passive Vibration Control;
- Active Vibration Control;
- Combined Passive & Active Vibration Control.

In the passive approach the damping of the structure is increase by using passive dampers (materials with significant visco-elasticity). This approach may increase considerably the total weight of structure and is best for high frequency modes.

In the active method, a smart structure has built-in sensors, processors and control mechanisms as well as actuators, so that the structure can sense a stimulus (mechanical or electrical) and process appropriately the information in a predetermined manner. Once the stimulus is removed, it reverts to its original state. Therefore, smart structures possess a highly distributed control system. Thus a complete control system involves distribution and integration of not only the sensing and control elements but also of the electronic components involved in signal conditioning, computing and power regulation (see Figure 2). Compared with conventional (passive) approach, this method of control offers numerous advantages such as reduced cost and better performance. One may find following active control schemes in the literatures:

- Discrete Distributed Control Systems: The continuous system must be discretize to incorporate spatially distributed sensors and actuators.
- Wave Absorbing Controller: Dynamic wave modeling of flexible structures can be used to design controllers.
- Spatially Discretize Control Systems: Applying discretize models of flexible structures, e.g. Finite Element Method or Assumed Mode Method, controllers have been derived.

For more references regarding the above schemes please check reference Yousefi-Koma (1997).

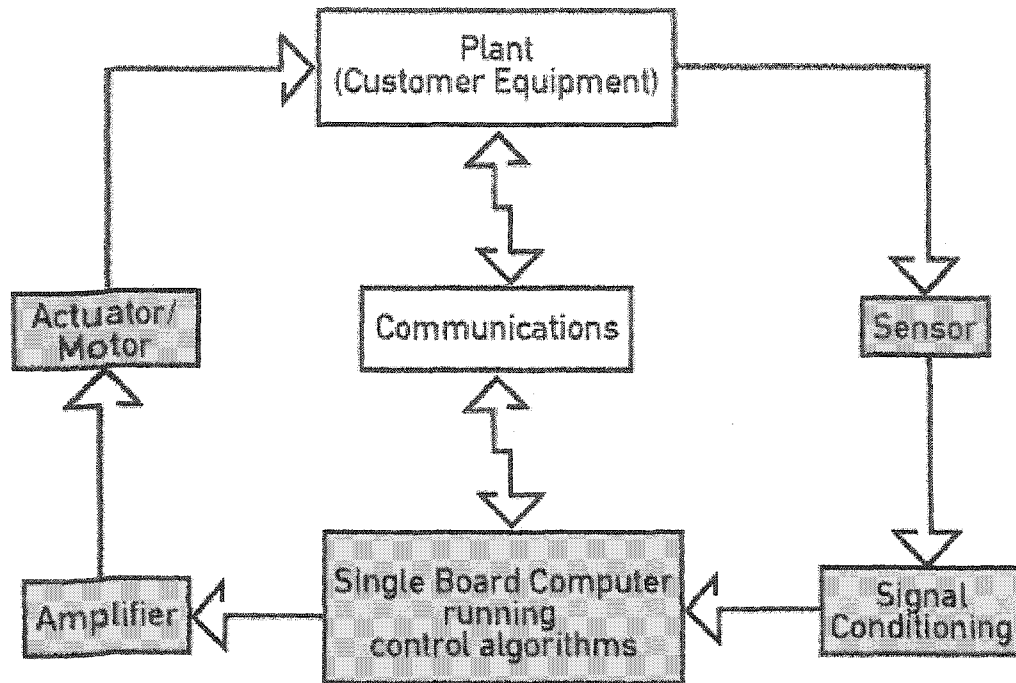


Figure 2 Schematic for active vibration control

In combined passive and active vibration control some benefits of this kind of control is

- Less expensive overall vibration suppression systems;
- Relaxed actuator sensor requirements;
- More robust closed loop systems;
- Overall more reliable systems.

1.2.5 Modeling

One of the engineering challenges is the modeling of the actuation mechanisms in the flexible structures. Extensive research has been done analytically as well as experimentally on the implementation of the mechanics of structure and electrical energy of the piezoelectric actuators Tzou (1989), Samanta (1996), Carpenter (1997) and Crawley (1987). So far, almost all of the studies were based on the conventional beam or plate theories to formulate a special finite element with piezoelectric as additional layers. Much research effort has been devoted to finite element formulation for the electromechanical coupling effects of piezoelectric materials, and fully electromechanical-coupled piezoelectric elements. These elements have just recently become available in commercial FEA software. Before the new piezoelectric capability was developed in commercial FEA codes Swanson (2000), the induced strain actuation function of piezoelectric materials had been modeled using analogous thermal expansion/contraction characteristics of structural materials. This method was helpful in the studies of the resulting stress distribution in actuators and host substructures, and the overall deformation of integrated structures under static actuation. However, the intrinsic electromechanical coupling effects of piezoelectric materials cannot be modeled, the dynamic actuation response of piezoelectric actuators on host substructures is difficult to implement by this method.

Additionally, the use of piezoelectric materials to control the vibration of structures has been extensively studied Konis (1994), Reddy (1997), Donthireddy (1996), Crawley (1992) and Sung (1992); however, their use in controlling the shape of structures has received less attention. With proper selection and placement of piezoelectric actuators, it is feasible to generate enough forces on a structure in order to control its shape. The changes in shape of composite plates for specified applied voltages to the piezoelectric actuators have been studied in reference Konis (1994). Recent advances in design and manufacturing technologies have greatly enhanced the use of advanced fiber-reinforced

composite structures for aircraft and aerospace structural applications. As a consequence, the integration of composite structural design with the "smart system" concept could potentially result in a significant improvement in the performance of aircraft and space structures.

Modeling of non-linear piezoceramics for structural actuation has been discussed in reference Chan and Baruh (1994). The model is based on a description of polarization reversal behaviors of a single piezoelectric crystallite in a piezoceramic. The piezoceramic is then modeled as an aggregate of these crystallites rotated into random orientations. The model has directly incorporated effects of both electrical and mechanical external loads on piezoceramics using the principle of minimum potential energy. Non-linear behavior due to either material or geometrical nonlinearity can significantly influence the performance of distributed piezoelectric sensors and actuators in adaptive piezoelectric laminated structures. The mathematical modeling of a non-linear laminated anisotropic piezoelectric structure has been discussed in reference Tzou, Bao and Ye (1994). Geometric nonlinearity induced by large deformations is considered. A generic theory is proposed and its non-linear thermo-electromechanical equations have been derived based on the variational principle. Thermo-electromechanical couplings among the elastic, electric, and temperature fields are discussed, and non-linear components have been identified.

According to reference Lalande, Chaudhry and Rogers (1994), piezoelectric actuators have been used for active shape, vibration and acoustic control of structures because of their adaptability and lightweight. Their ability to be easily integrated into structures makes them very attractive in structural control since all the moving parts encountered with conventional actuators are eliminated. Structural control is achieved by simply embedding PZT actuators in the structure or bonding them on the surface of the structure.

Circular geometry's are used in a wide variety of applications and are often easily manufactured, but the full three-dimensional vibration properties of these solids have not yet been investigated in detail. The knowledge of natural frequencies of components is of great interest in the study of responses of structures to various excitations and this study is fundamental for high-risk plants. Among plates of various shapes, circular plates have a particular importance due to their axial symmetry. Southwell (1992) derived equations for a circular plate clamped around the inner boundary and free at the outside edge. One can also be observed that the frequency equation for other combinations of boundary conditions could be found by proper rearrangement of his work. In addition, there are in the literature some interesting numerical investigations. Vogel and Skinner (1965) studied nine combinations of boundary conditions. Leissa (1993) gave data and references.

Applications of distributed piezoelectric sensors and actuators have been the subjects of recent interest in the fields of smart structures, structure vibration control and acoustic noise isolation. There have been many researches focused on applications to vibration control and suppression Crawley and Deluis (1990), Bailey and Hubbarg (1985), Fanson and Chen (1986). In recent years, there has been a surge of interest in using piezoelectric patches attached to optical surfaces in hope of attaining high precision of optical mirrors with minimal additional weight. Heyliger and Ramirez (2000) studied the free vibration characteristics of laminated circular piezoelectric plates using a discrete-layer model of the weak form of the equation of period motion. Dimitiadis, Fuller and Rogers (1991) have modeled the vibration of two-dimensional structures excited by a piezoelectric actuator for rectangular plate and by Van Niekerk, Tongue and Packard (1995) and Tylikowski (2001) for circular plates. Van Niekerk, Tongue and Packard presented a comprehensive static model for a circular actuator and a coupled circular plate. Their static results were used to predict the dynamic behavior of the coupled system, particularly to reduce acoustic transmissions. The axisymmetric vibrations for laminated circular plates have also been studied by Jiarang and Jianqiao (1990) using an exact approach. Circular plates composed entirely or in part by piezoelectric layers introduce

the electrostatic potential as an additional variable and increase the complexity of solution because of the coupling between the elastic and electric variables and the additional boundary conditions.

1.2.6 Polarization

A material that can be polarized under an electrical field is called a dielectric. Polarizability is a property inherent in all dielectrics Heyliger (1986). One type is electronic polarization, caused by shifts in electron clouds of the material away from their equilibrium position for an applied field. Polar materials have additional contributions to the material polarizability from orientation polarization of the dipoles for an applied electric field. In all cases, application of the electric field to the dielectric material induces a volume of polarization. The field created in the materials is offset by additional charges, which have collected on the electrodes. Thus, the dielectric constant is used as a measure of the charge storage capacity of the material.

One way to describe the polarization state of the material is the volume charge density. Alternatively, it can be described in terms of the surface charge on the material, which exactly cancels the net volume charge. The polarization P of a material is related to the electrical displacement D and applied electric field E^e through the following:

$$D = \epsilon_0 E^e + P \quad (1.1)$$

where $(36\pi 10^9)^{-1}$ (F/m) is the dielectric of vacuum (the permittivity of the vacuum). Note that these parameters are vector quantities. Since the electrical displacement and electric field are related through the material dielectric constant in linear dielectrics by:

$$D = \epsilon E^e \quad (1.2)$$

where $\epsilon = \epsilon_r \epsilon_0$ the absolute permittivity of the dielectric and ϵ_r its relative one.

Then the polarization in terms of the applied field as

$$P = (\epsilon - \epsilon_0)E^e \quad (1.3)$$

Generally, ϵ is much larger than one in most dielectrics, so the polarization can be approximated by electric displacement. In most cases, it is easier to measure the electrical displacement directly, and the terms are often used interchangeably.

Note that the polarization vanishes with zero electric field. That is, the removal of the field causes the material return to its original non-polarized state, and the internal field no longer needs to be cancelled by additional charges on the electrodes. In contrast to pure dielectrics, the phenomenon of piezoelectricity is described as electric polarization produced by a mechanical stress or strain. In these cases, the polarization of piezoelectric materials is non-vanishing even after the field is removed.

1.2.7 Piezoelectricity

In an unstressed one-dimensional dielectric medium, the dielectric displacement D (charge per unit area, expressed in Cb/m^2) is related to electric field E^e (V/m) and the polarization P (Cb/m^2) by equation 2.1. Hook's law, the stress-strain relationship no electric field applied is:

$$\sigma = C\varepsilon \quad (1.4)$$

where C is the stiffness of the material, σ is the stress (N/m^2) and ε is the strain.

For a piezoelectric material, the electrical and mechanical constitutive equations are coupled. A strain ε in the material induces a polarization $e\varepsilon$ by the direct piezoelectric effect. The total induced polarization is given by:

$$P = (\epsilon - \epsilon_0)E^e + e\epsilon \quad (1.5)$$

Conversely, an applied electric field E^e tends to align the internal dipoles, inducing stresses $-eE^e$ in the material by the inverse piezoelectric effect. The coupled equations finally become:

$$\sigma = C^E \epsilon - eE^e \quad (1.6)$$

$$D = e\epsilon + \epsilon^s E \quad (1.7)$$

where e is the piezoelectric constant relating the stress to the electric field E^e in the absence of mechanical strain and C^E refers to the stiffness when the electric field is constant. In second equation, e relates the electric charge per unit area D to the strain under a zero electric field (short-circuited electrodes); e is expressed in $NV^{-1}m^{-1}$ or Cb/m^2 . ϵ^s is the permittivity under constant strain. Equation 2.6 is the starting point for the formulation of the equation of a piezoelectric actuator, while equation 2.7 is that for sensor.

1.2.8 Shape estimation

Shape control for flexible structures is of great importance especially in low-weight aerospace applications. Shape control is an important task of smart structures and, in general, it means control of position or alignment of a certain number of points on the structure so as to track a desired value. The solution technique of real-time shape control is robust real shape estimation. Another aspect in adaptive systems capability is the realization of structures with precise shapes. Miura (1991) proposed a concept where the surface shape of a truss antenna was adjusted by changing the natural length of truss cable members. Belvin, Edighoffer and Herstrom (1989) reported the shape adjustment of

a 15-meter mesh antenna. The shape adjustment algorithm uses the linearized influence coefficients between adjustment cables and mesh surface. Mitsugi, Yasaka and Miura (1990) studied the shape control concept of the tension truss antenna, where inextensible cables and static determinate conditions are assumed. Tabata et al. (1991) have studied shape adjustment for the hybrid tension truss antenna, and it also uses flexible cables for precise shape forming. Kirby et al. (1997) examined the approximation of the strain field of a cantilever beam using both linear and quadratic local basis functions. Davis et al. (1994) assumed that the strain measured at any point could be written as a linear combination of a set of polynomials forming the strain basis functions, which upon successive integration and application of the boundary conditions yielded the displacements at any point. In a subsequent study, Kirby et al. (1995) approximated the strain distribution as a linear combination of sine function and polynomials. Bartley-cho et al. (2001) investigated three shape estimation techniques: a distributed sensor network, flight deflection measurement system, and fiber Bragg system. Jones et al. (1996) used wavelength division multiplexed fiber Bragg grating sensors to determine deformation of a cantilever honeycomb plat under arbitrary loading conditions.

CHAPTER 2

MODELING OF ALUMINIUM BEAM WITH PIEZOELECTRIC

In this chapter, the modelling of piezoelectric patch interactions with the beam structures is developed. The contributions due to piezoelectric can be categorised into two types, namely, internal and external moments and forces. Both contributions are discussed here, and a general model describing the structural dynamics when the piezoelectric as actuators and sensors are bonded to the beams is presented. Modal analysis is done for determining the natural frequencies and vibration mode shapes of the structures. Then, the harmonic analysis is performed for analysing the steady-state behaviour of the structures subjected to cyclic sinusoidal loads. Experimental results are presented and compared to finite element and analytical results. Relatively good agreement between the results of these three approaches is observed.

2.1 Introduction

One approach to controlling structural deformation is to incorporate into the structure elements in which actuation strain can be regulated. Actuation strain is a component of the strain that is due to stimuli other than mechanical stress. Actuation strain can be produced by adaptive materials, which were presented in chapter 2. In this thesis, the piezoelectric is used for actuation strain.

The contributions due to the piezoelectric can be categorised into two types, namely, internal (material) and external moments and forces. The internal moments and forces account for the material changes in the structure due to the presence of the piezoelectric and are present even when no voltage is being applied to the piezoelectric. The external contributions are due to the strain induced by the piezoelectric when voltage is applied, and they enter the equations of motion as external loads. Analytical solutions for the

mode shapes and natural frequencies of complex smart structures are quite complex. The finite element method provides a relatively easy way to model the system. Commercial finite element programs have become highly developed in the past few years and their utility has increase with the development of faster computers. The analysis method presented in this chapter makes use of the availability of highly refined commercial finite element programs ANSYS and ABAQUS to perform static and dynamic analysis. The next section presents the review of the finite element formulation.

2.2 Piezoelectric finite element formulation

To perform finite element analysis involving piezoelectric effects, coupled field elements, which take into, account structural and electrical coupling are needed. The coupled-field element should contain all necessary nodal degrees of freedom and include electrical-structural coupling in the element matrices. In the following, the piezoelectric finite element formulation employed in commercial FEM codes is briefly described (Swanson, Inc, 1993).

2.2.1 Equilibrium Equations

The mechanical response of piezoelectric elements can be described by the equation of motion

$$\{\text{div}[\sigma]\} + \{f\} = \rho\{\ddot{u}\} \quad (2.1)$$

where σ , f , ρ and \ddot{u} are stresses, body force in a unit volume, density and accelerations, respectively. On the other hand, the electrical response of piezoelectric elements can be expressed by the Maxwell's equation

$$\left\{ \frac{\partial D}{\partial x} \right\} = \{0\} \quad (2.2)$$

where D is the electric displacement.

2.2.2 Constitutive Relationships

The linear direct and converse constitutive relationships for piezoelectric elements are the basic equations for actuators and sensors, respectively. These equations are derived based on the following assumptions:

- The piezoelectric sensors and actuators are thin compared with the beam plate thickness;
- The poling direction of the actuators is in the positive z -direction;
- Only uniaxial loading of the actuators in the x -direction is considered when an electric field is introduced;
- The piezoelectric material is homogeneous, transversely isotropic and linearly elastic.

The constitutive equation of the actuator is given by

$$\{\sigma\} = [c]\{\varepsilon\} - [e]\{E^e\} \quad (\text{Direct effect}) \quad (2.3)$$

where

- σ and ε denote the stress and strain vectors, respectively;
- c denotes the stiffness tensor (fourth order) under constant electric field conditions;
- e is a third order tensor of piezoelectric stress coefficients (constants);
- E^e denotes the applied electric field vector or the electrical potential gradient vector,

$$E_i^e = \frac{\partial \varphi}{\partial x_i};$$

while, the constitutive equation for sensor is

$$\{D\} = [e]^T \{\varepsilon\} + [\epsilon] \{E^e\} \quad (\text{Converse effect}) \quad (2.4)$$

where D denotes the electric displacement (electric flux density) vector and ϵ denotes the dielectric constants tensor (second order) at constant mechanical strain (under constant electric field conditions).

Equation (2.3) and (2.4) are the usual structural and electrical constitutive equations respectively, except for the coupling terms involving the piezoelectric stress coefficients e .

For a piezoelectric finite element, using element shape functions and nodal solution variables can approximate the displacements and electrical potentials within the element domain:

$$\{u_c\} = [N^u]^T \{u\} \quad (2.5)$$

$$V_c = \{N^V\}^T \{V\} \quad (2.6)$$

The strains and electrical potential gradients, i.e., electrical fields, can then be obtained as:

$$\{\varepsilon\} = [B_u] \{u\} \quad (2.7)$$

$$\{E\} = -[B_V] \{V\} \quad (2.8)$$

where B_u and B_V are the spatial derivatives of the element shape functions, N^u and N^V , respectively.

With the application of variational principles on the mechanical equilibrium equation, equation (2.1) and the electrical flux conservation equation, equation (2.2), in conjunction with the approximate fields of equations (2.5-2.8) and the constitutive properties given in equations (2.3-2.4), the piezoelectric finite element system of equations can be derived in terms of nodal quantities:

$$\begin{bmatrix} [M] & [0] \\ [0] & [0] \end{bmatrix} \begin{Bmatrix} \{\ddot{u}\} \\ \{\ddot{V}\} \end{Bmatrix} + \begin{bmatrix} [C] & [0] \\ [0] & [0] \end{bmatrix} \begin{Bmatrix} \{\dot{u}\} \\ \{\dot{V}\} \end{Bmatrix} + \begin{bmatrix} [K] & [K^z] \\ [K^z] & [K^d] \end{bmatrix} \begin{Bmatrix} \{u\} \\ \{V\} \end{Bmatrix} = \begin{Bmatrix} \{F\} \\ \{L\} \end{Bmatrix} \quad (2.9)$$

where a dot above a variable denotes a time derivatives and $\{F\}$ is the mechanical force vector and $\{L\}$ is the electrical charge vector. Both mechanical force and electrical charge vectors include the body, surface, and nodal quantities.

$[M]$, $[C]$, $[K]$, $[K^z]$ and $[K^d]$ are mass matrix, damping matrix, displacement stiffness matrix, piezoelectric coupling matrix and dielectric conductivity matrix are expressed as:

$$[M] = \int_v \rho [N^u] [N^u]^T dv; \quad [C] = \int_v c [N^u] [N^u]^T dv \quad [K] = \int_v [B_u]^T [c] [B_u] dv;$$

$$[K^z] = \int_v [B_u]^T [e] [B_v] dv \quad [K^d] = - \int_v [B_v] [\Xi] [B_v] dv$$

where ρ is the mass density per unit volume; c is the structural damping.

The mechanical force vector consists of the body force vector, surface force vector and concentrated (point) force vector, as follows:

$$\{F\} = \{F^b\} + \{F^s\} + \{F^p\}$$

The electrical charge vector consists of the body charge vector, surface charge vector and point charge vector, as follows:

$$\{L\} = \{L^b\} + \{L^s\} + \{L^p\}$$

2.3 Analytical model

2.3.1 Analytical procedures

Prior to experimental, analytical models were produced to better understand what results were to be expected from the testing, and to set the test parameters correctly. Simple beam theory was used to obtain values for natural frequencies and mode shape of the specimens that were to be tested, which were followed by finite element solutions. These finite element models were created in ANSYS, and could accurately predict the behavior of structures for even complex geometry as well as plot their mode shape.

2.3.2 Simple beam theory

The beam depicted in Figure 3, is assumed to have length L , width b , thickness h and cantilever end conditions with the fixed end at $x = 0$ and free at $x = L$. It is assumed that the beam is homogeneous and constructed from a material, which essentially satisfies the Euler-Bernoulli hypothesis for displacement. Finally, it is assumed that a number n pair of identical piezoelectric is bonded to opposite sides of the beam. The Young's modulo, linear mass density for the beam and the piezoelectric are given in Table II. The bonding layer is taken to be negligible.

In this section, a detailed formulation of the beam vibration due to partially covered surface -bonded piezoelectric is presented. This cantilever beam is subdivided into five spanwise regions, namely, two composite (aluminium beam bonded with piezo-actuator materials) regions and three simple (aluminium beam) regions. Each segment of cantilever beam (Figure 3) is modelled as an Euler-Bernoulli beam. The solution for the beam as a whole is obtained in terms of the solutions of the entire component Euler-Bernoulli beams by satisfying the appropriate boundary conditions and continuity conditions.

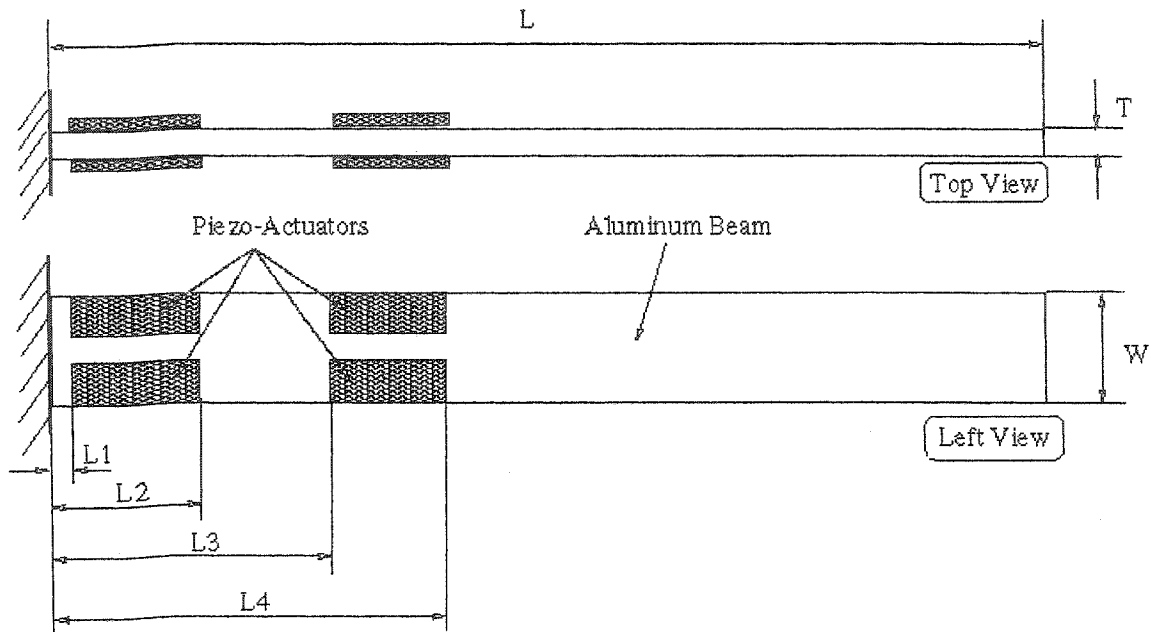


Figure 3 Schematic of a cantilever beam with double-sided piezo-actuators

Figure 4 shows an element of a thin beam with bonded piezoelectric excited in pure bending. For the following derivation it is assumed that the beam cross-section is symmetrical about the centreline and remains normal to the neutral surface. Under these assumptions and using deflection relations from Timoshenko and Goodier (1951), the longitudinal displacement u is given by:

$$u(x) = -z \frac{\partial w}{\partial x} \quad (2.10)$$

where w is out-of-plane displacement of the beam and z is the transverse co-ordinate of the beam section.

Using Hook's law in one dimension, the stress in the beam is given by

$$\sigma(z) = -zE_b \frac{\partial^2 w}{\partial x^2} \quad (2.11)$$

The stress in the piezoelectric is given by

$$\sigma(z) = -zE_p \frac{\partial^2 w}{\partial x^2} \quad (2.12)$$

where E_b and E_p are Young's modulus for the beam and piezoelectric respectively.

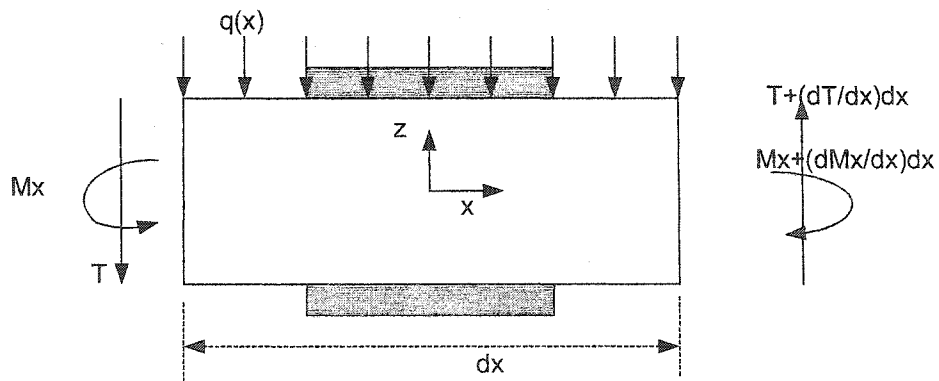


Figure 4 Beam element in bending

The resulting moment in the coupled structures can then be obtained by integrating the stress distribution over the coupled structures cross section such that

$$M_x(x) = \int_A \sigma(z)z dA \quad (2.13)$$

then

$$M_x(x) = \int_A \sigma(z)z dA = \int_0^b \int_{\frac{h}{2}-h_p}^{\frac{h}{2}+h_p} \sigma(z)z dz dy \quad (2.14)$$

Then

$$M_x(x) = -\left(E_b b \frac{h^3}{12} + \chi_p \sum_1^n E_b b_b a_3\right) \frac{\partial^2 w}{\partial x^2} \quad (2.15)$$

where n is the number of actuators and $a_3 = \frac{1}{3} \left(\left(\frac{h}{2} + h_p \right)^3 - \left(\frac{h}{2} \right)^3 \right)$.

where χ denotes the characteristic function over the i^{th} piezoelectric. Now, if we consider the beam element illustrated in Figure 4 with the resultant shear forces and moment acting as shown, and neglecting rotary inertia of the element, the condition of moment equilibrium gives

$$\frac{\partial M_x}{\partial x} dx = T dx \quad (2.16)$$

where M_x and T are the internal moment and the transverse shear force acting upon the element. Apply Newton's law of motion in the vertical direction gives

$$-q(x) + \frac{\partial T}{\partial x} = \rho_{\text{tot}} A \frac{\partial^2 w}{\partial t^2} \quad (2.17)$$

where $q(x)$ is the external load on the element (with units of force per unit length), A is the cross-sectional area of the beam and ρ_{tot} is the linear mass density of the total structures. $\rho_{\text{tot}} = \rho h b + n \chi_p b_b h_b \rho_p$: is piecewise constant with the characteristic function χ_p used to isolate the piezoelectric contributions.

Combining equation 2.17 and 2.16 we obtain

$$\frac{\partial^2 M_x}{\partial x^2} = \rho_{\text{tot}} A \frac{\partial^2 w}{\partial t^2} + q(x) \quad (2.18)$$

Finally, using the expression for bending moment from equation 2.15 and with $q(x)$ set to zero we obtain the Euler - Bernoulli thin beam equation of motion for each segment

$$\psi_i \frac{\partial^4 w_i}{\partial x^4} + \phi_i \ddot{w}_i = 0 \quad i = 1, \dots, 5 \quad (2.19)$$

where ψ_i and ϕ_i variables are listed in Table I for each segment and w_i represents the transverse displacement. Note that three non-dimensional parameters are defined as

follows :

$$\alpha = \frac{E_p}{E_b} \quad (2.20a)$$

$$\beta = \frac{h_p}{h} \quad (2.20b)$$

$$\gamma = \frac{\rho_p}{\rho} \quad (2.20c)$$

$$\kappa = \frac{b_p}{b} \quad (2.20d)$$

The second contribution from the piezoelectric is the generation of external moment and forces, which results from the property that when a voltage is applied, mechanical strains are induced in the x direction (see Figure 5). The magnitude of the induced free strains is taking to be

$$(\varepsilon_x)_{p1} = \frac{d_{31}}{h_p} V_1 \quad (2.21)$$

$$(\varepsilon_x)_{p2} = \frac{d_{31}}{h_p} V_2 \quad (2.22)$$

where d_{31} is a piezoelectric strain constant, and V_1 and V_2 are the applied voltages into the top and bottom piezoelectric. The induced external stress distribution in the individual patches is taken to be

$$(\sigma_x)_{p1} = -E_p \frac{d_{31}}{h_p} V_1 \quad (2.23)$$

Table I

Variables in the Euler-Bernoulli beam equation

i	x_i	ψ_i (flexural rigidity)	ϕ_i
1	$0 \leq x \leq l_1$	$\psi_b = \frac{1}{12} E_b b h^3$	$\phi_b = \rho b h$
2	$l_1 \leq x \leq l_2$	$\psi_{p1} = \psi_b (1 + n\alpha_{p1}\beta_{p1}\kappa_{p1}(3 + 6\beta_{p1} + 4\beta_{p1}^2))$	$\phi_{p1} = \phi_b (1 + n\kappa_{p1}\beta_{p1}\gamma_{p1})$
3	$l_2 \leq x \leq l_3$	$\psi_b = \frac{1}{12} E_b b h^3$	$\phi_b = \rho b h$
4	$l_3 \leq x \leq l_4$	$\psi_{p1} = \psi_b (1 + n\alpha_{p1}\beta_{p1}\kappa_{p1}(3 + 6\beta_{p1} + 4\beta_{p1}^2))$	$\phi_{p1} = \phi_b (1 + n\kappa_{p1}\beta_{p1}\gamma_{p1})$
5	$l_4 \leq x \leq l$	$\psi_b = \frac{1}{12} E_b b h^3$	$\phi_b = \rho b h$

$$(\sigma_x)_{p2} = -E_p \frac{d_{31}}{h_p} V_2 \quad (2.24)$$

The negative signs result from the conservation of forces when balancing the material and induced stresses in the patch. The external moment and force resultants due to the activation of the individual piezoelectric can be expressed as

$$M_x^e(x) = \int_A (\sigma_x) z dA \quad (2.25)$$

$$(M_x^e)_{p1} = b_p \int_{\frac{h}{2}}^{\frac{h}{2}+h_p} (\sigma_x)_{p1} z dA \quad (2.26)$$

$$(N_x^e)_{p1} = b_p \int_{\frac{h}{2}}^{\frac{h}{2}+h_p} (\sigma_x)_{p1} dA \quad (2.27)$$

$$(M_x^e)_{p2} = b_p \int_{\frac{h}{2}}^{\frac{h}{2}-h_p} (\sigma_x)_{p2} z dA \quad (2.28)$$

$$(N_x^e)_{p2} = b_p \int_{\frac{h}{2}}^{\frac{h}{2}-h_p} (\sigma_x)_{p2} dA \quad (2.29)$$

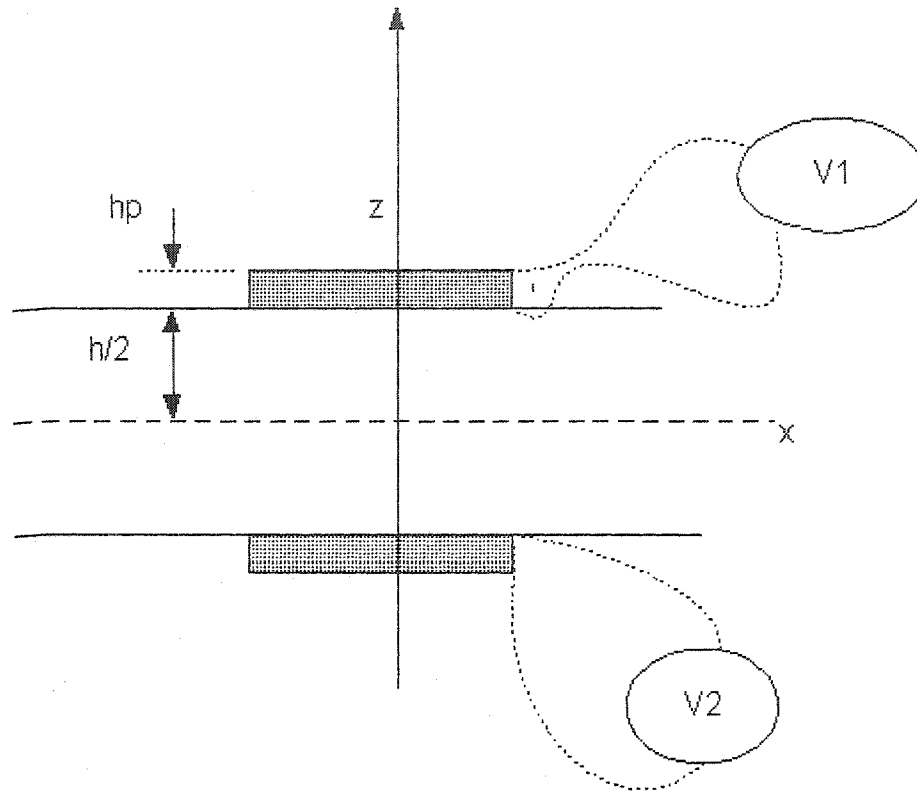


Figure 5 The activation of piezoelectric bonded to beam

Then, after integrating equations 2.26 and 2.28 the external moment for each piezoelectric are:

$$\left(M_x^e\right)_{p1} = -\frac{1}{2} E_p b_b (h + h_p) d_{31} V_1 \quad (2.30)$$

$$\left(M_x^e\right)_{p2} = -\frac{1}{2} E_p b_b (h + h_p) d_{31} V_2 \quad (2.31)$$

and, integrating equations 2.27 and 2.29 the external forces for each piezoelectric are

$$\left(N_x^e\right)_{p1} = -E_p b_p d_{31} V_1 \quad (2.32)$$

$$\left(N_x^e\right)_{p2} = -E_p b_p d_{31} V_2 \quad (2.33)$$

Note that, the voltage choice $V_1 = V_2 = V$ causes pure extension in the beam while pure bending occurs with the choice $V_2 = -V_1 = V$. Since the beam is clamped at $x = 0$, the boundary conditions are

$$w_1 = 0 \quad (\text{transverse displacement}) \quad (2.34)$$

$$\frac{\partial w_1}{\partial x} = 0 \quad (\text{normal slope}) \quad (2.35)$$

In order to satisfy the compatibility of displacements and equilibrium of forces at the junctions, the conditions of continuity have to be applied at these junctions. Continuity of transverse displacement, normal slope, bending moment and shear force at the junction $x = L_1$ are:

$$\left\{ \begin{array}{l} w_1 = w_2 \\ \frac{\partial w_1}{\partial x} = \frac{\partial w_2}{\partial x} \\ -\psi_1 \frac{\partial^2 w_1}{\partial x^2} = -\psi_2 \frac{\partial^2 w_2}{\partial x^2} + 2(M_x^e)_{p1} \\ -\psi_1 \frac{\partial^3 w_1}{\partial x^3} = -\psi_2 \frac{\partial^3 w_2}{\partial x^3} \end{array} \right. \quad (2.36)$$

Continuity of transverse displacement, normal slope, bending moment and shear force at the junction $x = L_2$ are:

$$\left\{ \begin{array}{l} w_2 = w_3 \\ \frac{\partial w_2}{\partial x} = \frac{\partial w_3}{\partial x} \\ -\psi_2 \frac{\partial^2 w_2}{\partial x^2} + 2(M_x^e)_{p1} = -\psi_3 \frac{\partial^2 w_3}{\partial x^2} \\ -\psi_2 \frac{\partial^3 w_2}{\partial x^3} = -\psi_3 \frac{\partial^3 w_3}{\partial x^3} \end{array} \right. \quad (2.37)$$

Continuity of transverse displacement, normal slope, bending moment and shear force at the junction $x = L_3$ are:

$$\left\{ \begin{array}{l} w_3 = w_4 \\ \frac{\partial w_3}{\partial x} = \frac{\partial w_4}{\partial x} \\ -\psi_3 \frac{\partial^2 w_3}{\partial x^2} = -\psi_4 \frac{\partial^2 w_4}{\partial x^2} + 2(M_x^e)_{p2} \\ -\psi_3 \frac{\partial^3 w_3}{\partial x^3} = -\psi_4 \frac{\partial^3 w_4}{\partial x^3} \end{array} \right. \quad (2.38)$$

Continuity of transverse displacement, normal slope, bending moment and shear force at the junction $x = L_4$ are:

$$\left\{ \begin{array}{l} w_4 = w_5 \\ \frac{\partial w_4}{\partial x} = \frac{\partial w_5}{\partial x} \\ -\psi_4 \frac{\partial^2 w_4}{\partial x^2} + 2(M_x^e)_{p2} = -\psi_5 \frac{\partial^2 w_5}{\partial x^2} \\ -\psi_4 \frac{\partial^3 w_4}{\partial x^3} = -\psi_5 \frac{\partial^3 w_5}{\partial x^3} \end{array} \right. \quad (2.39)$$

The moment and the shear force are free at the end of the beam $x = L$, the boundary conditions become

$$\frac{\partial^3 w_s}{\partial x^3} = 0 \quad (\text{shear force}) \quad (2.40)$$

$$\frac{\partial^2 w_s}{\partial x^2} = 0 \quad (\text{bending moment}) \quad (2.41)$$

Finally, equation (2.34) to (2.41) can be arranged as follows

$$[\Omega]\{K\} = \{\Gamma\} \quad (2.42)$$

where $[\Omega]$ is a 20 X 20 matrix and $\{\Gamma\}$ is a vector of twenty known coefficients, while $\{K\}$ is a vector of twenty unknown coefficients.

2.3.3 Modal Analysis

The free vibration analysis seeks to obtain the natural frequencies of the beam structure. External loading due to the actuators is not considered. The resulting equations after application of the boundary conditions and continuity equations are used to determine the natural frequency of the beam structure.

In any normal mode, by definition, no external load and $w_i(x,t) = \varphi_i(x)f_i(t)$, where $f_i(t)$ is a time function, and $\varphi_i(x)$ is the characteristic shape with some undetermined amplitude. We may also write

$$\frac{\partial^2}{\partial t^2} w_i(x,t) = \varphi_i(x) \frac{\partial^2}{\partial t^2} f_i(t) \quad \text{and} \quad \frac{\partial^4}{\partial x^4} w_i(x,t) = f_i(t) \frac{\partial^4}{\partial x^4} \varphi_i(x)$$

Substitution in equation 2.43 provides

$$\psi_i f_i(t) \frac{\partial^4 \phi_i(x)}{\partial x^4} + \phi_i(x) \ddot{f}_i(t) = 0 \quad i = 1, \dots, 5 \quad (2.43)$$

or

$$\frac{\psi_i}{\phi_i \phi_i(x)} \frac{\partial^4 \phi_i(x)}{\partial x^4} = -\frac{\ddot{f}_i(t)}{f_i(t)} \quad i = 1, \dots, 5 \quad (2.44)$$

Since the left side of equation (2.44) varies only with x and the right side only with t , each must be equal to a constant, which will be shown below, is equal to ω_i^2 . Thus, by setting each side equal to ω_i^2 , we may write the two equations

$$\ddot{f}_i(t) + \omega_i^2 f_i(t) = 0 \quad i = 1, \dots, 5 \quad (2.45)$$

$$\frac{d^4 \phi_i(x)}{dx^4} + \frac{\omega_i^2 \phi_i}{\psi_i} \phi_i(x) = 0 \quad i = 1, \dots, 5 \quad (2.46)$$

The solution for the first of these is

$$f_i(t) = c_1 \sin(\omega_i t) + c_2 \cos(\omega_i t) \quad i = 1, \dots, 5 \quad (2.47)$$

which merely indicates that the time function is harmonic with natural frequency ω_i , and hence that equation (2.44) is valid for normal modes. The solution of the equation (2.46) is

$$\phi_i(x) = A_i \cos(\lambda_i x) + B_i \sin(\lambda_i x) + C_i \cosh(\lambda_i x) + D_i \sinh(\lambda_i x) \quad i = 1, \dots, 5 \quad (2.48)$$

where $(\lambda_i)^4 = \frac{\omega_i^2 \phi_i}{\psi_i}$ and the constants a_i , b_i , c_i and d_i may be determined by the boundary

conditions. where λ_i is the i^{th} solution of the characteristic frequency equation :

2.3.4 Static Analysis

If the piezo-actuators (see Figure 3) are subjected to the application of a D.C. voltage, V , then the excitation frequency, ω , is zero and the beam structure bonded with piezo-actuators undergoes a static deflection. In this case, the relationships for deflection of the beam can be represented as

$$w_1 = 0 \quad \text{for } 0 \leq x \leq L_1 \quad (2.49)$$

$$w_2 = \eta_{p1}(L_1 - x)^2 \quad \text{for } L_1 \leq x \leq L_2 \quad (2.50)$$

$$w_3 = \eta_{p1}(L_1 - L_2)(L_1 + L_2 - 2x) \quad \text{for } L_2 \leq x \leq L_3 \quad (2.51)$$

$$w_4 = w_3 + \eta_{p2}(L_3 - x)^2 \quad \text{for } L_3 \leq x \leq L_4 \quad (2.52)$$

$$w_5 = w_3 + \eta_{p2}(L_3 - L_4)(L_3 + L_4 - 2x) \quad \text{for } L_4 \leq x \leq L_5 \quad (2.53)$$

where η_{p1} and η_{p2} are defined as follows :

$$\eta_{p1} = \frac{(M_x^e)_{p1}}{\Psi_{p1}} \quad (2.54)$$

$$\eta_{p2} = \frac{(M_x^e)_{p2}}{\Psi_{p2}} \quad (2.55)$$

Once again, if the same type of piezo-actuators are used for both locations then equation (2.54) and (2.55) are equal. For perfect bonding, these equations can be simplified as follow:

$$\eta = \eta_{p1} = \eta_{p2} = \frac{12\alpha\beta(1+\beta)}{1+2\alpha\beta(3+6\beta+4\beta^2)} \frac{d_{31}V}{h_p h} \quad (2.56)$$

where α and β are defined in equations (2.20a) and (2.20b), respectively.

2.4 Experimental approach

As explained previously, the natural frequencies and mode shapes of a cantilever beam bonded with piezoelectric elements can be predicted analytically and numerically (FEM). Experimental modal analysis has been conducted to verify the analytical and numerical approaches.

Among piezoelectric materials, plumbum zirconate titante has high coupling coefficients and piezoelectric charge coefficients. PZT BM500 of Sensor Technology Company is used for actuators. On the other hand, polarized homopolymer of VinyliDene Fluoride, PVDF, is the most popular piezoelectric material for sensors. They are thin, unobtrusive, self-powered, adaptable to complex contours, and available in a variety of configurations. The properties of the piezoelectric materials used in this study are presented in Table II.

Figures 6 and 7 represent the experimental set up and its schematic used in the first part of numerical results. The experimental set up consists of a cantilever aluminium beam with n piezoactuators. A non-contact laser displacement sensor, Keyence LB-72, was used to measure the displacement at the tip (or other points). A control panel instrument (Electro-Numeric RS-485) and a personal computer acquired the output data from the laser sensor at the same time. A function generator (synthesizer), Adret, was used to provide a harmonic signal to an amplifier, Kepco BOP 1000M, which supplied voltage to the piezoelectric actuator.

Table II

Properties of various piezoelectric materials

	PZT 500	PZT 532	PVDF
Curie temperature, °C	360	210	100
Piezoelectric constant, m/V	190×10^{-12}	200×10^{-12}	23×10^{-12}
Young's modulus, GPa	63	71	2-4
Thickness, mm	0.25	0.31	0.028
Length, mm	38	76	27
Width, mm	15.2	25.4	13
Density, kg/m ³	7600	7350	1780



Figure 6 Experimental set up

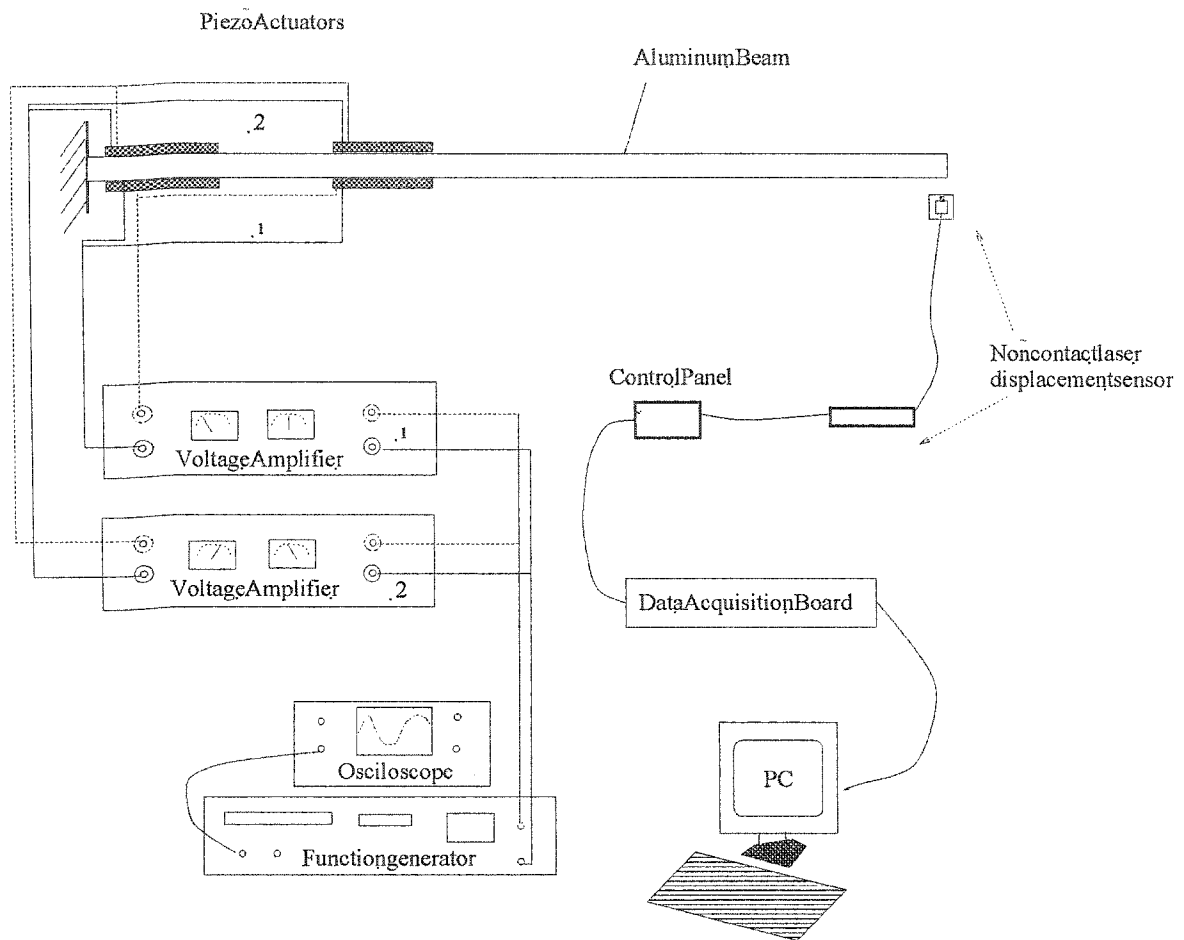


Figure 7 Schematic of experimental set up

2.5 Results and comparison

The objectives of this section are to 1) evaluate the adapted analytical technique for a cantilever beam bonded with piezo-electric elements; 2) examine the numerical results obtained with some commercial Finite Element Codes; 3) evaluate the experimental results obtained in our research group and finally, 4) compare the performance of these three approaches (i.e., analytical, numerical and experimental). Two following problems

are selected from reference Crawley and Deluis (1987) and Yousefi-Koma (1997), respectively. Two beam specimens were statically deformed with piezo-ceramic actuators and the tip deflections are measured. The first two natural frequencies are also determined by analytical, numerical and experimental approaches.

In the following examples, the cantilever beams are modelled with 4-node shell elements, while the piezoelectric materials are modelled with 3D 8-node brick elements.

2.5.1 Example 1

The schematic of this beam specimen is shown in Figure 3 and the geometrical and material properties are given in Table III. This example is taken from reference Crawley and Deluis (1987). The experimental set up (see Figure 6) used in this example is explained previously (Section 2.4).

Natural frequencies for beam A without any piezo-elements and with bonded piezo-actuators are presented in Tables IV and V, respectively. The discrepancy is within 4 % for beam with bonded piezo-actuators, while it is only about 1 % for beam without any piezo-elements. One can notice the better agreement between the numerical and analytical results than between the experimental and analytical ones. The numerical results listed in Tables IV and V show that the FEM can accurately predict the natural frequencies of an integrated piezo-actuator system, and that the prediction is validated by experiments.

Deflection of the beam under static piezoelectric actuation is presented in Figure 8. In general, good agreements between the three approaches are observed between 30 and 60 volts, however, better agreements are obtained for the low DC voltages between the numerical and analytical.

Table III

Beam A- Geometrical and material properties of test specimen

Beam	
Length, mm	400
Width, mm	38
Thickness, mm	3.18
Flexural modulus, GPa	70
Shear modulus, GPa	27
Density, Kg/m ³	2710
Actuator	
First actuator location, mm	5 - 43
Second actuator location, mm	102 - 140
Width, mm	15.2
Thickness, mm	0.25
Density, Kg/m ³	7600
Type (for more details see Table II)	BM 500

Table IV

Natural frequencies (Hz) for beam A without any piezo-elements

Mode number	Analytical	FEM	Discrepancy (%)
1	16.31	16.45	0.9
2	103.06	103.18	0.2

Table V

Natural frequencies (Hz) for beam A with bonded piezo-ceramics

Mode number	Analytical	FEA	Experimental	Δ_{FEA} (%)	Δ_{Exp} (%)
1	16.72	16.52	16.42	1.2	1.8
2	105.62	102.54	101.05	2.9	4.3

Finally, the tip amplitude of the beam versus AC voltage (harmonic analysis) is shown in Figure 9. The beam structure was excited in its first mode shape (i.e., natural frequency 16.42 Hz) using piezo-actuators. The voltages with the same magnitude were applied to the piezo-actuators and the driving voltages were equal in the phase for this mode shape. The actual measured tip amplitude of the beam, as well as the finite element results and the predicted amplitude based on reference Crawley and Deluis (1987), are also presented in Figure 9. We can notice that the finite element results are slightly less than the other results. On the other hand, good agreement is obtained between our experimental results and the ones from Crawley and Deluis (1987).

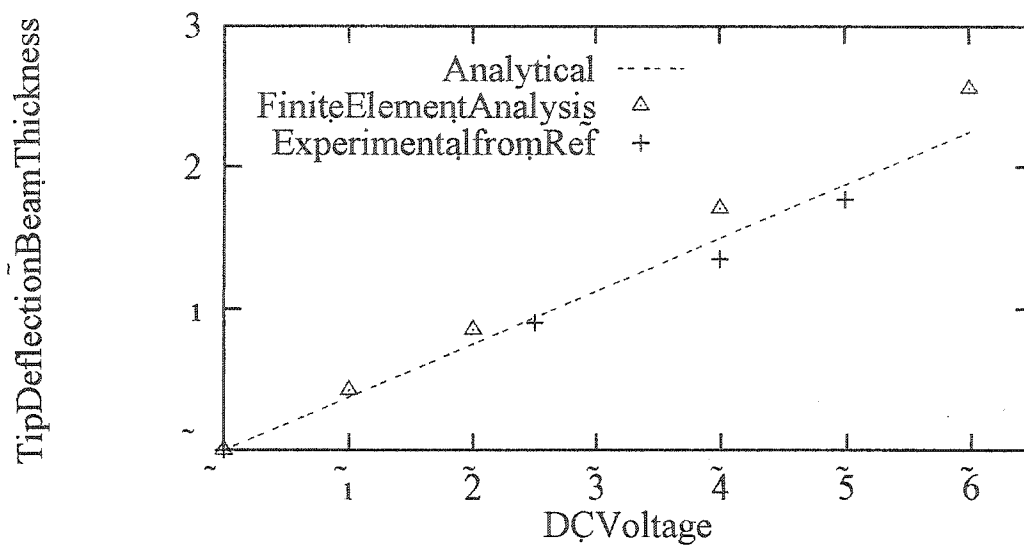


Figure 8 Deflection of the beam A under static piezoelectric actuation

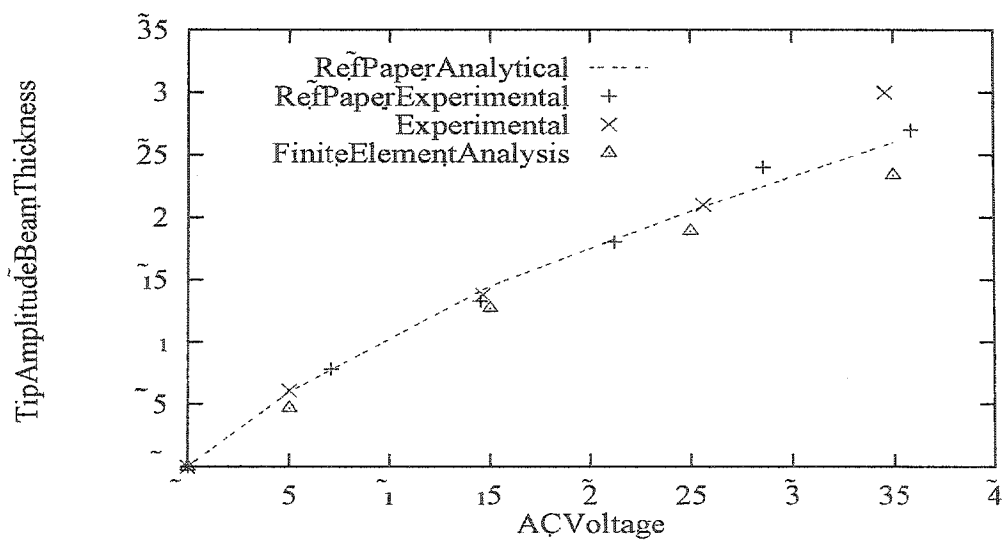


Figure 9 Tip amplitude of the beam A versus voltage

2.5.2 Example 2

The second example consists of a cantilever beam (Figure 10), which is taken from reference Yousefi-Koma (1997). The geometrical and material properties of aluminium beam with bonded piezoelectric sensors and actuators used in this example are presented in Table VI.

Natural frequencies for Beam B without any piezo-elements and with bonded piezo-elements are presented in Tables VII and VIII, respectively. We can notice a better agreement between the numerical and analytical results for the beam structure without any piezo-elements than for same beam with bonded piezo-elements. The numerical results listed in Tables VII and VIII show that the both finite element codes (i.e., ABAQUS and ANSYS) can predict well the natural frequencies. The difference of discrepancies between ABAQUS and ANSYS codes may be explained by the nature of the numerical procedures used in these two codes. Note that the Subspace method is used in ABAQUS code, while the Reduced method is applied in ANSYS.

Deflection of the beam under static piezo-electric actuation is presented in Figure 11. The experimental results for this example are taken from reference Yousefi-Koma (1997). Once again, good agreements between the three approaches are observed, however, the best agreements are obtained for the low DC voltages.

Table VI

Geometrical and material properties of test specimen

Beam	
Length, mm	508
Width, mm	25.4
Thickness, mm	0.8
Flexural modulus, GPa	72
Shear modulus, GPa	27
Density, Kg/m ³	2710
Sensor	
First PVDF location, mm	22-49
Second PVDF location, mm	129-156
Width, mm	13
Thickness, mm	0.028
Density, Kg/m ³	1780
Type (for more details see Table II)	PVDF
Actuator	
PZT location, mm	51-127
Width, mm	25.4
Thickness, mm	0.31
Density, Kg/m ³	7350
Type (for more details see Table II)	BM 532

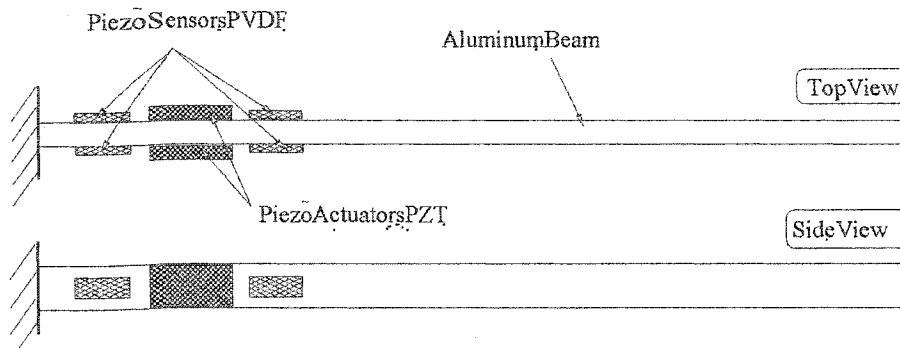


Figure 10 Beam B model with sensor and actuators

Table VII

Natural frequencies (Hz) for beam B without any piezo-ceramics

Mode number	Analytical	ABAQUS	ANSYS	$\Delta_{\text{ABAQUS}} (\%)$	$\Delta_{\text{ANSYS}} (\%)$
1	2.58	2.59	2.59	<0.1	<0.1
2	16.30	16.29	16.27	0.1	0.2

Table VIII

Natural frequencies (Hz) for beam B with piezoelectric

Mode number	Analytical	ABAQUS	ANSYS	$\Delta_{\text{ABAQUS}} (\%)$	$\Delta_{\text{ANSYS}} (\%)$
1	3.41	3.30	2.88	3.2	15.5
2	16.90	16.21	15.77	4.1	6.7

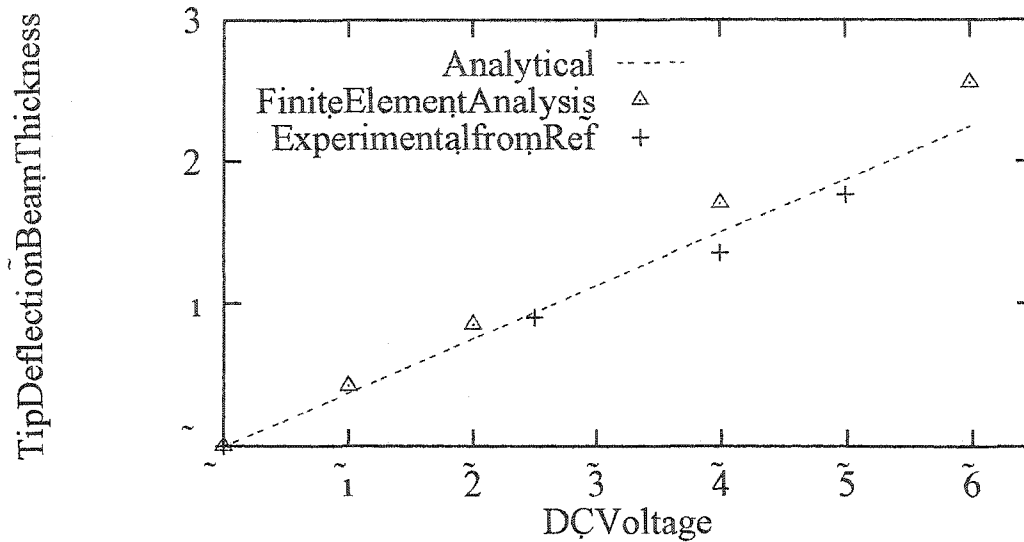


Figure 11 Deflection of the beam B under static piezoelectric actuation

2.6 Summary

At this point, a review of the finite element formulation was presented.

Theoretical model of piezoelectric patch interactions (actuators and/or sensors) with a thin aluminum beam structures are developed. This model is validated by comparing the natural frequencies and static deflection to those calculated by finite element approach and experimental results. Good results are observed. The next chapter will focus on modeling a laminate beam with piezoelectric.

CHAPTER 3

MODELING OF LAMINATED BEAM WITH PIEZOELECTRIC

In this chapter, the modeling of the dynamic response of composite structures with bonded and embedded piezoelectric actuators is presented. The first order shear deformation beam theory is used for the analysis to ensure accurate bending solutions. Experimental, theoretical and numerical modeling approaches are conducted into the active vibration control of laminate beam structures with bonded and embedded piezoelectric actuators. A modal analysis is performed to determine the natural frequencies and mode shapes of the structures. The natural frequency results obtained by the assumed-modes method and the theoretical solutions are validated through the experimental results obtained from Sung (1992) and finite elements. The assumed-modes method can accurately predict the natural frequencies and mode shape of the laminate beam. Finally, the effects of the number and locations of the actuators on the control system are also investigated using a static analysis of the model.

3.1 Introduction

Recent advances in design and manufacturing technologies have greatly enhanced the use of advanced fiber-reinforced composite structures for aircraft and aerospace structural applications. As a consequence, the integration of composite structural design with the "smart system" concept could potentially result in a significant improvement in the performance of aircraft and space structures. The objective of this investigation was to develop an analytical method for modeling the mechanical-electrical response of fiber-reinforced laminated composite structures containing distributed piezoceramics under static as well as dynamic mechanical or electrical loading. This chapter also introduces a modeling approach based on the Rayleigh-Ritz assumed mode shape to predict the behavior of a laminate beam excited by a patch of piezoelectric material

bonded to the surface of the beam. The model includes the inertia and stiffness of the actuator, and has been used to predict the frequency response of the composite beam. The experimental results obtained from Sung (1992) using T300/976 composite and PZT G1195 piezoelectric ceramics were used to verify the theory and the computer simulations. Finally, the effects of the number and locations of the actuators on the control system are also investigated.

3.2 Problem statement

Consider a fibre-reinforced laminated composite beam containing distributed piezoelectric ceramics as actuators that can be bonded on the surfaces or embedded inside structures. The ply orientation, θ and thickness, h of the laminate can be arbitrary. The goal of this paper is to determine the mechanical response of the structure for a given mechanical loading condition or electrical potential on the actuators.

3.3 Transverse vibration of laminate beam

In the first order shear deformation laminate plate theory (FSDT), the Kirchhoff hypothesis is relaxed by removing the third part, i.e., the transverse normal does not remain perpendicular to the midsurface after deformation. This amounts to including transverse shear strains in the theory. The inextensibility of transverse normal requires that the transverse displacement w not be a function of the thickness co-ordinate, z .

The linear constitutive relations for the k^{th} orthotropic lamina in the principal material co-ordinates of a lamina are:

$$\begin{Bmatrix} \sigma_1 \\ \sigma_2 \\ \tau_{12} \end{Bmatrix}^{(k)} = \begin{bmatrix} Q_{11} & Q_{12} & 0 \\ Q_{12} & Q_{22} & 0 \\ 0 & 0 & Q_{66} \end{bmatrix}^{(k)} \begin{Bmatrix} \varepsilon_1 \\ \varepsilon_2 \\ \gamma_{12} \end{Bmatrix}^{(k)} \quad (3.1)$$

where $Q_{ij}^{(k)}$ is the plane stress-reduced stiffness, and σ_i and ε_i are the stress and strain field components respectively.

In non-principal co-ordinates (generally orthotropic lamina), the stress-strain relationship is:

$$\begin{Bmatrix} \sigma_x \\ \sigma_y \\ \tau_{xy} \end{Bmatrix}^{(k)} = \begin{bmatrix} \bar{Q}_{11} & \bar{Q}_{12} & \bar{Q}_{16} \\ \bar{Q}_{12} & \bar{Q}_{22} & \bar{Q}_{26} \\ \bar{Q}_{16} & \bar{Q}_{26} & \bar{Q}_{66} \end{bmatrix}^{(k)} \begin{Bmatrix} \varepsilon_x \\ \varepsilon_y \\ \gamma_{xy} \end{Bmatrix}^{(k)} \quad (3.2)$$

The laminate constitutive equations for the first order theory are obtained using the lamina constitutive equation and the following relations:

$$\begin{Bmatrix} \tau_{yz} \\ \tau_{xz} \end{Bmatrix}^{(k)} = \begin{bmatrix} \bar{Q}_{44} & \bar{Q}_{45} \\ \bar{Q}_{45} & \bar{Q}_{55} \end{bmatrix}^{(k)} \begin{Bmatrix} \gamma_{yz} \\ \gamma_{xz} \end{Bmatrix}^{(k)} \quad (3.3)$$

where $\bar{Q}_{44} = Q_{44} \cos^2 \theta + Q_{55} \sin^2 \theta$

$$\bar{Q}_{45} = (Q_{55} - Q_{44}) \cos \theta \sin \theta$$

$$\bar{Q}_{55} = Q_{44} \sin^2 \theta + Q_{55} \cos^2 \theta$$

θ is the angle-measured counter clockwise from the x-co-ordinate (non-principal co-ordinates) to the material co-ordinate 1 (principal co-ordinates). The laminate

constitutive equations for symmetric laminates, in the absence of in-plane forces, are given by:

$$\begin{Bmatrix} M_{xx} \\ M_{yy} \\ M_{xy} \end{Bmatrix} = \begin{bmatrix} D_{11} & D_{12} & D_{16} \\ D_{12} & D_{22} & D_{26} \\ D_{16} & D_{26} & D_{66} \end{bmatrix} \begin{Bmatrix} \frac{\partial \phi_x}{\partial x} \\ \frac{\partial \phi_y}{\partial y} \\ \frac{\partial \phi_x}{\partial y} + \frac{\partial \phi_y}{\partial x} \end{Bmatrix} \quad (3.5)$$

$$\begin{Bmatrix} Q_{yz} \\ Q_{xz} \end{Bmatrix} = K \begin{bmatrix} A_{44} & A_{45} \\ A_{45} & A_{55} \end{bmatrix} \begin{Bmatrix} \frac{\partial w_0}{\partial y} + \phi_y \\ \frac{\partial w_0}{\partial x} + \phi_x \end{Bmatrix} \quad (3.6)$$

where A_{ij} is the “extensional stiffness,” D_{ij} the bending stiffness, defined in terms of the lamina stiffness \bar{Q}_{ij} (see reference Reddy (1997)), M_{xx} , M_{yy} and M_{xy} the moment resultants, and Q_{yz} and Q_{xz} are the transverse shear force resultant.

The linear constitutive equation in a piezoelectric can be expressed by the inverse and direct piezoelectric equations respectively.

$$\{\sigma\} = [Q_p]\{\varepsilon\} - [e]^T \{E\} \quad (3.7)$$

$$\{D\} = [e]\{\varepsilon\} - [\epsilon]^T \{E\} \quad (3.8)$$

where $\{\varepsilon\}$ is the strain tensor, $\{\sigma\}$ is the stress tensor, $\{D\}$ is the electric displacement, $\{E\}$ is the electric field intensity, $[Q_p]$ is the elastic stiffness matrix of piezoelectric ceramic, $[e]$ is the piezoelectric stress coefficient matrix, and $[\epsilon]$ is the permittivity constant matrix.

It should be noted that the piezoelectric stress coefficient matrix $[e]$ is expressed in terms of the commonly available strain coefficient matrix $[d]$, using the relation $[e] = [Q_p][d]$.

For a one-dimensional composite beam with actuators, the width in the y-direction is assumed to be free of normal stresses, i.e., $\sigma_y = \tau_{yz} = \tau_{xy} = 0$, while $\varepsilon_y \neq 0, \varepsilon_{yz} \neq 0$ and $\varepsilon_{xy} \neq 0$. We assume $M_{yy} = M_{xy} = Q_{yz} = \phi_y = 0$ everywhere in the beam, and that both w_0 and ϕ_x are functions of only x and t.

Following the beam theory of Timoshenko, the displacement field of the beam can be defined as

$$u(x, z, t) = u_0(x, t) + z\phi_x(x, t) \quad (3.9)$$

$$w(x, z, t) = w_0(x, t) \quad (3.10)$$

where u and w are the longitudinal and the transverse displacements at any point z from the middle plane; u_0 and w_0 are the longitudinal and transverse displacements of the beam middle plane, and ϕ_x is the rotation of the beam section. The longitudinal strain ε_x and shear strain γ_{xz} are given by

$$\varepsilon_x = \frac{\partial u}{\partial x} = \frac{\partial u_0}{\partial x} + z \frac{\partial \phi_x}{\partial x} \quad (3.11)$$

$$\gamma_{xz} = \frac{\partial w}{\partial x} + \frac{\partial u}{\partial z} = \frac{\partial w_0}{\partial x} + \phi_x \quad (3.12)$$

Therefore, the constitutive equation for the k^{th} layer of the laminate beam can be written as:

$$(\sigma_x)_k = (\bar{Q}_{11})_k (\varepsilon_x)_k \quad (3.13)$$

$$(\tau_{xz})_k = (\bar{Q}_{55} \gamma_{xz})_k \quad (3.14)$$

where $\bar{Q}_{11} = Q_{11} \cos^4(\theta) + 2(Q_{12} + 2Q_{66}) \sin^2(\theta) \cos^2(\theta) + Q_{22} \sin^4(\theta)$

$$\bar{Q}_{55} = Q_{44} \sin^2(\theta) + Q_{55} \cos^2(\theta)$$

$$Q_{11} = \frac{E_1}{1 - \nu_{12}\nu_{21}}, Q_{12} = \frac{\nu_{12}E_2}{1 - \nu_{12}\nu_{21}} = \frac{\nu_{21}E_1}{1 - \nu_{12}\nu_{21}}, Q_{22} = \frac{E_2}{1 - \nu_{12}\nu_{21}},$$

$$Q_{66} = G_{12}, Q_{44} = G_{23}, Q_{55} = G_{13}$$

and σ_x is the axial stress in the x-direction; τ_{xz} the shear stress in the x-z direction; E_i the modulus of elasticity; ν_{ij} the Poisson ratio; G_{ij} ($i, j = 1, 2, 3$) the shear modulus, and the subscript k denotes quantities belonging to the k^{th} layer.

The constitutive relations for the i^{th} actuator can be written as:

$$(\sigma_x^p(x, z))_i = \left(\frac{E_p}{1 - \nu_p^2} \varepsilon_x(x, z) - e_{31} E \right)_i \quad (3.15)$$

$$\left[\tau_{xz}^p(x) \right]_i = (G_p \gamma_{xz})_i \quad (3.16)$$

where E_p , G_p and ν_p are the modulus of elasticity, shear modulus, and Poisson ratio of the actuator, respectively; e_{31} is the piezoelectric z-x stress coefficient of the actuator; E the electric field intensity in the z direction in the actuator, and the subscript p indicates the piezoelectric.

The stress resultant-displacement relationships for the laminate beam can be obtained by integrating the stresses through the cross-sectional area of the beam.

$$\begin{bmatrix} N_{xx} \\ M_{xx} \end{bmatrix} = \begin{bmatrix} A_{11} & B_{11} \\ B_{11} & D_{11} \end{bmatrix} \begin{bmatrix} \frac{\partial u}{\partial x} \\ \frac{\partial \phi_x}{\partial x} \end{bmatrix} - \chi \begin{bmatrix} N_p \\ M_p \end{bmatrix} \quad (3.16)$$

$$[Q_{xz}] = [A_{55} \gamma_{xz}] \quad (3.17)$$

where $\{A_{11}, B_{11}, D_{11}\} = \sum_{k=1}^{n+n_p} \int_{z_{k-1}}^{z_k} (\bar{Q}_{11})_k (1, z, z^2) dz$; $A_{55} = k_s \sum_{k=1}^{n+n_p} \int_{z_{k-1}}^{z_k} \bar{Q}_{55} dz$

$\{N^p, M^p\} = \sum_{j=1}^{n_p} \int_{z_{j-1}}^{z_j} \left(\frac{E_p}{1-\nu_p^2} d_{31} E \right)_j (1, z) dz$, $d_{31} = e_{31} \frac{(1-\nu_p^2)}{E_p}$ is the piezoelectric z-x

strain coefficient; N_{xx} , M_{xx} are the longitudinal force and the moment per unit width of the beam; Q_{xz} is called the transverse shear force resultant; $\chi = 0$ for beam sections without actuators, and $\chi = 1$ for sections with actuators; n denotes the number of layers, n_p the number of actuators, and $k_s = 5/6$ is the shear correction factor. Here we consider the bending of symmetrically laminated beams according to the first order shear deformation laminate plate theory (FSDT). For symmetric laminates, the equations for bending deflection are uncoupled from those of the stretching displacements. If the in-plane forces are zero, the in-plane displacements (u_0, v_0) are zero, and the problem is reduced to one of solving for bending deflection and stress. From the equation of the symmetric laminate $B_{11} = 0$, we have

$$\frac{\partial \phi_x}{\partial x} = D_{11}^* M_{xx}, \quad \frac{\partial w_0}{\partial x} + \phi_x = A_{55}^* Q_{xz} \quad (3.18)$$

or

$$M(x) = bM_{xx} \text{ and } Q(x) = bQ_{xz} \quad (3.19)$$

The equation of motion

$$\frac{\partial Q_{xz}}{\partial x} + \varpi = I_0 \frac{\partial^2 w_0}{\partial t^2} \quad (3.20)$$

$$\frac{\partial M_{xx}}{\partial x} - Q_{xz} = I_2 \frac{\partial^2 \phi_x}{\partial t^2} \quad (3.20)$$

where $(I_0, I_1, I_2) = \int_{\frac{h}{2}-h_p}^{\frac{h}{2}+h_p} \rho(1, z, z^2) dz$, h and h_p are the thickness of beam and actuators respectively, A^* , D^* denote the inverse matrix of A and D respectively, ϖ is the applied load, and b is the width of the beam. From Equations (3.20) and (3.21), the equations of motion can be written in terms of the displacement function

$$\frac{b}{A_{55}^*} \left(\frac{\partial^2 w_0}{\partial x^2} + \frac{\partial \phi_x}{\partial x} \right) + \varpi b = b I_0 \frac{\partial^2 w_0}{\partial t^2} \quad (3.21)$$

$$\frac{b}{D_{11}^*} \frac{\partial^2 \phi_x}{\partial x^2} - \frac{b}{A_{55}^*} \left(\frac{\partial w_0}{\partial x} + \phi_x \right) = b I_2 \frac{\partial^2 \phi_x}{\partial t^2} \quad (3.22)$$

3.3.1 Static analysis

When the laminated beam problem is such that the bending moment $M(x)$ and $Q(x)$ can be readily written in terms of known applied loads (in statically determinate beam problems), Equation (3.18, 3.19, 3.20 and 3.21) can be used to determine ϕ_x , and then w_0 as:

$$\phi_x = \frac{M}{b} \frac{D_{11}^*}{A_{55}^*} x + C_1 \quad \text{and} \quad w_0(x) = -\frac{M}{2b} \frac{D_{11}^*}{A_{55}^*} x^2 - C_1 x + C_2$$

where $M = \frac{n_p d_{31} E_p V \frac{1}{2} \{(\frac{h}{2} + h_p)^2 - (\frac{h}{2})^2\}}{h_p (1 - \nu_p^2)}$, C_1 and C_2 are constants determined by

boundary conditions

$$0 \leq x \leq x_1 \quad w(x) = w_1(x) = \frac{dw_1}{dx} = 0;$$

$x_1 \leq x \leq x_2$ the boundary conditions are: at $x = x_1$, $w_1 = w_2$ and $\frac{dw_1}{dx} = \frac{dw_2}{dx}$,

$$\text{then } w(x) = w_2(x) = \frac{MD_{11}^*}{2} (x - x_1)^2;$$

for $x \geq x_2$, the boundary conditions are: at $x = x_2$, $w_2 = w_3$ and $\frac{dw_3}{dx} = \frac{dw_2}{dx}$

$$\text{then } w(x) = w_3(x) = \frac{MD_{11}^*}{2} (x_1 - x_2)(x_1 + x_2 - 2x)$$

where x_1 and x_2 are the positions of actuators.

When $M(x)$ and $Q(x)$ cannot be expressed in terms of known loads, Equations (3.22) and (3.23) can be used to determine $w_0(x)$ and $\phi_x(x)$.

For uniform loads, the deflexion is:

$$w_0(x) = -\frac{\omega L^4 D_{11}^*}{24} \left\{ 6\left(\frac{x}{L}\right)^2 - 4\left(\frac{x}{L}\right)^3 + \left(\frac{x}{L}\right)^4 \right\} - \frac{\omega A_{55}^* L^2}{2b} \left\{ \frac{2x}{L} - \left(\frac{x}{L}\right)^2 \right\} \quad (3.24)$$

where L is the length of beam.

3.3.2 Modal analysis

For modal analyses, we assume that the applied axial force and transverse load are zero and that the motion is periodic. For a periodic motion, we assume a solution in the form

$$w_0(x, t) = W(x)e^{i\omega t} \quad (3.25)$$

$$\phi_x(x, t) = \psi(x)e^{i\omega t} \quad (3.26)$$

where ω is the natural frequency of vibration, and Equations (3.22) and (3.23) become

$$\frac{b}{D_{11}^*} \frac{d^4 W}{dx^4} + \left(\frac{b}{A_{55}^*} \frac{I_0}{D_{11}^*} + bI_2 \right) \omega^2 \frac{d^2 W}{dx^2} - \left(1 - \frac{b}{A_{55}^*} \omega^2 I_2 \right) bI_0 \omega^2 W = 0 \quad (3.27)$$

or

$$p \frac{d^4 W}{dx^4} + q \frac{d^2 W}{dx^2} - rW = 0 \quad (3.28)$$

The general solution of equation (3.28) is:

$$W(x) = c_1 \sin \lambda x + c_2 \cos \lambda x + c_3 \sinh \mu x + c_4 \cosh \mu x \quad (3.29)$$

where $\lambda = \sqrt{\frac{1}{2p}(q + \sqrt{q^2 + 4pr})}$, $\mu = \sqrt{\frac{1}{2p}(-q + \sqrt{q^2 + 4pr})}$ and c_i , $i = 1, \dots, 4$ are constants, which are to be determined using the boundary conditions. Note that we have

$$(2\lambda^2 p - q)^2 = q^2 + 4pr \quad \text{or} \quad p\lambda^4 - q\lambda^2 - r = 0.$$

Alternatively, Equation (3.27) can be written, with W given by Equation (3.28) in terms of ω as :

$$P\omega^4 - Q\omega^2 + R = 0 \quad (3.30)$$

$$\text{where } P = \frac{I_2}{A_{55}^*}, Q = 1 + \left(\frac{1}{A_{55}^* D_{11}^*} + \frac{I_2}{I_0} \right) \lambda^2, R = \frac{\lambda^4}{D_{11}^* I_0}$$

Hence, there are two (sets of) roots of this equation (when $I_2 \neq 0$)

$$(\omega^2)_1 = \frac{1}{2P} (Q - \sqrt{Q^2 - 4PR}) \quad (3.31)$$

$$(\omega^2)_2 = \frac{1}{2P} (Q + \sqrt{Q^2 - 4PR}) \quad (3.32)$$

It can be shown that $Q^2 - 4PQ > 0$ (and $PQ > 0$), and therefore the frequency given by the first equation is the smaller of the two values.

3.4 Numerical approach

3.4.1 Assumed – modes method

To derive the equations of motion of the laminate beam based on the Rayleigh-Ritz method, both the strain energy, U and the kinetic energy, T of the beam, and the piezoelectric element must be determined. The strain and kinetic energy result from the deformation produced by the applied strain, which is induced by exciting the piezoelectric element.

$$U = \frac{1}{2} \int (\varepsilon_x \sigma_x + \varepsilon_{xz} \tau_{xz}) dv + \frac{1}{2} \int_p (\varepsilon_x^p \sigma_x^p + \varepsilon_{xz}^p \tau_{xz}^p) dv \quad (3.33)$$

$$T = \frac{1}{2} \int \rho (\dot{u}^2 + \dot{w}^2) dv + \frac{1}{2} \int_p \rho_p (\dot{u}^2 + \dot{w}^2) dv \quad (3.34)$$

where \dot{u} and \dot{w} are the velocity components in the x and z directions respectively.

The static or dynamic response of the laminate beam incorporating the piezoelectric actuator can be calculated by substituting the strain and kinetic energy into Lagrange's equation:

$$\frac{d}{dt} \left(\frac{\partial T}{\partial \dot{q}_i} \right) - \frac{\partial T}{\partial q_i} + \frac{\partial U}{\partial q_i} = F_i \quad (3.34)$$

where q_i represents the i^{th} generalised co-ordinate, F_i is the i^{th} generalised force, T and U are the kinetic energy and the strain energy for the laminate beam and actuator, respectively, dv shows volume differential, and indices p refer to the piezoelectric actuator, and ρ is the mass density.

As there are no external forces (the force applied by the piezoelectric element is included as an applied strain), and there is no added damping, Lagrange's equation is reduced to:

$$\frac{d}{dt} \left(\frac{\partial T}{\partial \dot{q}_i} \right) + \frac{\partial U}{\partial q_i} = 0 \quad (3.36)$$

The assumed-modes method consists of assuming a solution of free vibration problem in the form of a series composed of linear combination of admissible functions ϕ_i , which are functions of spatial co-ordinates, multiplied by time-dependent generalised co-ordinates $q_i(t)$. These admissible functions satisfy the natural boundary condition. For the laminate beam, the transverse displacement is approximately expressed as:

$$w(x, t) = \sum_{i=1}^n \phi_i(x) q_i(t) \quad (3.37)$$

where $\phi_i(x) = \left(\frac{x}{L}\right)^i$. Using the shape function expressed in Equation (3.37), substituting for the potential and kinetic energy terms, the equation of motion can be written as

$$[M]\{\ddot{q}\} + [K]\{q\} = [B_v]\{v\} \quad (3.38)$$

where $[M]$ and $[K]$ are the mass and stiffness matrices, and $[B_v]$ is the input matrix used to apply forces to the structure by piezoelectric actuators. Vector q represents the beam response modal amplitudes, and v is the vector of applied voltage on piezoelectric.

We attempt to find the natural motion of the system, i.e. response without any forcing function. The form of response or solution is assumed as:

$$\{q(t)\} = \{\phi\}e^{i\omega t} \quad (3.39)$$

where $\{\phi\}$ is the mode shape (eigenvector) and ω is the natural frequency of the motion. In other words, the motion is assumed to be purely sinusoidal due to zero damping in the system. The general solution turns out to be a linear combination of each mode, as in:

$$\{q(t)\} = \sum_{j=1}^n c_j \{\phi_j\} e^{i\omega_j t} \quad (3.40)$$

where each constant (c_j) is evaluated from initial conditions. Substituting Equation (3.39) into Equation (3.38) with $\{v\} = 0$ yields

$$(-\omega^2[M] + [K])\{\phi\}e^{i\omega t} = 0 \quad (3.42)$$

the above equation has a nontrivial solution if $(-\omega^2[M] + [K])$ becomes singular. In others words, there exist n number of ω which satisfy

$$\det(-\omega^2[M] + [K]) = 0 \quad (3.42)$$

Since the mass matrix is positive definite, and the stiffness matrix is at least positive semi-definite, all ω_j is positive. Using Maple, the mass and stiffness of the matrices are computed from:

$$M_{ij} = m \int_0^L \phi_i \phi_j dx \quad (3.43)$$

$$K_{ij} = bD \int_0^L \phi_i \phi_j dx \quad (3.44)$$

where $m = hb\rho + n_p h_p b_p \rho_p$, and $D = \frac{1}{D_{11}^*} + n_p E_p \frac{1}{3} [(\frac{h}{2} + h_p)^3 - (\frac{h}{2})^3]$

3.4.2 Finite element method

The natural frequencies were also obtained by using the finite element software package, ANSYS. The piezoelectric actuator patches were modelled using solid5 piezoelectric elements, and the laminate beam, using shell99 structural elements. Figure 19 illustrates the finite element mesh, which consists of 40 elements for each piezoelectric actuator, and 750 elements for the laminate beam structure. The fixed-free boundary condition was applied by constraining the nodal displacements in both the x and y directions at the left end of the beam. A modal analysis was performed for the structures using the block Lanczos method.

3.5 Results and comparisons

Numerical and analytical results are presented to show the static and dynamic behaviour of laminated beams with piezoelectric actuators. In order to verify the proposed and the assumed-modes approaches, numerical calculations were generated from a cantilevered

laminated composite beam with piezoelectric actuators, as shown in Figure 12. The dimensions are also shown in the same Figure. The beam is made of AS/3506 graphite-epoxy composites, and the piezoceramic is PZT BM532. The adhesive layers are neglected. The material data is given in Table IX. The stacking sequence of the composite beam is $[0/\pm 45]_n$. A constant voltage (equal amplitude) with an opposite sign was applied to the piezoelectric on each side of the beam. Due to the converse piezoelectric effect, the distributed piezoelectric actuators contract or expand depending on negative or positive active voltage. In general, for an upward displacement, the upper actuators need a negative voltage and the lower actuators need a positive one. The control of static deformation and modal analysis for the beam under the distribution piezoelectric are analysed. Figure 13 shows the shape of the cantilever beams for various specified voltages. It is observed that the deformation of the laminate beams increases with increases in applied voltage. A uniformly distributed load of $1 (N/m^2)$ is applied to the beam. It is clear from Figure 14 that the structure reverts to the undeformed position as the specified voltages are increased. To investigate the effect of the number and placement of the actuator pairs on the deformation control, three sets of the actuator pairs are considered: three pairs, (the left, the middle and the right); two pairs (the left and the middle ones, the left and the right) and one pair, located at the end of the beam. The comparison of Figures 14 to 17 reflects the fact that a lower voltage is needed to eliminate the deflection caused by the external load when more actuators are used (Figure 15 to 17). When one pair of actuators is used, as shown in Figure 14, a very high active voltage is needed to delete the deformation, and the beam is also not smoothly flattened. Figure 15 shows that below a certain active voltage, the beam can be flattened quite smoothly by two pairs of actuators placed in the left and the middle positions of the beam. It is not necessary to cover the structures entirely with piezoelectric. Figure 18 shows the calculated centreline deflection of the composite beam with one pair of the actuators at different positions. It is seen that the location of the actuators has a significant effect on the control of the deformation.

Table IX Material properties

	PZT-G_1195N	PZT- (BM532)	T300/976	AS/3501
E_1 (GPa)	63	71.4	150	144.8
E_2 (GPa)	63	71.4	9	9.65
G_{12} (GPa)	24.8	26.8	7.10	7.10
ν_{12}	0.3	0.33	0.3	0.3
G_{13} (GPa)	24.2	--	7.10	7.10
G_{23} (GPa)	24.2	--	2.50	5.92
ρ (Kg/m ³)	7600	7350	1600	
d_{31} (pm/V)	254	200		

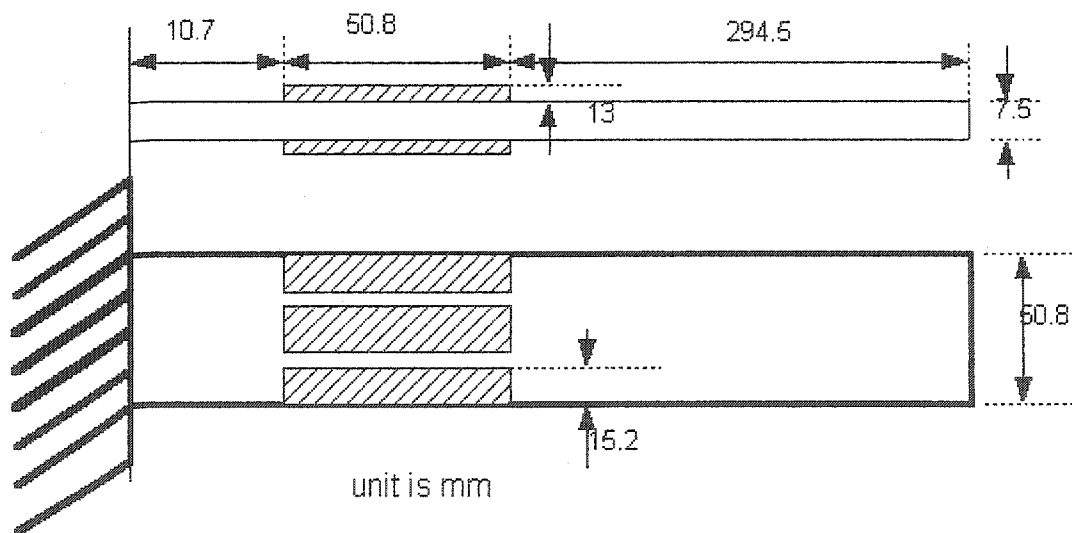


Figure 12 Laminate beam with piezoceramics

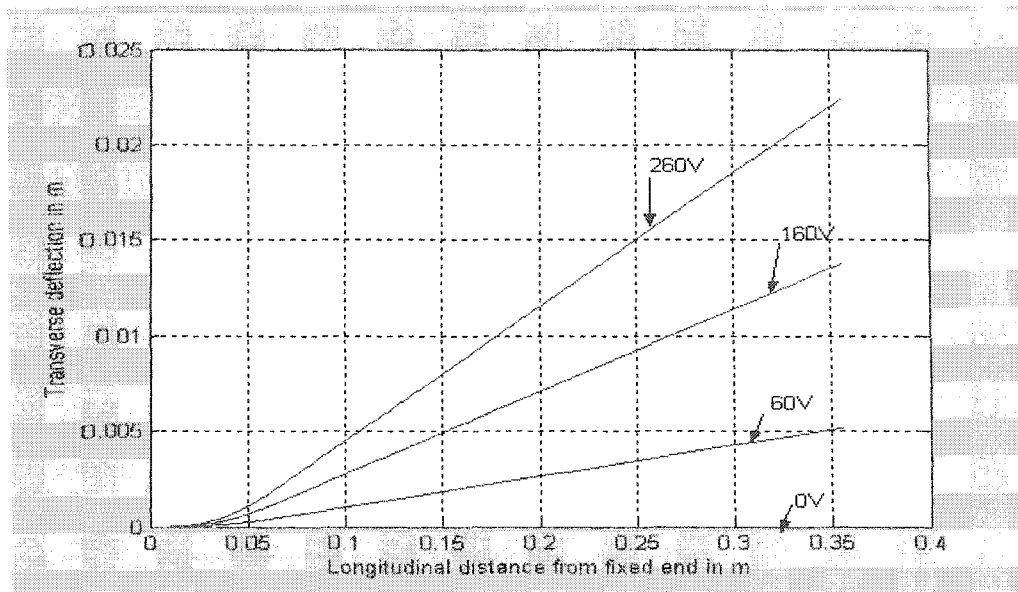


Figure 13 Effect of actuator voltage on transverse deflection

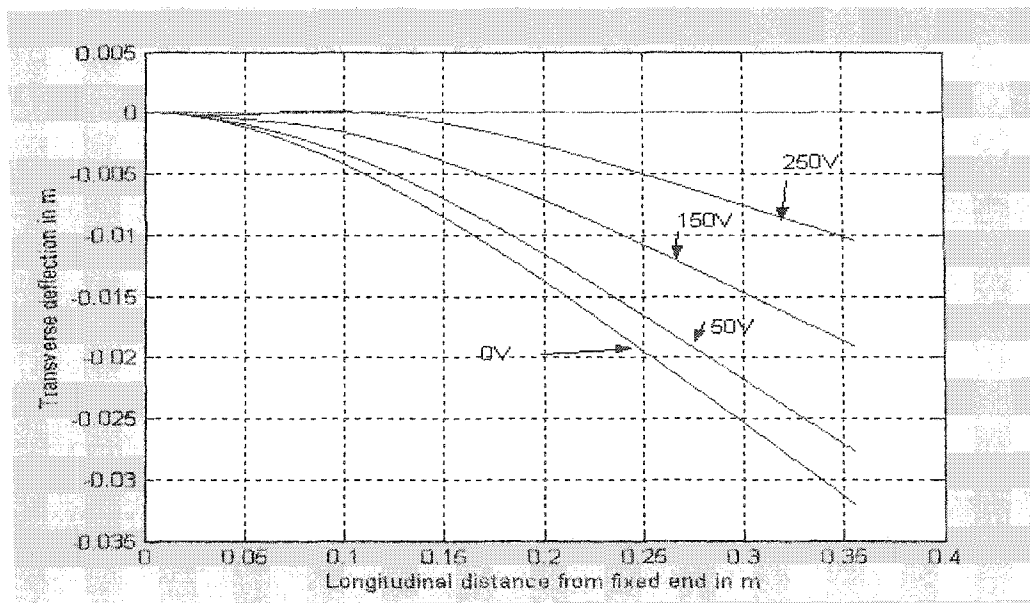


Figure 14 One pair of actuators located at the left of the beam

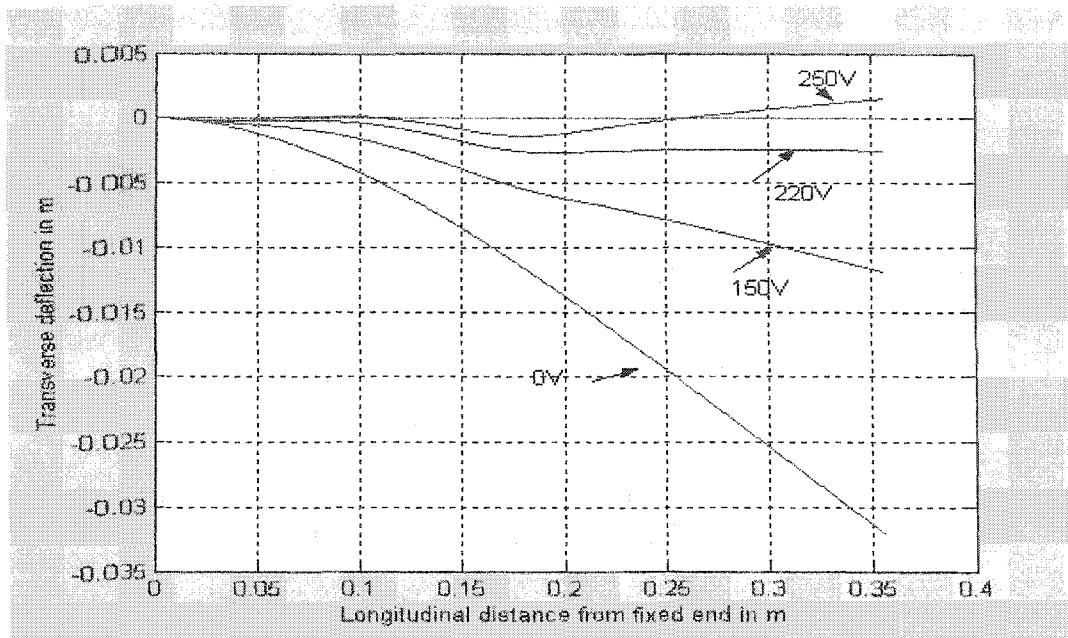


Figure 15 Two pairs of actuators located at the left and the middle of the beam

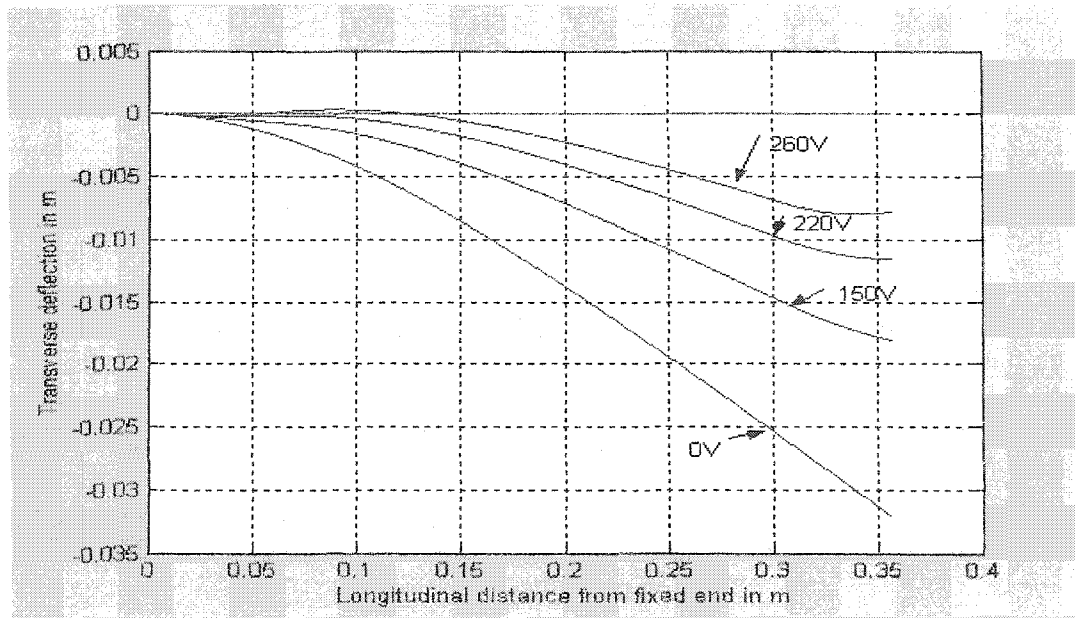


Figure 16 Two pairs of actuators: located at the left end and at the right end

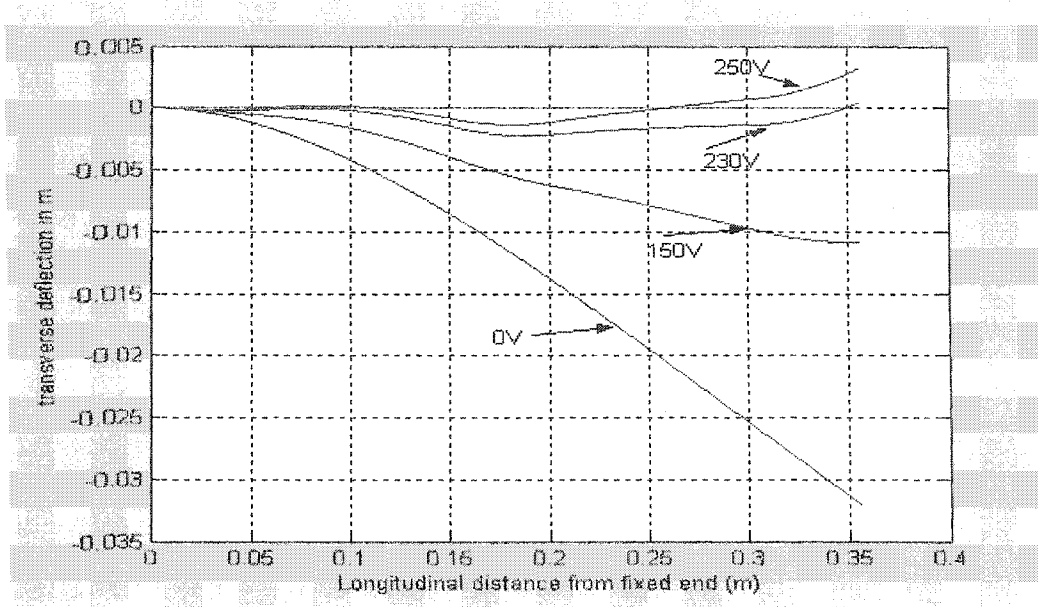


Figure 17 Three pairs of actuators located at: left end, $L/4$ and $3L/4$

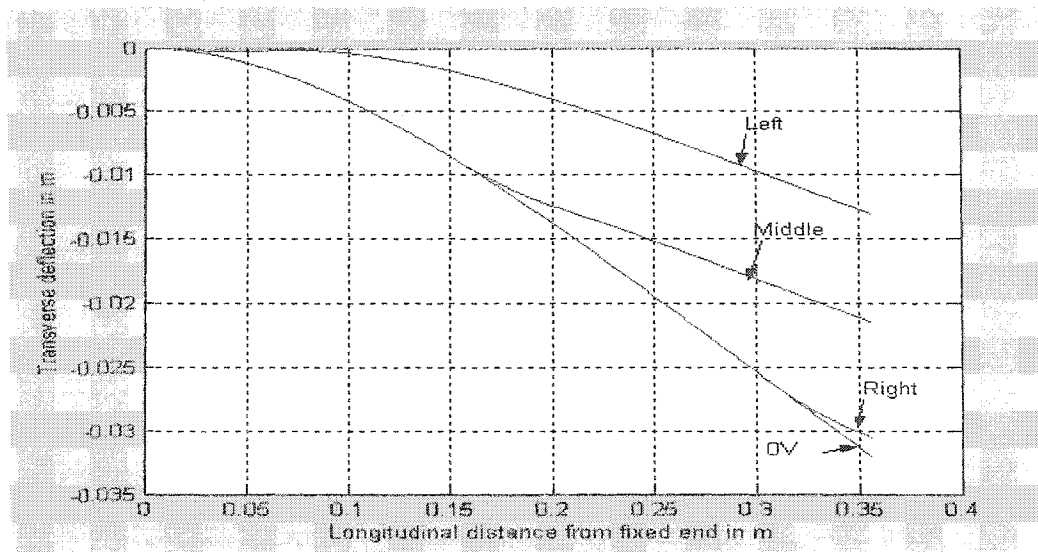


Figure 18 One pair of actuators at different positions (220V)

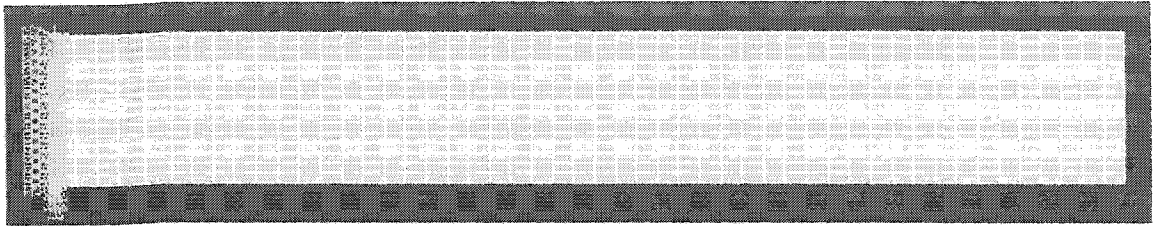


Figure 19 Finite element mesh of the laminate beam

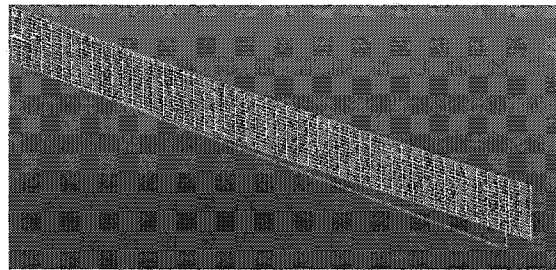


Figure 20 Mode shape 1

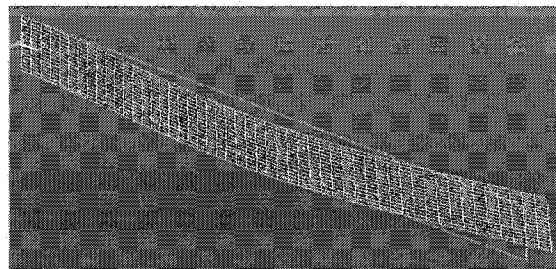


Figure 21 Mode shape 2

The natural frequencies for composite beams with no piezo elements and with bonded piezo-elements are presented in Tables X and XI, respectively. The beam is made of T300/976 graphite-epoxy composites and the piezoceramic is PZT G1195N. This example is taken from reference Sung et al. (1992). The discrepancy is 12.6% for a composite beam with bonded piezoactuators, while it is only about 1.6% for a beam without any piezoelectric. It can be observed that there is a better agreement between the numerical results and the analytical ones than between that of the experimental results and the analytical ones. The numerical results listed in Tables X and XI show that the assumed-modes method could accurately predict the natural frequencies of an integrated piezo-actuator system. Figures 20 and 21 show the first mode shape and the second mode shape of laminate beams using the finite element method.

Table X

Natural frequencies (Hz) of the beam without piezoelectric

Modes	F.E 1	Theory-2	Assumed-modes -3	%Error (1-2)	%Error (2-3)
1	7.99	8.02	8.02	0.2	0
2	49.82	50.66	50.57	1.6	0.1

Table XI

Natural frequencies (Hz) of the beam with 6 piezoelectric

Mode	F.E-0	Exper.-1	Theo.- 2	Ass.-modes -3	%Err.1 -2	%Err.1 -3	%Err.2-3
1	9.24	9.25	9.42	9.52	1.8	2.8	1.0
2	54.4	51.9	59.44	56.44	12.6	8.0	5.2

3.6 Summary

An analytical method for modeling the mechanical–electrical response of fibre-reinforced laminated composite structures containing distributed piezoceramics under static as well as dynamic mechanical or electrical loading is presented. The first order shear deformation beam theory is used for the analysis to ensure accurate bending solutions. The assumed-modes method was also presented. Experimental results obtained from reference Sung et al. (1992) using T300/976 composite and PZT G1195 piezoelectric ceramics were also conducted in order to verify the theory and the computer simulations. Finally, the effects of the number and locations of the actuators on the control system are also investigated. The investigation shows that in designing smart structures with distributed piezoelectric actuators, the number and the location of the actuators must be given careful consideration.

CHAPTER 4

MODELING OF CIRCULAR PLATE WITH PIEZOELECTRIC

In this chapter, an analytical approach for modeling of a circular plate structures containing distributed piezoelectric under static as well as dynamic mechanical or electrical loading was presented. The analytical approach used in this chapter is based on the Kirchhoff plate model. Experiments using a thin circular aluminum plate structure with distributed piezoelectric actuators were also conducted to verify the analysis and the computer simulations. This chapter also introduces a modeling approach based on the Rayleigh-Ritz assumed mode shape method to predict the behavior of a thin circular plate excited by a patch of piezoelectric material bonded to the surface of the plate. The model includes the added inertia and stiffness of the actuator and has been used to predict the natural frequencies and mode shape of the plate. Note that the finite element is very attractive; the substructuring analysis in ANSYS is used to extract eigenmodes of the system.

4.1 Introduction

Vibration suppression of space structures is very important because they are lightly damped due to the material used and the absence of air damping. Thus, the modes of the structure must be known very accurately in order to be affected by the controller while avoiding spillover. This problem increases the difficulty of predicting the behavior of the structure and consequently it might cause unexpected on-orbit behavior.

These difficulties have motivated researchers to use the actuation strain concept. One of the mechanisms included in actuation strain concept is the piezoelectric actuator effect where as the strain induced through a piezoelectric actuator is used to control the deformation of the structure. It can be envisaged that using this concept in conjunction

with control algorithms can enhance the ability to suppress modes of vibration of flexible structures.

Circular geometries are used in a wide variety of applications and are often easily manufactured, but the full three-dimensional vibration properties of these solids have not been yet investigated in detail. The knowledge of natural frequencies of components is of great interest in the study of responses of structures to various excitations and this study is fundamental for high-risk plants. Among plates of various shapes, circular plates have a particular importance, due to their axial symmetry.

The next section presents the analytical model, while the following sections address the numerical and experimental comparison of this model on a circular plate.

4.2 Plate model

The structure under consideration consists of a thin circular plate with piezoceramic patches bonded on one side. The plate is clamped around the inner boundary (radius R_1) and free at the outside edge (radius R_2) as illustrated in Figure 22. The free patches generate strains in response to an applied voltage. When the plate is bonded to an underlying structure, these strains lead to the generation of in plane forces and /or bending moments. In this chapter, we will only consider the bending moments generated by the patches and will consider them as an input to the model describing the transverse vibrations of a plate.

Moreover the circular plate is assumed to be made of linearly elastic, homogeneous and isotropic material. The dynamic extensional strain on the plate surface is calculated by considering the dynamic coupling between the actuators and the plate, and by taking into account a perfect bonding (infinite shear stiffness).

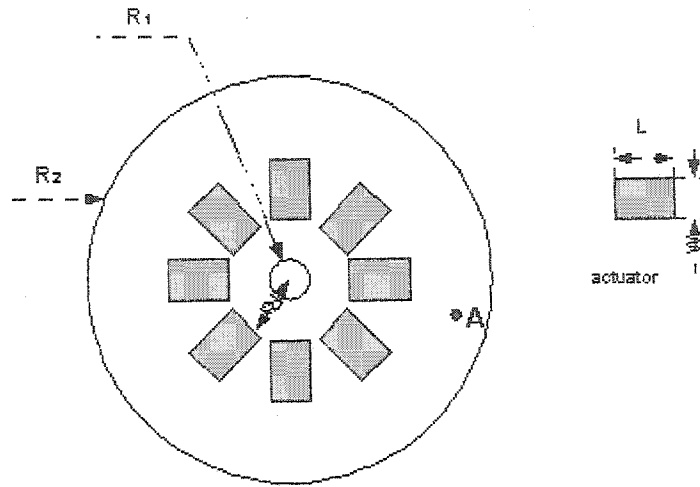


Figure 22 Circular plate with piezoelectric patches

The plate motion is described by partial differential equations relating stresses and electric displacements with strains and electric field. The ratio of the radius of the plate to its thickness is more than ten, and the Kirchhoff assumption for thin plates is applicable and the shear deformation and rotary inertia can be omitted. For wave propagation in such a structure, the displacement field is assumed as follow:

$$u_z = u_z(r, \theta, t) = w(r, \theta, t) \quad (4.1)$$

$$u_r = u_r(r, \theta, t) = -z \frac{\partial u_z}{\partial r} \quad (4.2)$$

$$u_\theta = u_\theta(r, \theta, t) = -z \frac{\partial u_z}{r \partial \theta} \quad (4.3)$$

where u_z , u_r and u_θ are the displacements in transverse z -direction, radial r -direction, and tangential θ -direction of the plate, respectively.

The poling direction of the piezoelectric material is assumed to be in the z-direction. When external an electric potential is applied across the piezoelectric layer, a differential strain is induced that results in the bending of the plate. The strain in the plate and piezoelectric with respect to the radial and tangential directions and the shear component are given by

$$\varepsilon_{rr} = \frac{\partial u_r}{\partial r} \quad (4.4)$$

$$\varepsilon_{\theta\theta} = \frac{u_r}{r} + \frac{1}{r} \frac{\partial u_\theta}{\partial \theta} \quad (4.5)$$

$$\varepsilon_{r\theta} = \frac{1}{2} \left(\frac{\partial u_\theta}{\partial r} - \frac{u_\theta}{r} + \frac{1}{r} \frac{\partial u_r}{\partial \theta} \right) \quad (4.6)$$

The constitutive equations of piezoelectric ceramic are expressed as

$$\{\sigma\} = [C_p] (\{\varepsilon\} - [d]^T \{E\}) \quad (4.7)$$

$$\{D_e\} = [e] \{\varepsilon\} + [\varepsilon^s] \{E\} \quad \{E\} = [d] \{\sigma\} + [\varepsilon^\sigma] \{E\} \quad (4.8)$$

where $\{\sigma\}$ is the stress tensor, $\{\varepsilon\}$ is the strain tensor $[C_p]$ is the elastic stiffness matrix of piezoelectric ceramic, D_e is the electric displacement, $[e]$ is piezoelectric constant, $[\varepsilon^s]$ is permittivity constant under constant strain condition, and $[\varepsilon^\sigma]$ is permittivity constant under constant stress condition. The last two equations give:

$$[e] = [d][C_p]$$

and
$$[\varepsilon^s] = [\varepsilon^\sigma] - [d][C_p][d]^T$$

for the plate

$$\{\sigma\} = [C]\{\epsilon\} \quad (4.9)$$

where $[C]$ is the elastic stiffness matrix of the plate.

In order to satisfy the assumptions, an electric field E^e is applied along the z-direction, i.e., $E_1^e = 0$, $E_2^e = 0$ and $E_3^e = E^e$, and thus the following conditions need to be satisfied: $d_{32} = d_{31}$, $d_{36} = 0$ and $d_{24} = d_{15}$ also for piezoceramic material, $e_{32} = e_{31}$ and $e_{36} = 0$.

The relationship between the electric field E^e and the applied voltage is given by

$$\{E^e\} = \{L_\phi\}\phi \quad (4.10)$$

where

$$\{L_\phi\} = \begin{Bmatrix} -\frac{\partial}{\partial x} & -\frac{\partial}{\partial y} & -\frac{\partial}{\partial z} \end{Bmatrix}$$

Hence, when a constant voltage is applied to the network along the z-direction, the electrical field generated is $\begin{Bmatrix} 0 & 0 & \frac{d\phi}{dz} \end{Bmatrix}^T$. It should be noted that, although we can only supply the electric power with constant voltage (electrode field), the piezoceramic can be coated with different types of electrode to produce spatially distributed electric fields. Thus, we may consider that the applied voltage $\phi(x, t)$ is represented as a product of two quantities of $V(t)$ and $B(x)$, in which $V(t)$ is the input voltage power and $B(x)$ defines the electrode profile. Similarly, the following relation can obtain the electric charge from electrical displacement:

$$\{Q\} = \int_S \{D_e\} dS \quad (4.11)$$

where $\{Q\}^T = [Q_1 \ Q_2 \ Q_3]$, and S denotes the surface area of the electrode.

The radial stresses in the piezolayers are assumed to be uniformly distributed in the direction perpendicular to the plate because of the plate's small thickness.

The equations of each piezoelectric layer have the following form

$$\sigma_r = \frac{E_p}{1-\nu_p^2} \left(\frac{\partial u_r}{\partial r} + \nu_p \left(\frac{u_r}{r} + \frac{1}{r} \frac{\partial u_\theta}{\partial \theta} \right) \right) - \frac{V d_{3r} E_p}{h_p (1-\nu_p)} \quad (4.12)$$

$$\sigma_\theta = \frac{E_p}{1-\nu_p^2} \left(\frac{u_r}{r} + \frac{1}{r} \frac{\partial u_\theta}{\partial \theta} + \nu_p \frac{\partial u_r}{\partial r} \right) - \frac{V d_{3\theta} E_p}{h_p (1-\nu_p)} \quad (4.13)$$

$$D_3 = d_{3r} \frac{du_r}{dr} + d_{3\theta} \frac{u_r}{r} - \epsilon_{33} \frac{V}{h_p} \quad (4.14)$$

where σ_r , σ_θ and τ are respectively, radial stress, circumferential stress and shear stress on the interface surface, d_{3r} and $d_{3\theta}$ are transverse piezoelectric constants in the radial and circumferential directions, respectively. V is the voltage acting in the direction perpendicular to plate. E_p and ν_p are the modulus and Poisson ratio of the actuator. D_3 is the electrical displacement and ϵ_{33} is a permittivity coefficient.

The constitute equations of the plate

$$\sigma_r = \frac{E}{1-\nu^2} \left(\frac{\partial u_r}{\partial r} + \nu \left(\frac{u_r}{r} + \frac{1}{r} \frac{\partial u_\theta}{\partial \theta} \right) \right) \quad (4.15)$$

$$\sigma_\theta = \frac{E}{1-\nu^2} \left(\frac{u_r}{r} + \frac{1}{r} \frac{\partial u_\theta}{\partial \theta} + \nu \frac{\partial u_r}{\partial r} \right) \quad (4.16)$$

$$\tau_{r\theta} = \frac{E}{2(1+\nu)} \left(\frac{\partial u_\theta}{\partial r} + \frac{1}{r} \frac{\partial u_r}{\partial \theta} - \frac{u_\theta}{r} \right) \quad (4.17)$$

where E and ν are the modulus and Poisson ratio of the material of the plate.

Assume that, the radial stresses in the piezolyers are uniformly distributed in the direction perpendicular to plate (small thickness).

For the radial actuator motion, the dynamics equation is expressed as follows:

$$\left(r \frac{\partial \sigma_r}{\partial r} + \sigma_r - \sigma_\theta\right) h_p - \tau r = \rho_p h_p r \frac{\partial^2 u_r}{\partial t^2} \quad (4.18)$$

$$\text{or } r\tau = \left(r \frac{\partial \sigma_r}{\partial r} + \sigma_r - \sigma_\theta\right) h_p - \rho_p h_p r \frac{\partial^2 u_r}{\partial t^2} \Rightarrow \frac{\partial}{\partial r}(r\tau) = \frac{\partial}{\partial r} \left(\left(r \frac{\partial \sigma_r}{\partial r} + \sigma_r - \sigma_\theta\right) h_p - \rho_p h_p r \frac{\partial^2 u_r}{\partial t^2} \right)$$

$$\text{Then } h \frac{\partial}{\partial r}(r\tau) = \frac{E_p h_p h^2}{2(1-\nu_p^2)} \left[r \frac{\partial^4 w}{\partial r^4} + 2 \frac{\partial^3 w}{\partial r^3} - \frac{1}{r} \frac{\partial^2 w}{\partial r^2} + \frac{1}{r^2} \frac{\partial^2 w}{\partial r^2} \right] + \frac{\rho h_p h^2}{2} \frac{\partial^3 w}{\partial r \partial t^2} + \frac{\rho h_p h^2 r}{2} \frac{\partial^4 w}{\partial r^2 \partial t^2} \quad (4.18b)$$

$$D_p = \frac{E_p h_p h^2}{2(1-\nu_p^2)} \chi_i(r, \theta)$$

The balance of the moments has the form:

$$\frac{\partial(rM_r)}{\partial r} - M_\theta - r\Gamma + hr\tau = 0 \quad (4.19)$$

Using Hook's law we express the moments by the plate transverse displacement in the following form:

$$M_r = -D \left(\frac{\partial^2 w}{\partial r^2} + \nu \frac{\partial w}{r \partial r} \right) \quad \text{and} \quad M_\theta = -D \left(\frac{\partial w}{r \partial r} + \nu \frac{\partial^2 w}{\partial r^2} \right) \quad (4.20)$$

$$D(r, \theta) = \frac{E h^3}{12(1-\nu^2)}$$

where T is the shear force, M_r and M_θ are internal plate moments and D is the plate cylindrical stiffness, h_p is the thickness of the actuator, ρ_p is the modified density of the actuator, and t is the time. Differentiating equation (4.19) with respect to r

$$r \frac{\partial^2 M_r}{\partial r^2} + 2 \frac{\partial M_r}{\partial r} - \frac{\partial M_\theta}{\partial r} - \frac{\partial(T_r)}{\partial r} + h \frac{\partial(r\tau)}{\partial r} = 0 \quad (4.21)$$

The equation of the transverse plate motion is obtained:

$$\frac{\partial(T_r)}{\partial r} = \rho h r \frac{\partial^2 w}{\partial t^2} \quad (4.22)$$

where ρ is the density for combined structures given by $\rho = \rho_1 + n\rho_p\chi_i(r, \theta)$ whole ρ_1, ρ_p and n are the density coefficient for the plate, the patches and the number of piezoelectric respectively. $\chi_i(r, \theta)$ is the characteristic function, which has a value of 1 in the region covered by the i^{th} patch and 0 elsewhere.

Taking into account a perfect bonding the plate transverse displacement is related to the radial actuator displacement by

$$u_r = -\frac{h}{2} \frac{\partial w}{\partial r} \quad (4.23)$$

Substituting equation (4.22) and (4.18b) into equation (4.21). Finally, the equation for modeling the transverse motion is obtained by:

$$\nabla^4 w + \rho \frac{h}{D_p + D} \frac{\partial^2 w}{\partial t^2} - \frac{\rho_p h_p h^2}{2(D_p + D)} \nabla^2 \left(\frac{\partial^2 w}{\partial t^2} \right) = \frac{P}{D_p + D} \quad (4.24)$$

where $\nabla^4 = \frac{1}{r} \frac{\partial}{\partial r} \left\{ r \frac{\partial}{\partial r} \left[\frac{1}{r} \frac{\partial}{\partial r} \left(r \frac{\partial}{\partial r} \right) \right] \right\}$ is biharmonic operator in the polar co-ordinates,

n is the number of actuators and P is the external surface force.

The displacement in the transverse z -direction w of the circular plate integrated piezoceramics actuators is governed by equation (4.24).

4.2.1 Modal Analysis

To obtain the natural frequencies and modes, all external mechanical and electric excitations are assumed to be zero. The first studies of equation (4.24) were those of Poisson (1829) and Kirchhoff (1850) and the classical methods of finding the solution are based on the separation of variables. In the case of axisymmetric boundary conditions, the solution takes the form

$$w(r, \theta, t) = \sum_{m=0}^{\infty} \sum_{n=0}^{\infty} g_{mn}(r) \cos(m\theta) f_{mn}(t) \quad (4.25)$$

where

$$g_{mn}(r) = A_{mn} J_m \left(\lambda_{mn} \frac{r}{R_2} \right) + B_{mn} Y_m \left(\lambda_{mn} \frac{r}{R_2} \right) + C_{mn} I_m \left(\lambda_{mn} \frac{r}{R_2} \right) + D_{mn} K_m \left(\lambda_{mn} \frac{r}{R_2} \right) \quad (4.26)$$

in which m and n are the numbers of nodal diameters and circles, $f_{mn}(t) = e^{i\omega_{mn}t}$, B_{mn} , C_{mn} and D_{mn} are the mode shape constants that are determined by the boundary conditions, J_m , Y_m are the Bessel function of the first and second kinds, I_m and K_m are the modified Bessel functions of the first and the second kind, and λ_{mn} is the frequency parameter, which is also determined by the boundary and joint conditions.

Note that, the circular plate has been subdivided into two sections, inner ring or outer ring who $\chi = 0$ and middle composite plate (patch) whom $\chi = 1$.

Substituting $w(r, t) = f(t)g(r)$ into equation (4.25) we have for each section

$$\nabla^4 g_1(r) - \lambda_1^4 g_1(r) = 0 \quad \text{for } \chi=0: R_1 \leq r \leq R_3 \text{ or } R_1 \leq r \leq R_2$$

$$\nabla^4 g_2(r) + \lambda^4 \frac{\rho_p h_p h^2}{2\rho h} \nabla^2 g_2(r) - \lambda^4 g_2(r) = 0 \quad \text{for } \chi=1: R_3 \leq r \leq R_3 + l_p$$

$$\nabla^4 g_3(r) - \lambda_1^4 g_3(r) = 0 \quad \text{for } \chi=0: R_3 + l_p \leq r \leq R_2$$

where $g_i(r)$ $i = 1, 2, 3$ is the amplitude of the z-direction displacement and ω is the natural frequency. The modal functions can be written in explicit form as:

$$\begin{aligned} g_1(r) &= C_1 J_0(\kappa r) + C_2 Y_0(\kappa r) + C_3 I_0(\kappa r) + C_4 K_0(\kappa r) \\ g_2(r) &= C_5 J_0(\alpha r) + C_6 Y_0(\alpha r) + C_7 I_0(\beta r) + C_8 K_0(\beta r) \\ g_3(r) &= C_9 J_0(\kappa r) + C_{10} Y_0(\kappa r) + C_{11} I_0(\kappa r) + C_{12} K_0(\kappa r) \end{aligned} \quad (4.27)$$

where J_0 and Y_0 are the Bessel functions of the first and second kinds, respectively, and I_0 and K_0 are modified Bessel function of the first and the second kind, respectively.

The frequency parameter, λ_{mn} , is related to the circular frequency, ω_{mn} , of the plate with piezoceramic

$$\begin{aligned} \kappa^2 &= \frac{\rho h \omega^2}{D}, \quad \alpha^2 = \frac{1}{2} \left[\sqrt{\left(\frac{\rho h^2 h_p \omega^2}{2(D + D_p)} \right)^2 + \frac{4\rho_p h_p}{D_p + D} \omega^2} + \frac{\rho_p h_p h^2}{2(D_p + D)} \omega^2 \right], \\ \beta^2 &= \frac{1}{2} \left[\sqrt{\left(\frac{\rho h^2 h_p \omega^2}{2(D + D_p)} \right)^2 + \frac{4\rho_p h_p}{D_p + D} \omega^2} - \frac{\rho_p h_p h^2}{2(D_p + D)} \omega^2 \right] \end{aligned}$$

4.2.2 Boundary and joint conditions

The plate is clamped at $r = R_1$ inner radius and free at $r = R_2$ outside radius. Then the boundary conditions are:

$$g_1(R_1) = 0, \quad \frac{dg_1}{dr}(R_1) = 0 \quad (4.28)$$

$$M_r(R_2) = 0, \quad Q_r(R_2) = 0 \quad (4.30)$$

where $Q_r = -D\left(\frac{\partial}{\partial r}(\nabla^2 w)\right)$ is the shear force.

At The joints between sections, the continuity in plate deflection, slope and radial moment have to be satisfied

$$g_1(R_1) = g_2(R_3), \quad \frac{dg_1}{dr}(R_1) = \frac{dg_2}{dr}(R_3) \quad (4.31)$$

$$g_2(R_3 + l_p) = g_3(R_3 + l_p), \quad \frac{dg_2}{dr}(R_3 + l_p) = \frac{dg_3}{dr}(R_3 + l_p) \quad (4.32)$$

$$M_{r1}(R_3) = M_{r2}(R_3) \quad \text{and} \quad M_{r2}(R_3 + l_p) = M_{r3}(R_3 + l_p) \quad (4.33)$$

Note that twelve unknown coefficients, C_i , $i = 1, 2, \dots, 12$, in equation (4.28)-(4.33) represent the amplitudes of the left and the right travelling and decaying flexural waves in each section and can be determined with the boundary and joint conditions, which can be arranged into the following matrix equation

$$[D]\{C\}=0 \quad (4.34)$$

where $[D]$ is a 12×12 matrix and $\{C\}$ are 12×1 vectors. Once again, the coefficient vector $\{C\}$ can be obtained by solving equation (4.34). Thus, the vibration field can be determined with equation (4.28)-(4.33).

4.3 Energy method

In developing the Rayleigh-Ritz model of a circular plate excited by piezoelectric bonded to the surface of the plate, a number of assumptions must be made. The piezoelectric is assumed to be perfectly bonded to the surface of the plate. The magnitude of the strains induced by the piezoelectric element is a linear function of the applied voltage.

To derive the equations of motion of the circular plate based on the Rayleigh-Ritz method, both the strain energy U and kinetic energy result T from the deformation produced by the applied strain, which is induced by exciting the piezoelectric element.

4.3.1 Strain energy

The strain energy of piezo-actuator is

$$U_p = \int_{V_p} U_{p0} dV$$

where dV shows volume differential, indices p refer to the piezoelectric actuator and

U_{p0} is piezoelectric strain energy density function given by

$$U_{p0} = \int \{\sigma\}^T d\{\varepsilon\} \quad (4.35)$$

Substitution of equation (4.13) into (4.35) leads to

$$U_p = \frac{1}{2} \int_{V_p} \{\epsilon\}^T [C_p] (\{\epsilon\} - 2[d]^T \{E\}) dV \quad (4.36)$$

The strain energy of the annular plate is given by

$$U = \frac{1}{2} \int_V \{\epsilon\}^T [C] \{\epsilon\} dV \quad (4.37)$$

4.3.2 Kinetic Energy

To obtain the kinetic energy, the velocity components in r-direction, θ -direction and z-direction are needed. The velocity components are differencing equations (4.4 to 4.6). Using these velocity components, the kinetic energies of piezoelectric actuators are obtained as

$$T_p = \frac{1}{2} \int_{V_p} \rho_p \{\dot{u}\}^T \{\dot{u}\} dV \quad (4.38)$$

For the annular plate the kinetic energy is given by:

$$T = \frac{1}{2} \int_V \rho_1 \{\dot{u}\}^T \{\dot{u}\} dV \quad (4.39)$$

where $\{u\}^T = \{u_r \quad u_\theta \quad u_z\}$ (see equations 4.1-4.3)

4.3.3 Electric energy

The electric energy generated by the actuator is

$$W_p = \int_{V_p} W_{p0} dV \quad (4.40)$$

where W_{p0} is the charged energy density function given by

$$W_{p0} = \int_{V_p} \{D_e\}^T d\{E^e\} \quad (4.41)$$

Thus, after using equation (4.8) in (4.41), we have

$$W_p = \frac{1}{2} \int_{V_p} \{E^e\}^T ([\epsilon^s] \{E^e\} + 2[e] \{\epsilon\}) dV \quad (4.42)$$

The associated variational forms of above energy functions are

$$\partial U_p = \int_{V_p} \partial\{\epsilon\}^T [C_p] (\{\epsilon\} - 2[d]^T \{E\}) dV \quad (4.43)$$

$$\partial U = \int_V C_{ij} \partial\epsilon_{ij} \epsilon_{ij} dV \quad (4.44)$$

$$\partial T_p = \int_{V_p} \rho_p \partial\{\dot{u}\}^T \{\dot{u}\} dV \quad (4.45)$$

$$\partial T = \int_V \rho \partial\{\dot{u}\}^T \{\dot{u}\} dV \quad (4.46)$$

$$\partial W_p = \int_{V_p} \partial\{E^e\}^T ([\epsilon^s] \{E^e\} + 2[e] \{\epsilon\}) dV \quad (4.47)$$

4.4 Lagrange's equation

The total Lagrangian functional L is

$$L = \int_V L_0(r, \theta, t) dV \quad (4.48)$$

and the Lagrangian density L_0 is defined as

$$L_0(r, t) = T_0(r, t) - U_0(r, t) + W_0(r, t) \quad (4.49)$$

where $U_0(r, t) = U + U_p$ = flexural energy density

$T_0(r, t) = T + T_p$ = kinetic energy density

$W_0(r, t) = W + W_p$ = work done by external load and electrical power

4.4.1 Equation of Motion

The static or dynamic response of the plate excited by the piezoelectric actuator can be calculated by substituting the strain and kinetic energy into Lagrange's equation

$$\frac{d}{dt} \left(\frac{\partial T_0}{\partial \dot{q}_i} \right) - \frac{\partial T_0}{\partial q_i} + \frac{\partial U_0}{\partial q_i} = Q_i \quad (4.50)$$

where q_i represents the generalized coordinate and Q_i is the i^{th} generalized force. As there are no external forces (the force applied by the piezoelectric element is included as an applied strain) or gyroscopic terms and there is no added damping, Lagrange's equation reduces to:

$$\frac{d}{dt} \left(\frac{\partial T_0}{\partial \dot{q}_i} \right) + \frac{\partial U_0}{\partial q_i} = 0 \quad (4.51)$$

Now the equation of motion can be obtained by using the expression obtained for the strain and kinetic energy, and the assumed shape functions for flexural motion

$$w(r, \theta, t) = \sum_{i=1}^n \phi_i(r, \theta) q_i(t) \quad (4.52)$$

where ϕ_i is the assumed displacement. Using the shape functions expressed T_0 and U_0 , the equation of motion of the plate in the form is

$$[M] \{\ddot{q}\} + [K] \{q\} = [B_v] \{V\} \quad (4.53)$$

where $[M]$ and $[K]$ are the mass, and stiffness matrices and $[B_v]$ is the voltage-to-force transformation vector. Vector q represents the plate response modal amplitudes and V is the applied voltage.

$[M]$, $[K]$ and $[B_v]$ will be determined by the assumed mode method for vibration control of smart structures.

4.5 Model for vibration control

4.5.1 Assumed-modes method

The assumed-modes method consists of assuming a solution of the free vibration problem in the form of a series composed of a linear combination of admissible functions ϕ_i , which are functions of spatial coordinates, multiplied by time-dependent generalized coordinates $q_i(t)$. These admissible functions satisfy the natural boundary condition.

In developing the Assumed-Modes Methods of the annular plate Figure 23 excited by a patch of piezoelectric material bonded to the surface of the plate, a number of assumptions must be made. The patch of piezoelectric material is assumed to be perfectly bonded to the surface on the plate.

Assume that, the admissible functions for annular plate are given by these equations

$$\phi_i(r, \theta) = \frac{r - R_1}{R_2 - R_1} \cos(i\theta), i = 0, 1, 2, \dots \quad (4.54)$$

$$\phi_j(r, \theta) = \frac{r - R_1}{R_2 - R_1} \cos(j\theta), j = 0, 1, 2, \dots \quad (4.55)$$

These functions verified the geometry boundary conditions: at $r = R_1$, $\phi_i(r, \theta) = 0$.

4.5.2 Plate

For an annular plate alone the strain energy is given by

$$U = \frac{D}{2} \int_0^{2\pi} \int_{R_1}^{R_2} \left(\left(\frac{\partial^2 w}{\partial r^2} + \frac{1}{r} \frac{\partial w}{\partial r} + \frac{1}{r^2} \frac{\partial^2 w}{\partial \theta^2} \right)^2 - 2(1-\nu) \left(\frac{\partial^2 w}{\partial r^2} \left(\frac{1}{r} \frac{\partial w}{\partial r} + \frac{1}{r^2} \frac{\partial^2 w}{\partial \theta^2} \right) + 2(1-\nu) \left(\frac{\partial}{\partial r} \left(\frac{1}{r} \frac{\partial w}{\partial \theta} \right) \right) \left(\frac{\partial}{\partial r} \left(\frac{1}{r} \frac{\partial w}{\partial \theta} \right) \right) \right) r dr d\theta \quad (4.56)$$

Substituting equation (4.52) into (4.56) than the stiffness matrix is given by:

$$K_{ij} = D \int_0^{2\pi} \int_{R_1}^{R_2} \left(\left(\frac{\partial^2 \phi_i}{\partial r^2} + \frac{1}{r} \frac{\partial \phi_i}{\partial r} + \frac{1}{r^2} \frac{\partial^2 \phi_i}{\partial \theta^2} \right) \left(\frac{\partial^2 \phi_j}{\partial r^2} + \frac{1}{r} \frac{\partial \phi_j}{\partial r} + \frac{1}{r^2} \frac{\partial^2 \phi_j}{\partial \theta^2} \right) - (1-\nu) \left(\frac{\partial^2 \phi_i}{\partial r^2} \left(\frac{1}{r} \frac{\partial \phi_j}{\partial r} + \frac{1}{r^2} \frac{\partial^2 \phi_j}{\partial \theta^2} \right) + \frac{\partial^2 \phi_j}{\partial r^2} \left(\frac{1}{r} \frac{\partial \phi_i}{\partial r} + \frac{1}{r^2} \frac{\partial^2 \phi_i}{\partial \theta^2} \right) \right) + 2(1-\nu) \left(\frac{\partial}{\partial r} \left(\frac{1}{r} \frac{\partial \phi_i}{\partial \theta} \right) \right) \left(\frac{\partial}{\partial r} \left(\frac{1}{r} \frac{\partial \phi_j}{\partial \theta} \right) \right) \right) r dr d\theta \quad (4.57)$$

The mass matrix is

$$M_{ij} = \rho \int_0^{2\pi} \int_{\frac{h}{2}}^{\frac{h}{2}} \int_{R_1}^{R_2} \left(\phi_i \phi_j + z^2 \frac{\partial \phi_i}{\partial r} \frac{\partial \phi_j}{\partial r} + \frac{z^2}{r^2} \frac{\partial \phi_i}{\partial \theta} \frac{\partial \phi_j}{\partial \theta} \right) r dr d\theta dz \quad (4.58)$$

4.3.3 Actuator

For the actuator, the shape of the piezoelectric sheet actuators used for controlling the annular plate is defined in Figure 23 or 24. For this analysis, rectangular piezoelectric actuator are desired due to the cost and availability of rectangular piezoelectric ceramics, but modeling difficulties prevented the piezoelectric to be modeled as purely rectangular. In the Figure, the sides of the actuator with length l are modeled as straight edges while the edges with length l have radius R_3 and R_3+l . Since the width L of the piezoelectric is small in comparison to the radius and size of the annular plate, the actuator shape is considered to be a reasonable approximation of a rectangular patch.

As shown, attaching the piezoelectric patches on a circular plate requires that the θ coordinate of the length l is functions of the radial position as expressed in equation:

$$\theta_1(r) = \theta_i - \text{Arcsin} \frac{L}{2r} \quad (4.59)$$

$$\theta_2(r) = \theta_i + \text{Arcsin} \frac{L}{2r} \quad (4.60)$$

For the each actuator the stiffness matrix is given by:

$$\begin{aligned} K_{ij}^p = & D_p \int_{\theta_1(r)}^{\theta_2(r)} \int_{R_3}^{R_3+l} \left(\left(\frac{\partial^2 \phi_i}{\partial r^2} + \frac{1}{r} \frac{\partial \phi_i}{\partial r} + \frac{1}{r^2} \frac{\partial^2 \phi_i}{\partial \theta^2} \right) \left(\frac{\partial^2 \phi_j}{\partial r^2} + \frac{1}{r} \frac{\partial \phi_j}{\partial r} + \frac{1}{r^2} \frac{\partial^2 \phi_j}{\partial \theta^2} \right) \right. \\ & - (1 - \nu_p) \left(\frac{\partial^2 \phi_i}{\partial r^2} \left(\frac{1}{r} \frac{\partial \phi_j}{\partial r} + \frac{1}{r^2} \frac{\partial^2 \phi_j}{\partial \theta^2} \right) + \frac{\partial^2 \phi_j}{\partial r^2} \left(\frac{1}{r} \frac{\partial \phi_i}{\partial r} + \frac{1}{r^2} \frac{\partial^2 \phi_i}{\partial \theta^2} \right) \right) + \\ & \left. 2(1 - \nu_p) \left(\frac{\partial}{\partial r} \left(\frac{1}{r} \frac{\partial \phi_i}{\partial \theta} \right) \right) \left(\frac{\partial}{\partial r} \left(\frac{1}{r} \frac{\partial \phi_j}{\partial \theta} \right) \right) \right) r dr d\theta \end{aligned} \quad (4.61)$$

$$M_{ij}^p = \rho_p \int_{\theta_1(r)}^{\theta_2(r)} \int_{\frac{h}{2}}^{\frac{h}{2}+h_p} \int_{R_3}^{R_3+l} \left(\phi_i \phi_j + z^2 \frac{\partial \phi_i}{\partial r} \frac{\partial \phi_j}{\partial r} + \frac{z^2}{r^2} \frac{\partial \phi_i}{\partial \theta} \frac{\partial \phi_j}{\partial \theta} \right) r dr d\theta dz \quad (4.62)$$

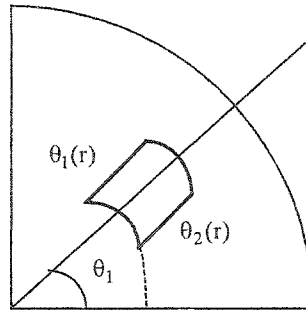


Figure 23 Geometry of piezoelectric sheet actuator

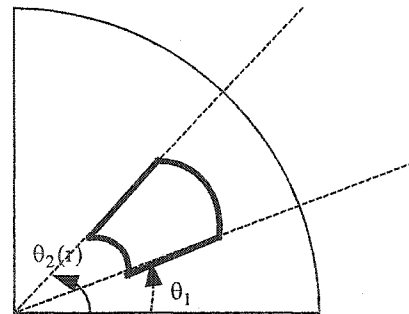


Figure 24 Geometry of piezoelectric sheet actuator

The input matrix is given by

$$B_v = \int_{V_p} [B_1]^T [D]^T [G] dv \quad (4.63)$$

where $B_1 = L\phi(r, \theta)$

$$\{L\} = \left\{ -z \frac{\partial^2}{\partial r^2} - \frac{z}{r} \frac{\partial}{\partial r} - \frac{z}{r^2} \frac{\partial^2}{\partial \theta^2} - \frac{z}{r} \frac{\partial^2}{\partial \theta \partial r} + \frac{z}{r^2} \frac{\partial}{\partial \theta} \right\}^T = \{L_1 \quad L_2 \quad L_3\}$$

and for 5 frequencies

$$\phi(r, \theta) = [\phi_1 \quad \phi_2 \quad \phi_3 \quad \phi_4 \quad \phi_5]$$

then

$$[B_1] = \begin{bmatrix} L_1 \phi_1 & L_1 \phi_2 & L_1 \phi_3 & L_1 \phi_4 & L_1 \phi_5 \\ L_2 \phi_1 & L_2 \phi_2 & L_2 \phi_3 & L_2 \phi_4 & L_2 \phi_5 \\ L_3 \phi_1 & L_3 \phi_2 & L_3 \phi_3 & L_3 \phi_4 & L_3 \phi_5 \end{bmatrix}$$

note that here $z = h/2$

For 4 actuators

$$[G] = \begin{bmatrix} 0 & 0 & 0 & 0 \\ 0 & 0 & 0 & 0 \\ \frac{1}{h_1} & \frac{1}{h_2} & \frac{1}{h_3} & \frac{1}{h_4} \end{bmatrix}$$

In our case the piezoceramic has the same thickness than $h_1 = h_2 = h_3 = h_4 = h$.

The matrix of piezoelectric $[d]$ constant has the form (2D)

$$[d] = \begin{bmatrix} 0 & 0 & 0 \\ 0 & 0 & 0 \\ d_{13} & d_{13} & 0 \end{bmatrix}$$

The stiffness matrix under constant electric field condition is

$$[C_p] = \frac{E_p}{1-\nu_p^2} \begin{bmatrix} 1 & \nu_p & 0 \\ \nu_p & 1 & 0 \\ 0 & 0 & \frac{1-\nu_p}{2} \end{bmatrix}$$

than $[D_p]^T = [C_p][d]^T$

Not that, the accuracy of the assumed mode method depends on the shape functions of the structures, but the finite element method is very attractive to extract the mass and stiffness matrices and vector load.

4.5.4 Mass, stiffness and load vector extraction

To obtain the modeling matrices M , K and B_v , we recall that the eigenfunctions are orthogonal with respect to the mass and stiffness matrices. Furthermore, if the eigenfunctions are normalized with respect to the mass matrix, then we have the following orthogonality conditions with respect to the mass and stiffness matrices, respectively.

$$\phi^T M \phi = I \quad (4.64)$$

$$\phi^T K \phi = \omega_n^2 \quad (4.65)$$

where ϕ_i is the modal matrix whose columns is the eigenfunctions for the n modes and ω_n^2 is a diagonal matrix of the eigenvalues. Hence, the system matrices M and K can be found by manipulating equations 4.64 and 4.65. In this work, the eigenfunction obtained from the finite element package ANSYS compute the mass and stiffness matrices and vector load. They are two ways in ANSYS to extract these matrices; first one gives only the information defining the mass and stiffness matrices. This information is defined in the file *jobname.full* created by ANSYS after performing a modal analysis. This file

contains the information in binary format that needs to be converted and extracted from the file. This procedure is described in the Guide to Interfacing with ANSYS. In our case, the mass and stiffness matrices and the load vector were extracted after performing the substructuring analysis.

4.6 Experimentation

An experimental investigation was carried out in order to verify the applicability of the analytical approach discussed in this chapter. The experimental system consists of a thin circular aluminum plate with bonded eight piezoceramic actuators as shown in Figure 25. A non-contact laser displacement sensor, Keyence LB-72, was used to measure the displacement at point A. A data acquisition board and a personal computer acquired the output data from the laser sensor. A function generator was used to provide a signal to an amplifier, KEPCO BOP 1000M, which supplied voltage to the piezoelectric actuators. As explained previously, the natural frequencies and mode shapes of a circular plate bonded with piezoelectric elements can be predicted analytically and numerically (FEA). Experimental modal, static and harmonic analysis have been conducted to verify the analytical and numerical approaches.

The properties and the physical dimension of plate and piezoactuators are given in Table XII. For a circular plate of this size, experimental results provide a basis for comparison between measured experimental, analytic and simulation natural frequencies.

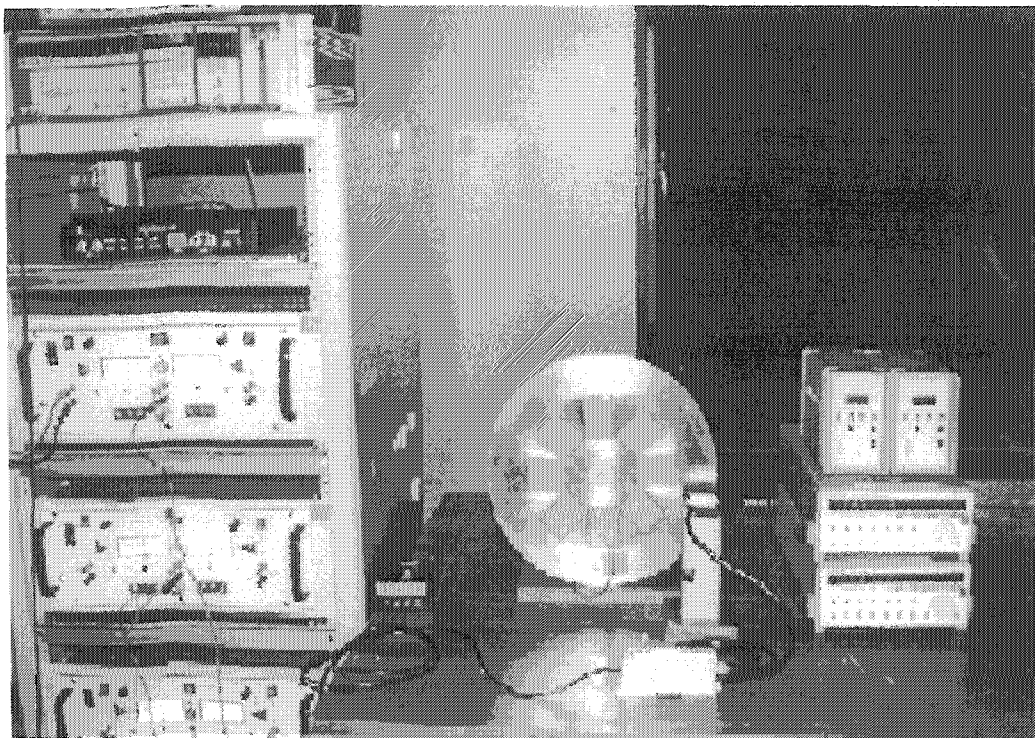


Figure 25 Experimental set up

Table XII

Dimension and material properties of plate and piezoelectric

Aluminum 3003-H14	PZT (BM532)	Units
$\rho = 2730$	$\rho = 7350$	Kg/m^3
$E = 69 \cdot 10^9$	$E_p = 71.4 \cdot 10^9$	Pa
$\nu = 0.33$	$\nu = 0.3$	
$R_1 = 0.019, R_2 = 0.17, R_3 = 0.056$	$L = 0.0508, W = 0.03683$	m
$h = 0.0008$	$h_p = 0.00025$	m
	$d_{31} = 200 \cdot 10^{-12}$	V/m

4.7 Results and comparisons

In order to verify the proposed analysis and the finite element approach, numerical calculations were generated to compare with the experimental results from the circular plate with distributed eight piezoceramics bonded on the surface of the plate. The schematic of this plate is shown in Figure 22 while the dimensions and the material properties are given in Table XII.

The piezoelectric actuator patches were modeled using solid5 piezoelectric elements and the aluminum circular plate by shell63 structural elements of a commercial finite element code (ANSYS).

The static response of the structure was determined by applying a constant voltage to the five piezoelectric actuators. The deflections of the circular plate at the point A (node 988) were recorded by the non-contact laser displacement sensors. Figure 27 shows the comparison of the deflection of a circular plate between the finite element and the experimental results. Good agreements between the two methods are observed.

The natural frequencies and modes shapes can be predicted by equation 4.24. Experimental modal analysis has been conducted to verify the analytical and finite element prediction. The first five natural frequencies as obtained by analytical prediction, finite element and experimental modal testing are shown in Table XIII and Figure 27. The circular plate model analytically predicts 25.5Hz and 26.6Hz for the first bending mode and first torsional mode; and these validate by the modal testing results of 24.9 and 26.5Hz. The discrepancy is within 2.3 %. The experimental data listed in Table XIII and Figure 27 shows that the circular plate model can accurately predict the frequencies of an integrated piezoelectric actuators system, and that the prediction is validated by experiments.

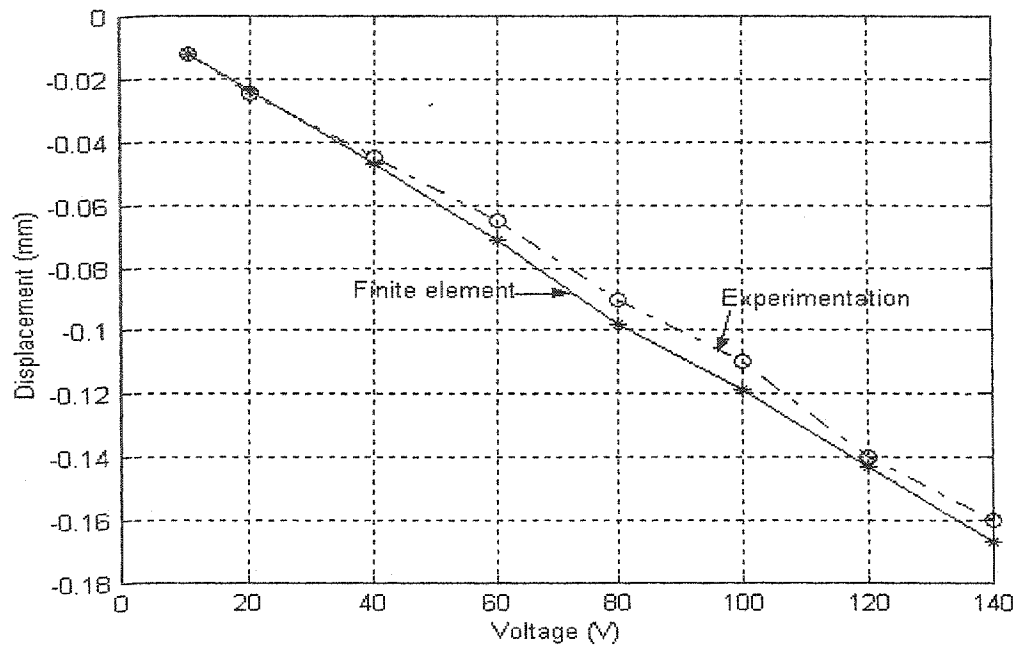


Figure 26 Tip deflection on the circular plate in terms of the input voltage

Table XIII

Natural frequencies for circular plate with eight actuators

Mode number	Analytical	FEA	Experimental	Δ_{FEA} (%)	Δ_{Exp} (%)
1	25.0	24.4	24.9	2.2	0.1
2	25.0	24.4	24.9	2.2	0.1
3	26.6	29.2	26.5	9.7	0.3
4	33.6	37.7	33.5	10	0.2
5	33.6	37.7	33.5	10	0.2

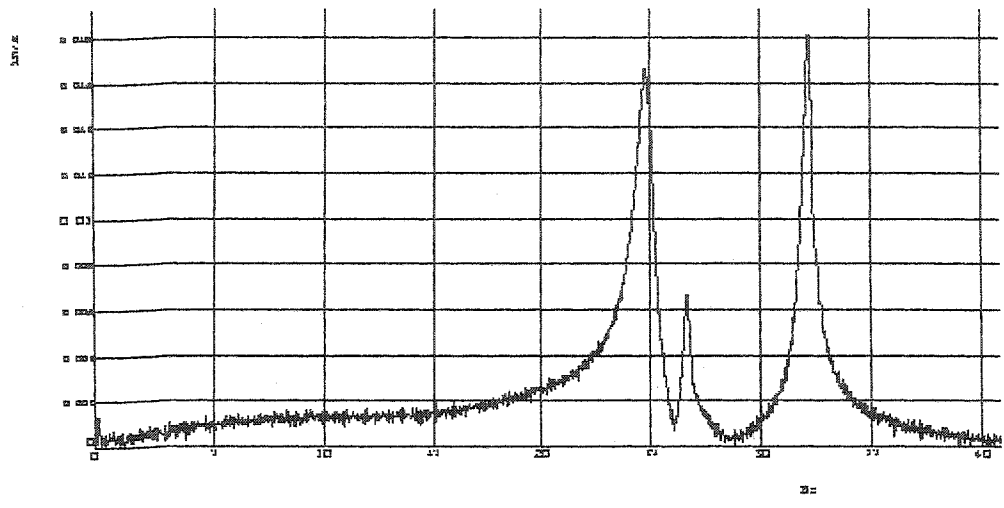


Figure 27 Experimental modal analysis

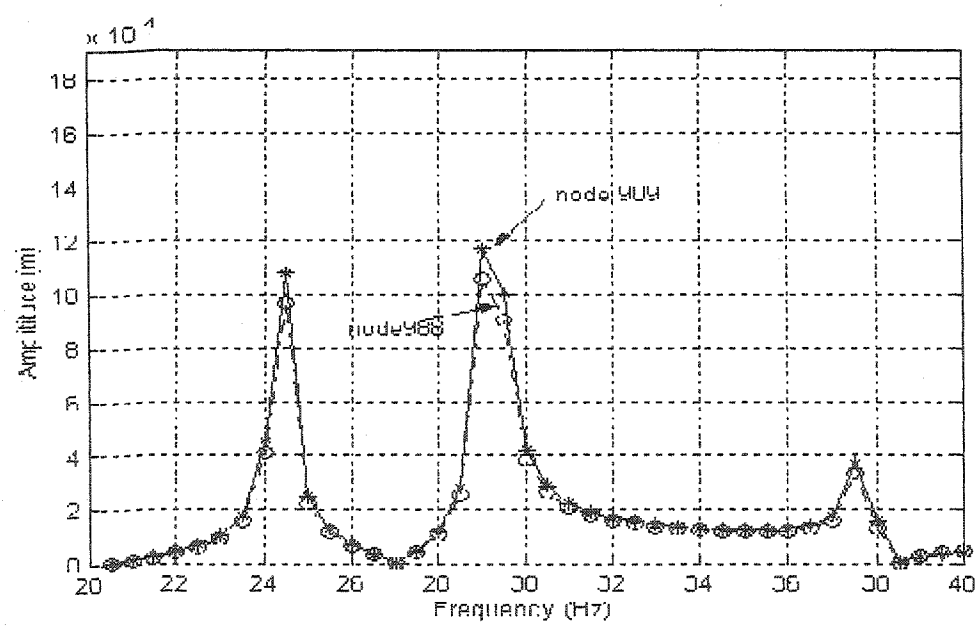


Figure 28 Response of the modal displacement at nodes 988 and 909

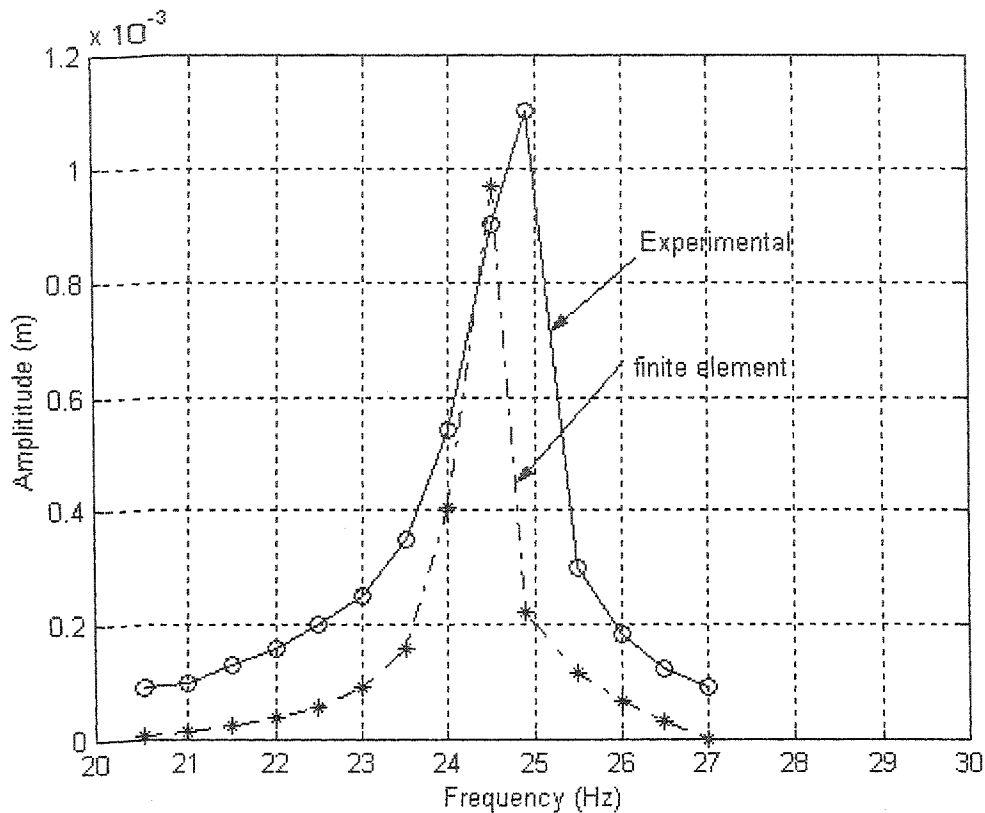


Figure 29 Frequency of the nodal displacement at point A

Finally, the frequency response of the structure with eight actuators subjected to dynamic piezoelectric actuation was also obtained. The frequency response of the nodal displacement at the point A (node988) and the free end of circular plate (node 909) is shown in Figure 28. The responses at the two nodal locations appear to have the same frequency response profile but differ in magnitude. The results obtained using the finite element method and experimental result are shown in Figure 29. Comparable results were obtained. On the other hand, this discrepancy can be attributed to amplifier characteristics and the presence of environmental noise, which was verified by observing the poor coherence between the applied voltage signal and the acceleration signal measured during the experiments.

4.7.1 Obtaining matrices using assume mode model

The objectives of this section are to evaluate the analytical and assume mode models for annular plate with surface-mounted piezoceramic patch clumped in inner radius, examine the numerical results obtained with commercial finite element code ANSYS, and compare the performance of these two approaches with finite element method. The geometrical and material properties are given in Table XIV.

Table XIV

Material properties of plate structure (2) and piezoelectric

Aluminium 3003-H14	PZT (BM532)	Units
$\rho = 2730$	$\rho = 7350$	Kg/m^3
$E = 69 \cdot 10^9$	$E_p = 71.4 \cdot 10^9$	Pa
$\nu = 0.33$	$\nu = 0.3$	
$R_1 = 0.04, R_2 = 0.17, R_3 = 0.065$	$L = 0.048, W = 0.038$	m
$h = 0.000508$	$h_p = 0.0003$	m
	$d_{31} = 200 \cdot 10^{-12}$	V/m

Modal analysis was performed for the structure using the Block Lanczos method. Table XV and XVI presents the first five natural frequencies for annular plate without any piezoelements and with bonded piezoceramics actuators. The discrepancy is within 10 % for annular plate with bonded piezoceramics actuators, while it is only about 1.6 % for annular plate without any piezoelements. Figure 30 – 34 shows the first lowest modes shape of the plate with piezoceramic.

Finally, the frequency response of the structure with 8 actuators subject to dynamic piezoelectric actuation in one side was also obtained. Electrical loading was applied in side of the plate as $V1 = 0$ and $V2 = 140$ volt in the other faces for each eight actuators. The frequency response of the nodal displacement at the free end of the annular plate and the center of the piezoelectric patch is shown in Figure 35. The responses at the two nodal locations appear to have the same frequency response profile but differ in magnitude.

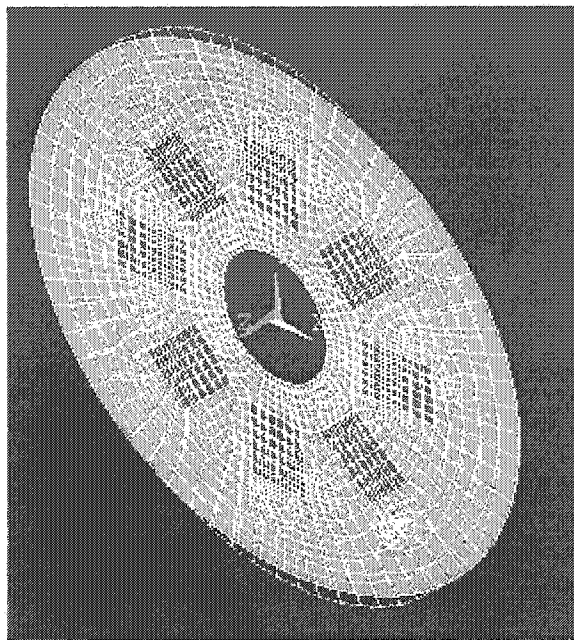


Figure 30 Mode 1

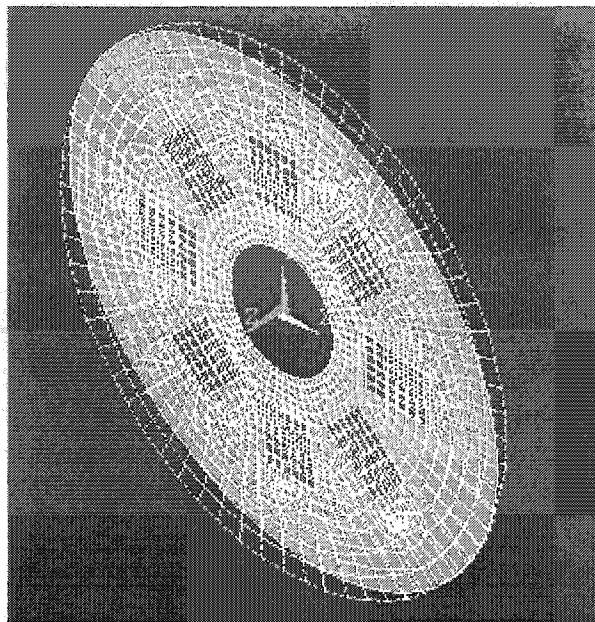


Figure 31 Mode 2

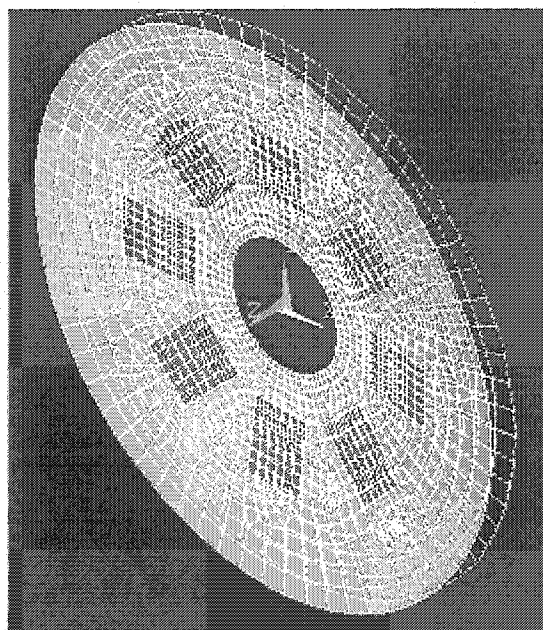


Figure 32 Mode 3

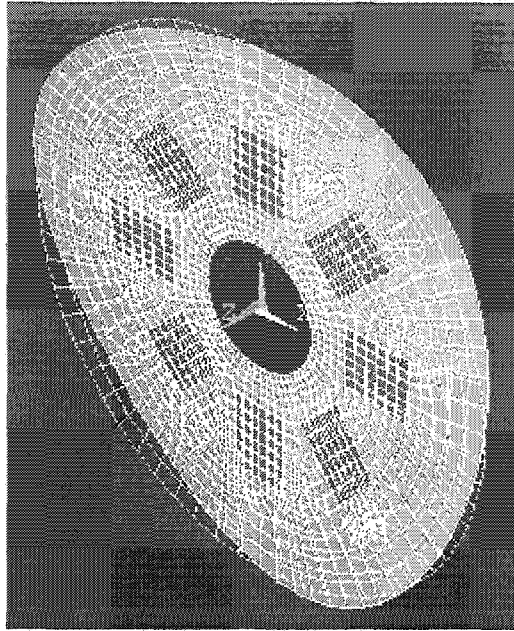


Figure 33 Mode 4

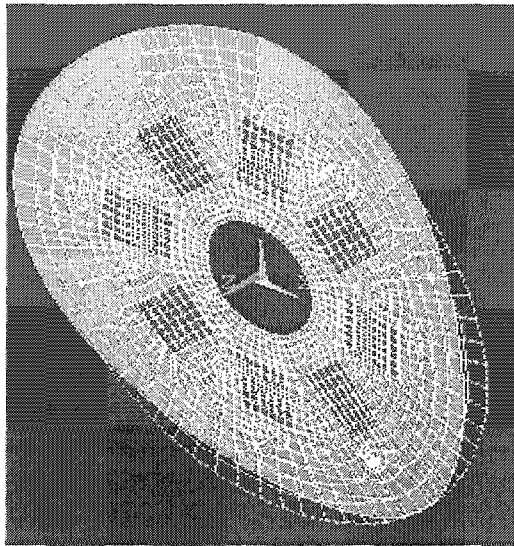


Figure 34 Mode 5

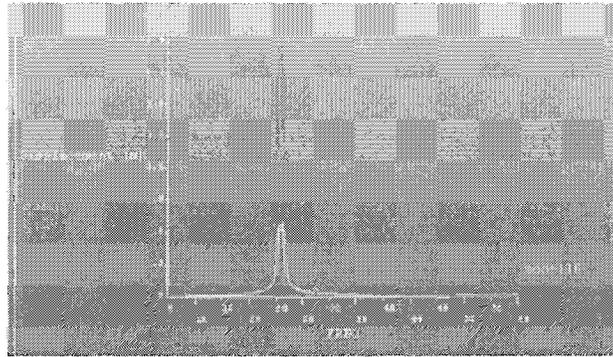


Figure 35 Frequency response at the free end and the centre of the actuator

Table XV

Natural frequencies (Hz) of the plate with 8 piezoelectric

Modes	Theory	FEA	Error %
1	26.1	23.79	8.1
2	26.1	23.79	8.1
3	27.7	24.91	7.7
4	34	30.84	10
5	34	30.86	10

Now, the assume-mode method is used to calculate the mass, stiffness, and input matrices for vibration control of the annular plate with 8 piezoceramic and calculate the natural frequencies. The result shows a good agreement between finite element and this method Table XVI and XVII. The Maple software was used to calculate thesis matrices.

Table XVI

Natural frequencies ω for annular plate without actuators

Modes	Assume-mode	FEA	Error %
1	152.39	150.41	1.3
2	152.39	150.41	1.3
3	183.8	178.54	2.86
4	331.77	228.58	31.10
5	331.77	228.58	31.10

Table XVII

Natural frequencies ω for annular plate with actuators

Modes	Assume-mode	FEA	Error %
1	165.13	152.37	7.7
2	165.13	152.37	7.7
3	200.53	182.84	8.8
4	353.21	236.76	32.9
5	353.21	236.76	32.9

vibration. A substructure analysis can be condensing a group of regular finite elements into a single super element by using the generation pass. The condensation is done by identifying a set of master degrees of freedom, which are mainly used to define the interface between the super element and other elements and capture dynamic characteristics for dynamic analyzes. The size of the matrices is defined by the number of master nodes multiplied by the degree of freedom associated to each master node. In our study, height master nodes associated with one degree of freedom each (u_z) were selected. The mass and stiffness matrices are 8 X 8 and the load vector is 8 X 1. The location of these master nodes was taken in the center of each actuator Figure 36. These locations were chosen after several finite element computation .The modal analysis was done by performing the Block Lanczos and Reduced mode extraction method. The natural frequencies were compared for these two methods Table XVIII. Note that, Block Lanczos method is independent of the master nodes but Reduced mode extraction method depends on master nodes. The schematic of this plate is shown in Figure 22 while the dimensions and the material properties are given in Table XIV.

We applied the method described below, and we did static and substructure analysis applying different voltage loads to the piezoceramic actuators according to the matrix V. The i th column of matrix V is the voltage applied to 8 piezoceramic actuators for the i^{th} time. The i^{th} column of the matrix F is the i^{th} vector load.

The stiffness matrix K is given by

$$[K] = \begin{bmatrix} 6814.5951 & -4322.1307 & 2510.0879 & -459.13263 & 163.00 & -657.27072 & 2914.3463 & -4891.8933 \\ -4322.1307 & 6802.0513 & -5395.1334 & 2186.0492 & -652.73766 & 272.26689 & -654.48444 & 226.70033 \\ 2510.0 & -5395.1334 & 8704.6277 & -4675.1893 & 2637.1262 & -765.38972 & 309.66975 & -733.45816 \\ -459.13263 & 2186.0492 & -4675.1893 & 6182.0674 & -4759.372 & 2729.1376 & -649.17194 & 176.88525 \\ 163.00924 & -652.73766 & 2637.1262 & -4759.3721 & 8407.4499 & -6503.2263 & 3138.7566 & -531.08816 \\ -657.27072 & 272.26689 & -765.38972 & 2729.1376 & -6503.2263 & 11408.712 & -7665.3349 & 2847.1881 \\ 2914.3463 & -654.48444 & 309.66975 & -649.17194 & 3138.7566 & -7665.3349 & 11600.324 & -6102.8671 \\ -4891.8933 & 2267.0033 & -733.45816 & 176.88525 & -531.08816 & 2847.1881 & -6102.8671 & 7286.1081 \end{bmatrix}$$

Table XVIII

Natural frequencies (Hz) for circular plate with actuators

Modes	Reduced (8 master nodes)	Bolck Lanczos	Error %
1	25.5	24.4	4
2	25.5	24.4	4
3	30.9	29.2	5
4	40.1	37.7	5
5	40.1	37.7	5

The mass matrix M is given by

$$[M] = \begin{bmatrix} 0.03396 & 0.00529 & -0.00543 & 0.00072 & 0.00000 & 0.00069 & -0.00667 & 0.00115 \\ 0.00529 & 0.03450 & 0.00248 & -0.00286 & 0.00129 & -0.00042 & 0.00180 & -0.00386 \\ -0.00543 & 0.00248 & 0.03876 & 0.00596 & -0.00704 & 0.00229 & -0.00075 & 0.00169 \\ 0.00072 & -0.00286 & 0.00596 & 0.03621 & 0.00301 & -0.00563 & 0.00074 & -0.00006 \\ 0.00000 & 0.00129 & -0.00704 & 0.00301 & 0.04180 & 0.00707 & -0.00579 & -0.00008 \\ 0.00069 & -0.00042 & 0.00229 & -0.00563 & 0.00707 & 0.04659 & 0.01012 & -0.00415 \\ -0.00667 & 0.001805 & -0.00075 & 0.00074 & -0.00579 & 0.01012 & 0.04367 & 0.0065 \\ 0.00115 & -0.00386 & 0.00169 & -0.00006 & -0.000083 & -0.00415 & 0.00659 & 0.03477 \end{bmatrix}$$

$$[V] = \begin{bmatrix} 200 & 0 & 0 & 0 & 0 & 0 & 0 & 150 \\ 200 & 200 & 0 & 0 & 0 & 0 & 0 & 150 \\ 0 & 200 & 200 & 0 & 0 & 0 & 0 & 150 \\ 0 & 0 & 200 & 200 & 0 & 0 & 0 & 150 \\ 0 & 0 & 0 & 200 & 200 & 0 & 0 & 150 \\ 0 & 0 & 0 & 0 & 200 & 200 & 0 & 150 \\ 0 & 0 & 0 & 0 & 0 & 200 & 200 & 150 \\ 0 & 0 & 0 & 0 & 0 & 0 & 200 & 200 \end{bmatrix}$$

and

$$[F_z] = \begin{bmatrix} 0.00415 & -0.0979 & 0.07090 & 0.001450 & -0.01152 & 0.0955 & -0.06813 & -0.04788 \\ -0.0307 & -0.1227840 & -0.2556716 & 0.00539 & -0.010647 & -0.01803 & 0.01077 & -0.2061085 \\ -0.1466434 & 0.1395746 & 0.1658368 & -0.1040485 & 0.048945 & -0.01066 & -0.003642 & 0.04561 \\ 0.01766 & -0.2298646 & -0.1262212 & -0.1048581 & -0.1573156 & 0.0702 & -0.00761 & -0.2050650 \\ -0.001789 & 0.0843 & -0.09328 & 0.1080839 & -0.0332 & -0.2498542 & 0.08238 & -0.03240 \\ -0.007374 & -0.02283 & 0.01512 & -0.2636266 & 0.1443018 & 0.08730 & -0.3608548 & -0.1563777 \\ 0.03270 & -0.0007097 & 0.00291 & 0.07304 & -0.3028275 & 0.078975 & 0.280401 & -0.03540 \\ -0.1584589 & 0.01321 & -0.02038 & -0.00685 & 0.08231 & -0.2324949 & -0.1714760 & -0.1632792 \end{bmatrix}$$

To find the input matrix, there are two methods. First one according to substructure analysis we determinate the matrix $[F_z]$ and the matrix $[V]$ is given:

$$[B_v] = [F_z][V]^{-1}$$

The second method is based on both the result of static and substructure analysis. The $[q]$ matrix is from the results of static analysis. $[K]$ is from the results of substructure analysis, it exists:

$$[K][q] = [F_z] \text{ and } [B_v] = [K][q][v]^{-1}$$

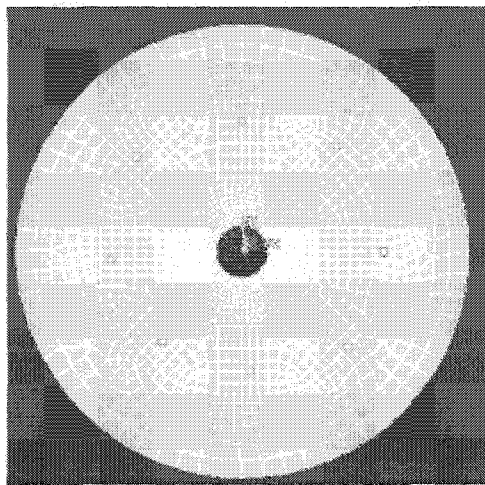


Figure 36 Location of master nodes

4.8 Summary

An analytical approach for modeling circular plate structures with integrated distributed piezoelectric actuators under static as well as dynamic mechanical or electrical loading is developed. The mathematical solution based on the Kirchhoff plate model for free vibration is presented. The validity of the theory is established by examining static as well as dynamic analysis of the circular plate containing eight bonded actuators. The equations governing the dynamics of the plate and relating the strains in the piezoelectric elements to the strain induced in the system are derived for circular plate using the partial differential equation. Modal analysis is done to determine the natural frequencies and mode shapes of the structures while the harmonic analysis is performed to analyze the steady-state behavior of the structures subjected to cyclic sinusoidal loads. Numerical simulation results are obtained using finite element approach. Experiments using a thin aluminum circular plate structure with distributed piezoelectric ceramics PZT BM532 were also conducted to validate the analysis and the computer simulations. Relatively good agreements between the results of these three approaches are observed. Finally, the results show that the model can predict natural frequencies and mode shapes of the plate very accurately. This chapter introduces also a modeling approach based on the Rayleigh-Ritz assumed mode shape method. The model has been used to predict the natural frequencies and mode shape of the plate. Finally, the substructuring analysis in ANSYS is used to extract the mass and stiffness matrices and load vector of the system for active control application eventually.

CHAPTER 5

SHAPE ESTIMATION OF STRUCTURES

In this chapter, an algorithm has been developed to determine deflection of rectangular and circular structures under arbitrary loading and boundary conditions.

5.1 Introduction

To estimate the shape of the surface from strain sensors for continuous structures can use either one of two techniques, namely, approximation of the strain field with global basis functions or approximation of the strain with local basis functions.

This chapter focuses on the shape estimation of thin and composite structures. The next challenge is to estimate the deformed shape for these structures. Note that, we can apply the finite element method and easily estimate the deformed shape of the above structure, but in space (real environment), running a well-known commercial FE code on a powerful workstation is neither practical nor possible. For this reason, a mathematical model to estimate quickly the deformed shape of the above structure was developed. This chapter proposes a shape estimation method to estimate the deformed shape of the flat structures. The strain field is represented by a two-dimensional bi-polynomial function for rectangular plate and by stress function for circular plate. The coefficients of each function are determined based on the relationship of strain, displacement, and strain compatibility. The strain field is constructed by a least squares smoothing procedure. This shape estimation method is verified by the finite element method, and by experimental results.

5.2 Model for rectangular plate

5.2.1 Assumptions

Assume that an aluminium and laminate flat structures with strain gages installed on its surface are subjected to an in-plane force as shown in Figure 37 and 38. The strain components have been measured, using strain gage, at limited number of positions. Using a FE code the strain components are extracted for a limited number of nodes. These values can be considered as the measured strains from the strain gages. The advantage of this approach is clear because the experimental measurement of strain components is not cost effective.

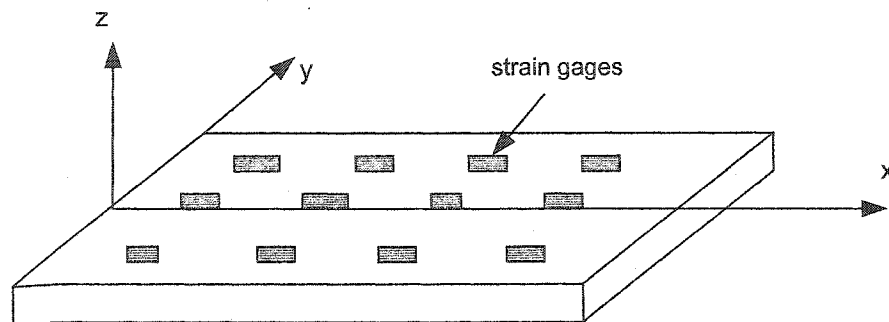


Figure 37 Geometry of flat plate subjected force in z -direction

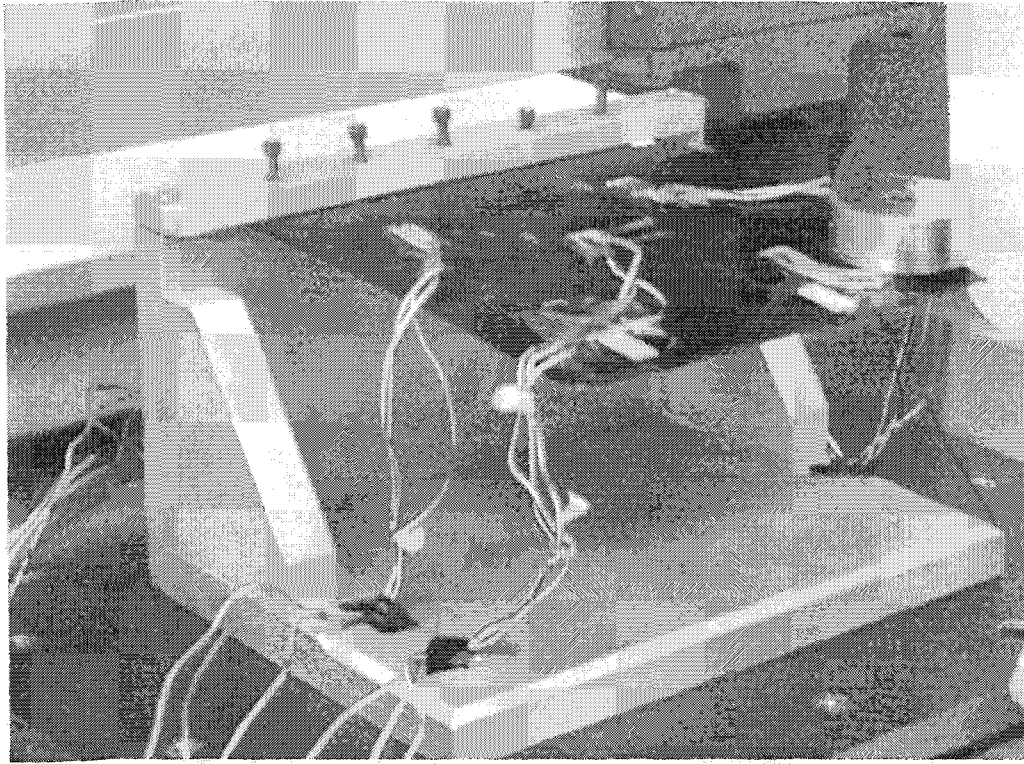


Figure 38 Geometry of Laminate plate with strain gages

It is well known that for plates, the results Kirchhoff plate bending theory are very similar to those for Euler Bernoulli beam theory. One of the most important assumptions for both theories is that the transverse deformation is neglected.

5.2.2 Method

A strain-displacement relationship exists such that:

$$\varepsilon_x = -z \frac{\partial^2 w}{\partial x^2} \quad (5.1)$$

$$\varepsilon_y = -z \frac{\partial^2 w}{\partial y^2} \quad (5.2)$$

$$\varepsilon_{xy} = -z \frac{\partial^2 w}{\partial x \partial y} \quad (5.3)$$

where ε_x , ε_y and ε_{xy} are the linear strain in direction x and y, and the angular strain respectively, z is the distance from the neutral axis of the plate to the sensor location, and w is the out-of-plane displacement function.

5.2.3 Least Squares Method

The great mathematician Gauss developed the method of least squares in the early nineteenth century. This analytical technique is the best available for extracting information from sets of experimental observations, in the sense that any values calculated have statistical errors, but they are normally distributed about their true value with least possible standard deviation. In the present context, the data points are given by strain gage sensor.

The method of least squares is used to model the strain field using the measured strains from known locations on the plate. Firstly a polynomial in x and y that describes the strain field for every location on the plate is defined. A two-dimensional strain field that has the complete linear or quadratic or cubic polynomial terms is assumed. Three cases are study here. For the case of a cubic polynomial the terms are as follows:

$$\varepsilon_x(x, y) = a_1 + a_2x + a_3y + a_4x^2 + a_5xy + a_6y^2 + a_7x^2y + a_8xy^2 + a_9x^3 + a_{10}x^2y^2 + a_{11}x^3y + a_{12}x^3y^2 \quad (5.4)$$

$$\varepsilon_y(x, y) = b_1 + b_2x + b_3y + b_4x^2 + b_5xy + b_6y^2 + b_7x^2y + b_8xy^2 + b_9x^3 + b_{10}x^2y^2 + b_{11}x^3y + b_{12}x^3y^2 \quad (5.5)$$

$$\begin{aligned} \varepsilon_{xy}(x, y) = & c_1 + c_2x + c_3y + c_4x^2 + c_5xy + c_6y^2 + \\ & c_7x^2y + c_8xy^2 + c_9x^3 + c_{10}x^2y^2 + c_{11}x^3y + c_{12}x^3y^2 \end{aligned} \quad (5.6)$$

For a quadratic polynomial the terms are:

$$\varepsilon_x(x, y) = a_1 + a_2x + a_3y + a_4x^2 + a_5xy + a_6y^2 \quad (5.7)$$

$$\varepsilon_y(x, y) = b_1 + b_2y + b_3x + b_4y^2 + b_5xy + b_6x^2 \quad (5.8)$$

$$\varepsilon_{xy}(x, y) = c_1 + c_2x + c_3y + c_4x^2 + c_5xy + c_6y^2 \quad (5.9)$$

Finally for a linear polynomial the terms are:

$$\varepsilon_x(x, y) = a_1 + a_2x + a_3y \quad (5.10)$$

$$\varepsilon_y(x, y) = b_1 + b_2x + b_3y \quad (5.11)$$

$$\varepsilon_{xy}(x, y) = c_1 + c_2x + c_3y \quad (5.12)$$

the compatibility equation is

$$2 \frac{\partial^2 \varepsilon_{xy}}{\partial x \partial y} = \frac{\partial^2 \varepsilon_x}{\partial y^2} + \frac{\partial^2 \varepsilon_y}{\partial x^2} \quad (5.13)$$

The unknown parameters a_i , b_i and c_i , $i = 1, 2 \dots m$ ($m = 3$, or 6 or 12) in the above equations can be determined from the strain compatibility relations strain-displacement relationship and the boundary conditions using a least squares fitting technique. The fitting is performed by converting the strain field given in terms of polynomial terms (linear, quadratic or cubic) into the following matrix form:

$$[X]\{c\} = \{s\} \quad (5.14)$$

where s is the vector containing the target readings (given by the experiment or finite element method), c is the vector containing the coefficients (to be determined), and X is the matrix of generalized coordinates corresponding to a location of the strain gages .

Then, an error function to be minimized is defined by the sum of differences between the strain computed by the cubic, quadratic or linear polynomial terms and the finite element method or experimental results Lancaster (1986).

$$E(\epsilon_x(x, y)) = \sum_{i=1}^n (\epsilon_x(x_i, y_i) - \epsilon_x^{FE}(x_i, y_i)) \quad (5.15)$$

$$E(\epsilon_y(x, y)) = \sum_{i=1}^n (\epsilon_y(x_i, y_i) - \epsilon_y^{FE}(x_i, y_i)) \quad (5.16)$$

$$E(\epsilon_{xy}(x, y)) = \sum_{i=1}^n (\epsilon_{xy}(x_i, y_i) - \epsilon_{xy}^{FE}(x_i, y_i)) \quad (5.17)$$

These error function will have a minimum only if $\frac{\partial E}{\partial a_j} = 0$, $\frac{\partial E}{\partial b_j} = 0$ and $\frac{\partial E}{\partial c_j} = 0$ for $j=1, \dots, m$.

Note that n is the number of measurement locations and $m = 12$ for a cubic approximation, $m = 6$ for a quadratic approximation and $m = 3$ for linear approximation.

Then the error function can be expressed as

$$[X]^T [X] \{c\} = [X]^T \{s\} \quad (5.18)$$

Then, the vector containing the coefficients is given by:

$$\{c\} = [[X]^T [X]]^{-1} [X]^T \{s\} \quad (5.19)$$

where $[[X]^T [X]]^{-1}$ is the pseudo-inverse matrix.

For a linear approximation

The field of the strain is assumed linear, equations 5.10, 5.11 and 5.12.

The compatibility equation 5.13 is verified. Introducing equation 5.10 into equation 5.1 and double integration about x of this equation, then the deflection of the plate is obtained

$$w(x, y) = -\frac{1}{z} \left(\frac{a_1}{2} x^2 + \frac{a_2}{6} x^3 + \frac{a_3}{2} x^2 y + x f_1(y) + f_2(y) \right) \quad (5.20)$$

where $f_1(y)$ and $f_2(y)$ are function of y only. Using equations 5.2 and 5.11 gives

$$b_1 + b_2 x + b_3 y = x \frac{\partial^2 f_1}{\partial y^2} + \frac{\partial^2 f_2}{\partial y^2} \quad (5.21)$$

and equations 5.3 and 5.12 gives

$$c_1 + c_2 x + c_3 y = a_3 x + \frac{\partial f_1}{\partial y} \quad (5.22)$$

Then $c_2 = a_3$ and $c_1 = \text{constant}$ and f_1 become

$$f_1(y) = c_1 y + \frac{c_3}{2} y^2 + K_1 \quad (5.23)$$

where K_1 is a constant. Equation 5.21 involves $c_3 = b_2$, $b_1 = \text{constant}$ and $f_2(y)$ become

$$f_2(y) = \frac{b_1}{2} y^2 + \frac{b_3}{6} y^3 + K_2 y + K_1 \quad (5.24)$$

Finally, the field of strain becomes

$$\varepsilon_x(x, y) = a_1 + a_2x + a_3y \quad (5.25)$$

$$\varepsilon_y(x, y) = b_1 + b_2x + b_3y \quad (5.26)$$

$$\varepsilon_{xy}(x, y) = c_1 + a_3x + b_2y \quad (5.27)$$

and the deflection given by equation (5.20)

$$\text{where } f_1(y) = c_1 + \frac{b_2}{2}y^2 + K_1 \text{ and } f_2(y) = K_3 + K_2y + \frac{b_2}{2}y^2 + \frac{b_3}{6}y^3$$

K_1 , K_2 and K_3 were determined by the boundary condition.

At $x = 0$ and y

$$w(x, y) = 0, \quad \frac{\partial w}{\partial x}(x, y) = 0 \quad \text{and} \quad \frac{\partial w}{\partial y}(x, y) = 0$$

Then

$$K_1 = -(c_1y + \frac{b_1}{2}y^2) \text{ and } K_2 = -(b_1y + \frac{b_3}{2}y^2) \quad (5.28)$$

The same method was applied for the case quadratic and cubic polynomial approximation.

For a quadratic approximation

The field of strain and the deflection for a quadratic polynomial approximation are

$$\varepsilon_x(x, y) = a_1 + a_2x + a_3y + a_4x^2 + a_5xy + a_6y^2 \quad (5.29)$$

$$\varepsilon_y(x, y) = b_1 + b_2x + b_3y + b_4x^2 + b_5xy + b_6y^2 \quad (5.30)$$

$$\varepsilon_{xy}(x, y) = c_1 + a_3x + b_3y + \frac{a_5}{2}x^2 + 2a_6xy + \frac{b_5}{2}y^2 \quad (5.31)$$

and the deflection

$$w(x, y) = -\frac{1}{z} \left(\frac{a_1}{2}x^2 + \frac{a_2}{6}x^3 + \frac{a_3}{2}x^2y + \frac{a_4}{12}x^4 + \frac{a_5}{6}x^3y + \frac{a_6}{2}x^2y^2 + xf_1(y) + f_2(y) \right) \quad (5.32)$$

$$\text{where } f_1(y) = c_1y + \frac{b_3}{2}y^2 + \frac{b_5}{6}y^3 + g_1 \text{ and } f_2(y) = -\frac{b_1}{2}y^2 + \frac{b_2}{6}y^3 + \frac{b_4}{12}y^4 + g_2y + g_3$$

g_1 , g_2 and g_3 were determined by the boundary condition.

For a cubic approximation

The field of strain and the deflection for a cubic polynomial approximation are

$$\varepsilon_x(x, y) = a_1 + a_2x + a_3y + a_4x^2 + a_5xy + a_6y^2 + a_7x^2y + A_8y^3 \quad (5.33)$$

$$\varepsilon_y(x, y) = b_1 + b_2x + b_3y + b_4y^2 + b_5xy + a_6x^2 + B_6x^3 \quad (5.34)$$

$$\varepsilon_{xy}(x, y) = c_1 + a_3x + b_3y + \frac{a_5}{2}x^2 + 2a_6xy + \frac{b_5}{2}y^2 + \frac{a_7}{3}x^3 \quad (5.35)$$

and

$$\begin{aligned}
w(x, y) = & -\frac{1}{z} \left(\frac{a_1}{2} x^2 + \frac{a_2}{6} x^3 + \frac{a_3}{2} x^2 y + \frac{a_4}{12} x^4 + \frac{a_5}{6} x^3 y + \frac{a_6}{2} x^2 y^2 \right. \\
& \left. + \frac{a_7}{12} x^4 y + \frac{A_8}{20} x^5 + x f_1(y) + f_2(y) \right) \quad (5.36)
\end{aligned}$$

$$\text{where } f_1(y) = c_1 y + \frac{b_3}{2} y^2 + \frac{b_5}{6} y^3 + g_1$$

$$\text{and } f_2(y) = -\frac{b_1}{2} y^2 + \frac{b_2}{6} y^3 + \frac{b_4}{12} y^4 + \frac{B_6}{20} y^5 + g_2 y + g_3$$

g_1 , g_2 and g_3 were determined by the boundary condition.

Table XIX

Dimension and material properties of plate and piezoelectric

	PZT- (BM532)	Aluminium	AS/3501-6 graphite-epoxy
E_1 (GPa)	71.4	69	138
E_2 (GPa)	71.4	69	9
G_{12} (GPa)	71.4	69	6.9
ν_{12}	0.3	0.33	0.3
ρ (Kg/m ³)	7350	2730	1600
Length (m)	0.0508	0.28	0.265
Width (m)	0.03683	0.2	0.255
Thickness (m)	0.00025	0.00075	0.0029
d_{31} (pm/V)	200		

5.3 Model for circular plate

5.3.1 Description

The structure under consideration consists of a thin circular plate with piezoceramic patches bonded on one side and the strain gages in the others side. The plate is clamped around the inner boundary radius R_1 and free at the outside edge radius R_2 as illustrated in Figure 22. The patches generate strains in response to an applied voltage. When bonded to an underlying structure, these strains lead to the generation of in plane forces and /or bending moments. In this chapter, we will consider only the bending moments, which are generated by the patches and will consider them as an input to the model describing the transverse deformation of a plate. The circular plate is also assumed to be made of linearly elastic, homogeneous and isotropic material. On the other hand, using strain gages, one has measured the strain components at limited number of positions. This chapter develops a mathematical model to estimate quickly the deformed shape of the above circular structure.

5.3.2 Method

Equilibrium equations in cylindrical co-ordinates

$$\frac{\partial \sigma_{rr}}{\partial r} + \frac{\sigma_{rr} - \sigma_{\theta\theta}}{r} + \frac{1}{r} \frac{\partial \sigma_{r\theta}}{\partial \theta} + F_r = 0 \quad (5.37)$$

$$\frac{\partial \sigma_{r\theta}}{\partial r} + 2 \frac{\sigma_{r\theta}}{r} + \frac{1}{r} \frac{\partial \sigma_{\theta\theta}}{\partial \theta} + F_\theta = 0 \quad (5.38)$$

where σ_{rr} , $\sigma_{\theta\theta}$ and $\sigma_{r\theta}$ are the stress in r-direction, θ -direction and the shear stress respectively and F_r and F_θ are the body forces in r-direction and θ -direction respectively.

The displacement field is assumed as follows:

$$u_z = u_z(r, \theta, t) = w(r, \theta, t) \quad (5.39)$$

$$u_r = u_r(r, \theta, t) = -z \frac{\partial u_z}{\partial r} \quad (5.40)$$

$$u_\theta = u_\theta(r, \theta, t) = -z \frac{\partial u_z}{r \partial \theta} \quad (5.41)$$

where u_z , u_r and u_θ are the displacement in transverse z-direction, radial r-direction, and tangential θ -direction of the plate, respectively. The strain displacement relationship is

$$\varepsilon_{rr} = \frac{\partial u_r}{\partial r} \quad (5.42)$$

$$\varepsilon_{\theta\theta} = \frac{u_r}{r} + \frac{1}{r} \frac{\partial u_\theta}{\partial \theta} \quad (5.43)$$

$$\varepsilon_{r\theta} = \frac{1}{2} \left(\frac{\partial u_\theta}{\partial r} - \frac{u_\theta}{r} + \frac{1}{r} \frac{\partial u_r}{\partial \theta} \right) \quad (5.44)$$

where ε_{rr} and $\varepsilon_{\theta\theta}$ are the r-radial and θ -direction strain respectively.

Assume that the stress can be represented by Airy's Stress function ϕ such that

$$\sigma_{rr} = \frac{1}{r} \frac{\partial \phi}{\partial r} + \frac{1}{r^2} \frac{\partial^2 \phi}{\partial \theta^2} \quad (5.45)$$

$$\sigma_{\theta\theta} = \frac{\partial^2 \phi}{\partial r^2} \quad (5.46)$$

$$\sigma_{r\theta} = \frac{1}{r} \frac{\partial \phi}{\partial \theta} - \frac{1}{r} \frac{\partial^2 \phi}{\partial r \partial \theta} \quad (5.47)$$

ϕ has to satisfy the biharmonic equation $\nabla^4 \phi = 0$, where the body forces are zero or constants.

$$\text{Where} \quad \nabla^4 \phi = \left(\frac{\partial^2}{\partial r^2} + \frac{1}{r} \frac{\partial}{\partial r} + \frac{1}{r^2} \frac{\partial^2}{\partial \theta^2} \right) \left(\frac{\partial^2 \phi}{\partial r^2} + \frac{1}{r} \frac{\partial \phi}{\partial r} + \frac{1}{r^2} \frac{\partial^2 \phi}{\partial \theta^2} \right)$$

5.3.3 Application

5.3.3.1 Axisymmetric problem

In this case the stress is independent on θ then

$$\sigma_{rr} = \frac{1}{r} \frac{\partial \phi}{\partial r} \quad \sigma_{\theta\theta} = \frac{\partial^2 \phi}{\partial r^2} \quad \text{and} \quad \sigma_{r\theta} = 0$$

$$\nabla^4 \phi = 0$$

The solution of this equation is

$$\phi = C_1 r^2 \ln r + C_2 r^2 + C_3 \ln r + C_4$$

where C_i $i = 1 \dots 4$ are the constants.

Then the field stress

$$\sigma_{rr} = C_1(1 + 2 \ln r) + 2C_2 + C_3 \frac{1}{r^2} \quad (5.48)$$

$$\sigma_{\theta\theta} = C_1(3 + 2 \ln r) + 2C_2 - C_3 \frac{1}{r^2} \quad (5.49)$$

$$\sigma_{r\theta} = 0 \quad (5.50)$$

Hook's law, the strain in plane stress

$$\varepsilon_{rr} = \frac{1}{E}(\sigma_{rr} - \nu\sigma_{\theta\theta}) \quad (5.51)$$

$$\varepsilon_{\theta\theta} = \frac{1}{E}(\sigma_{\theta\theta} - \nu\sigma_{rr}) \quad (5.52)$$

$$\varepsilon_{r\theta} = \frac{1+\nu}{E}(\sigma_{r\theta}) \quad (5.53)$$

where E is Young modulus and ν is Poisson coefficient, then the field strain is:

$$\varepsilon_{rr} = \frac{1}{E} \left(\frac{C_3(1+\nu)}{r^2} + 2C_2(1-\nu) + C_1(1-\nu)(2\ln r + 1) - 2\nu C_1 \right) \quad (5.54)$$

$$\varepsilon_{\theta\theta} = \frac{1}{E} \left(-\frac{C_3(1+\nu)}{r^2} + 2C_2(1-\nu) + C_1(1-\nu)(2\ln r + 1) + 2C_1 \right) \quad (5.55)$$

Integrate the equation 5.54, we obtained the radial displacement :

$$u_r = \frac{1}{E} \left(-\frac{C_3(1+\nu)}{r} + 2C_2(1-\nu)r + C_1(1-\nu)(2r \ln r - r) - 2\nu r C_1 + \text{constant} \right) \quad (5.56)$$

Or, $\varepsilon_{\theta\theta} = \frac{u_r}{r}$, then

$$u_r = \frac{1}{E} \left(-\frac{C_3(1+\nu)}{r} + 2C_2(1-\nu)r + C_1(1-\nu)(2r \ln r - r) - 2\nu r C_1 \right) \quad (5.57)$$

Equations 5.56 and 5.57 involve the constant = 0 and $C_1 = 0$, then

$$u_r = \frac{1}{E} \left(-\frac{C_3(1+\nu)}{r} + 2C_2(1-\nu)r \right) \quad (5.58)$$

The deflection is given by w:

$$w(r) = -\frac{1}{z} \int u_r dr \quad (5.59)$$

$$w = -\frac{2}{h} \left(-\frac{1}{E} C_3 \ln(r) - \frac{\nu}{E} \ln(r) C_3 + \frac{1}{E} C_2 r^2 - \frac{\nu}{E} C_2 r^2 \right) + f_1 \quad (5.60)$$

where f_1 is the constant. This constant was calculated by the boundary condition, h is the thickness of the plate, C_i are the unknowns' coefficients.

5.3.3.2 Quasi axisymmetric problem

In this case, assume that the stresses are independent on θ but the displacements may be depend on θ , the field strain is:

$$\varepsilon_{rr} = \frac{\partial u_r}{\partial r} = \frac{1}{E} \left(\frac{C_3(1+\nu)}{r^2} + 2C_2(1-\nu) + C_1(1-\nu)(2\ln r + 1) - 2\nu C_1 \right) \quad (5.61)$$

$$\varepsilon_{\theta\theta} = \frac{u_r}{r} + \frac{\partial u_\theta}{r\partial\theta} = \frac{1}{E} \left(-\frac{C_3(1+\nu)}{r^2} + 2C_2(1-\nu) + C_1(1-\nu)(2\ln r + 1) + 2C_1 \right) \quad (5.62)$$

$$\varepsilon_{r\theta} = \frac{1}{2} \left(\frac{\partial u_\theta}{\partial r} - \frac{u_\theta}{r} + \frac{\partial u_r}{r\partial\theta} \right) \quad (5.63)$$

Integrating equation 5.61, it is obtained,

$$u_r = \frac{1}{E} \left(-\frac{C_3(1+\nu)}{r} + 2C_2(1-\nu)r + C_1(1-\nu)(2r \ln r - r) - 2\nu C_1 \right) + f(\theta) \quad (5.64)$$

Substituting into equation 5.42 we find

$$\frac{\partial u_\theta}{r \partial \theta} = \frac{1}{E} \left(C_1 - \frac{f(\theta)}{r} \right) \quad (5.65)$$

Integration we obtain

$$u_\theta = \frac{1}{E} (4C_1 r \theta - \int f(\theta) d\theta + g(r))$$

Substituting u_θ into shear strain expression:

$$\frac{\partial g(r)}{\partial r} - \frac{g(r)}{r} + \frac{1}{r} \int f(\theta) d\theta + \frac{1}{r} \frac{\partial f(\theta)}{\partial \theta} = 0$$

where f and g are the functions depend only on θ and r respectively.

then :

$$r \frac{\partial g(r)}{\partial r} - g(r) = C_5$$

$$\int f(\theta) d\theta + \frac{\partial f(\theta)}{\partial \theta} = -C_5$$

Solving above two equations, it is obtained:

$$g(r) = -C_5 + C_6 r$$

$$f(\theta) = C_7 \sin \theta + C_8 \cos \theta$$

The displacement u_r , is derived,

$$u_r = \frac{1}{E} \left(-\frac{C_3(1+\nu)}{r} + 2C_2(1-\nu)r + C_1(1-\nu)(2r \ln r - r) - 2\nu r C_1 + C_7 \sin \theta + C_8 \cos \theta \right) \quad (5.66)$$

$$u_\theta = \frac{1}{E}(4C_1 r \theta + C_7 \cos \theta - C_8 \sin \theta + C_6 r) \quad (5.67)$$

where C_i $i = 1 \dots 8$ are the constants.

The deflection is given by w :

$$w(r) = -\frac{1}{z} \int u_r dr \quad (5.68)$$

5.3.3.3 General case

For the general case the Airy's Stress function is

$$\phi = (C_1 r \ln r + C_2 r^3 + \frac{C_3}{r} + C_4 r) \sin \theta \quad (5.69)$$

The field strain is:

$$\varepsilon_{rr} = (2C_3 \frac{1+\nu}{r^3} + 2(1-3\nu)C_2 r + (1-\nu) \frac{C_1}{r}) \frac{\sin \theta}{E} \quad (5.70)$$

$$\varepsilon_{\theta\theta} = (2C_3 + 2C_3 \nu + 2(3-\nu)C_2 r^4 - (1-\nu)C_1 r^2) \frac{\sin \theta}{Er^3} \quad (5.71)$$

$$\varepsilon_{r\theta} = (-2C_3 - 2C_3 \nu + 2(1+\nu)C_2 r^4 + (1+\nu)C_1 r^2) \frac{\sin \theta}{Er^3} \quad (5.72)$$

$$u_r = \frac{1}{E} \left(-\frac{C_3(1+\nu)}{r^2} + C_2(1-3\nu)r^2 - C_1(1+\nu) + (1-\nu)C_1 \ln r - r \right) \sin \theta - 2\nu C_1 \cos \theta + C_5 \cos \theta + C_6 \sin \theta \quad (5.73)$$

$$u_\theta = \frac{1}{E} \left(-(1+\nu) \frac{C_3}{r^3} - (5+\nu)C_2 r^2 + (1-\nu)C_1 \ln r \right) \cos \theta + 2C_1 \theta \sin(\theta) - C_4 r - C_5 \sin \theta + C_6 \cos \theta \quad (5.74)$$

Finally, the deflection is given by the equations

$$w(r) = -\frac{1}{z} \int u_r dr \quad (5.75)$$

and the boundary conditions.

Now, strain field is defined by the equations 5.70 to 5.72 for every location on circular plate, the C_i terms are real-valued coefficients that define the individual contributions of each term to global strains function. The question remains: how may we estimate judiciously the coefficients C_i using the collected information about the strain field? What is the best fit? A very common method to respond to this question is known as the method of least squares.

The fitting is performed by converting equations 5.70 to 5.72 in the following matrix form:

$$[A]\{C\} = \{s\}$$

where s is the vector containing the target readings given by strain gage sensor, C is the vector containing the unknown coefficients C_i , and A is the matrix of generalized coordinate whose individual row correspond to the term of equations 5.70 to 5.72 at the target locations r and θ . The matrix A may be square or not depended of the number of the target readings, which is equal or greater than the number of terms in the shape function. In the last cases a pseudo-inverse matrix must be found. The C vector is solved by performing the following matrix operation:

$$\{C\} = [[A]^T [A]]^{-1} [A]^T \{s\} \quad (5.79)$$

5.5 Experimentation

In order to verify the applicability of the shape estimation method, experimental investigations have been initiated and a laboratory test arrangement has been developed at the CSA.

The experimental system consists of:

1. A laminate rectangular plate with glued five strain gages as shown in Figure 38. Figure 39 shows the setup used for this plate. The plate is made of AS/3506 graphite-epoxy composites. The material data and the dimensions of this plate are given in Table XIV. The stacking sequence of the composite plate is $[0_2/90_7/0_2]_S$.
2. A thin circular aluminium plate with bonded eight piezoceramic actuators on one-side and strain gages on other sides. Figure 40 shows the test set up with close-up views of the components. Four actuators were chosen to apply the voltage 150 voltages symmetrically. The output voltage was measured from conditioning amplifier and transformed to strain. A non-contact laser sensor instrument was used to measure the displacement at different points along the radius of plate.

The strain gage is connected to a Wheatstone Bridge Circuit and built into an amplifier. The model 563-H transducer - conditioning amplifier is used in this experimentation. This amplifier is a wide band; true differential DC instrumentation amplifier with built in transducer signal conditioning functions. The output of the basic amplifier is 10V at 10 mA. Strain gages are the small active devices that change resistance when subjected to a dimensional change. They are used in a bridge configuration having one active element (quarter bridge). To measure strain, one of the resistors is replaced by the strain gage. The output voltage V_0 can be calculated from Ohm's law. Also, using the relationship for change in resistance of a strain gage as a function of axial strain, resistance, and strain gage factor, namely

$$\frac{dR}{R} = S' \varepsilon \quad (5.80)$$

Finally,

$$V_o = \frac{1}{4} V_E S' (\varepsilon + \varepsilon_{th}) \quad (5.81)$$

where $S' = S \frac{R}{R + R_w}$, R is resistance of strain gages; R_w resistance of wire, S is the strain gage factor and V_E is the exciting voltage.

The strain gages used here has an electrical resistance $R = 350 \Omega$, the strain gage factor $S = 2.12$, $R_w = 0.172 \Omega$ and $V_E = 10V$. The strain due to the temperature is assumed to be zero. The output voltage was measured from conditioning amplifier and transformed to strain by using equation 5.81. A contact depth displacement instrument was used to measure the displacement at different points of plate.

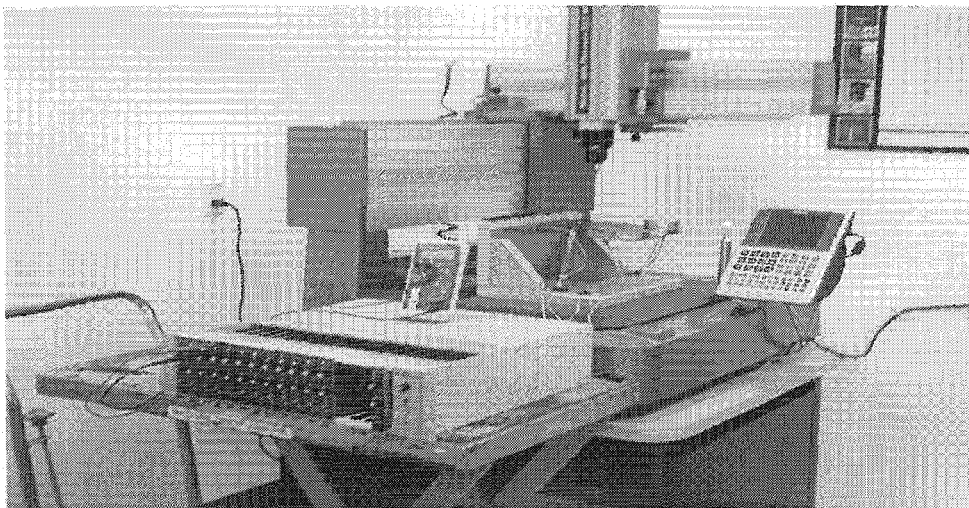


Figure 39 Set-up of Laminate plate with strain gages

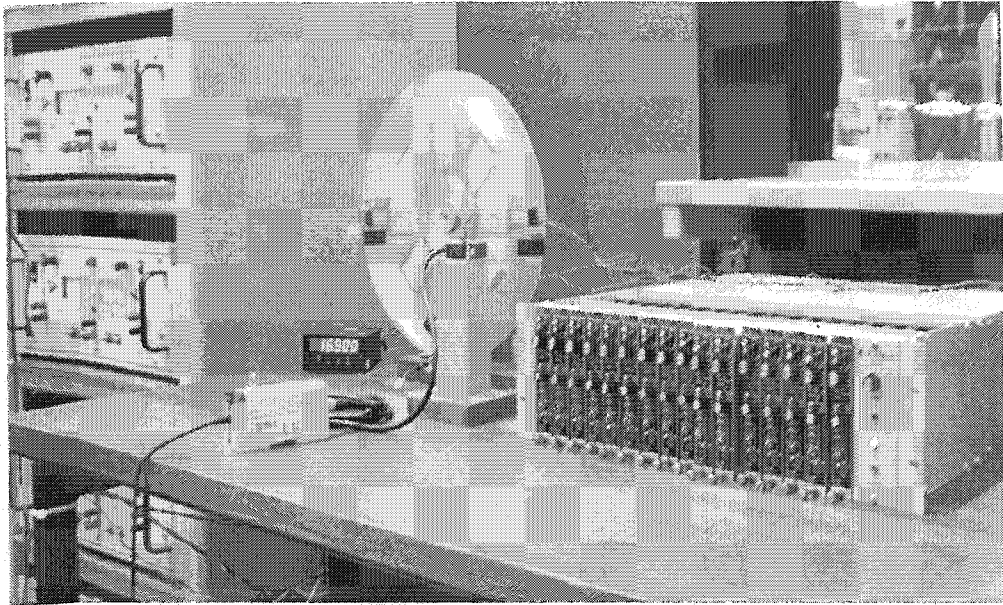


Figure 40 Experimental set up

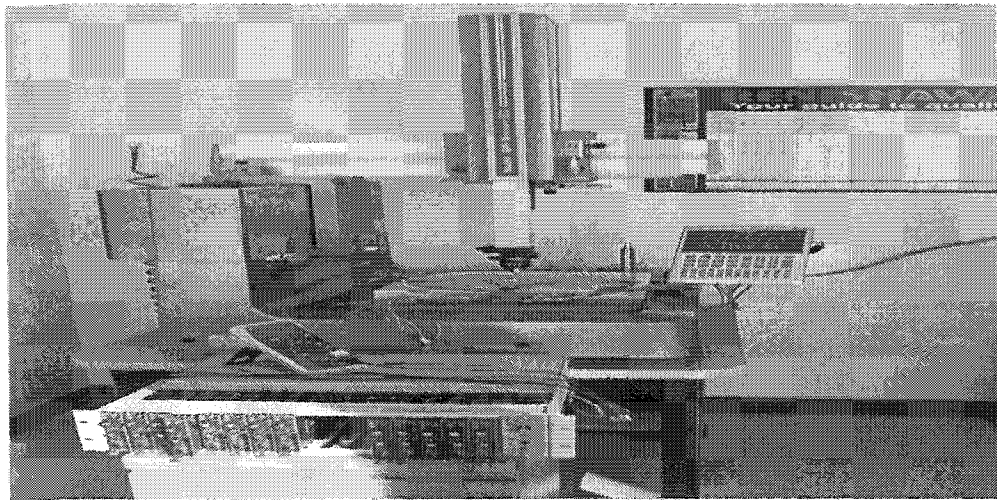


Figure 41 Experimental set up of simply supported circular plate

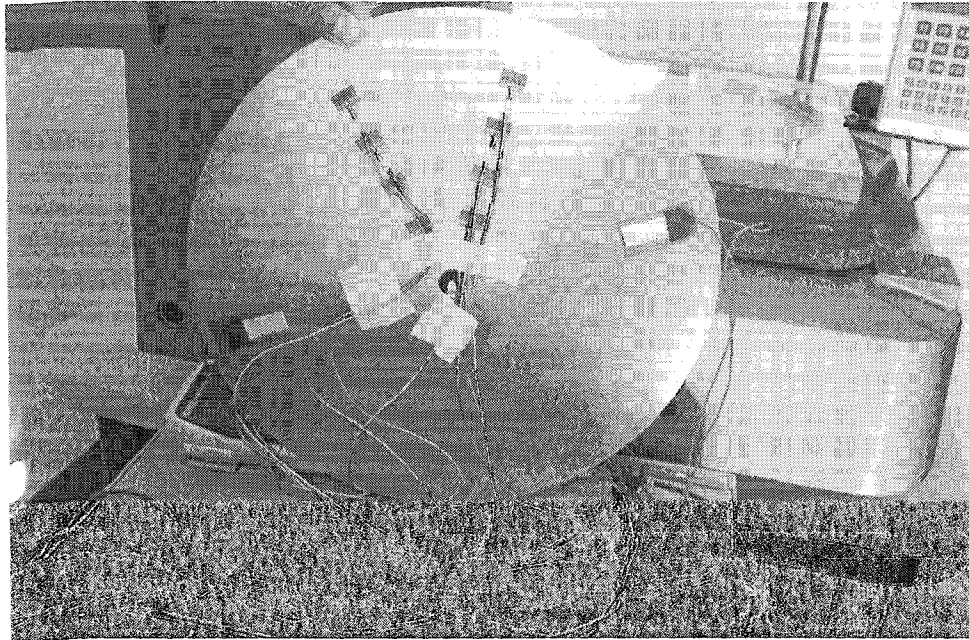


Figure 42 Placement of strain gages

5.5 Results and comparison

5.5.1 Rectangular plate

The proposed method was used to estimate the deformation of a clamped plate with strain gages and actuators bonded on its surface. The schematic of this plate is shown in Figure 37 while the dimensions and the material properties are given in Table XIV. In Figures 43, 44 and 45 the linear, quadratic and cubic approximations, respectively, were used for the strain field to estimate the shape of the plate. Two load cases were investigated. In the first one a concentrated force of 0.2 N was applied at location $x=0.28, y=0$ in positive z direction. In the second case a voltage 100V was applied to the two piezoelectric actuators as shown in Figure 37.

In order to verify the accuracy of the proposed shape estimation method, a commercial finite element method software (ANSYS) was used to generate the strain field for the plate. Various sets of strain information obtained from ANSYS were used also to determine the optimum strain gage locations necessary to produce the most accurate estimation of the plate deformation. It was decided that the strain field must be recovered from 4 nodes, 6 nodes, 12 nodes and 18 nodes. The reason is, because one cannot install too many strain gages in practice. The finite element method also produced out-of-plane displacements for the element locations.

In order to show the effectiveness of the proposed shape estimation method and the optimum sensor locations, the deformation of the plate with different strain gage sensors and FEM results are shown in Figures 43, 44 and 45. The applied loading in this case is 0.2 N acting at location $x = 0.28$ and $y = 0$. The method of least squares is used to model the strain field using the measured strains from known locations on the plate. A two-dimensional strain field that has the complete linear, quadratic and cubic polynomial terms was used in this method. Five sets of strain information 4, 6, 8, 12 and 18 strain gages were investigated. It is found that the accuracy is improved when the number of strain gage sensors is 12 and the approximation field strain is linear. The shape estimation error is approximately less than 0.1 percent compared with the finite element method for the linear, quadratic and cubic approximation.

In Figure 46, a load of 0.2 N is applied at location $x = 0.28$ and $y = 0$ in positive z direction. The rosette strain gages are installed on 12 numbers of locations of the plate. The location of the strain gage sensors was chosen after several trial-and-error optimization studies were performed (Figures 43, 44 and 45). The least squares displacement estimates (linear, quadratic and cubic) are compared to the FEM displacement results. For x -direction ($y = -0.1$), the displacement magnitude match very well (Figure 46). Figure 46 shows a least square displacement estimate is quite as accurate as the FEM solution when the strain field has linear, quadratic and cubic

polynomial terms and 12 strain gages. The maximum error for three approximations is less than 2 %.

In Figure 47, we consider the same plate and an isotropic BM532 piezoceramic patches are applied on the top of the plates in the manner shows in Figure 37. 100 volts was applied across two symmetric patches placed in the left end of the plate. The rosette strain gages are installed on 12 numbers of locations of the plate. The linear polynomial terms are used to approximate the field strain. The deflections along $y = -0.1$ was calculated by the finite element method and shape estimation method. These results were then compared in Figure 47. The results in this Figure show good agreement between the proposed method and finite element method.

In Figure 48, a load of 0.2 N is applied at one of the free corners of plate ($x=0.28, y=-0.1$) in the positive z direction and the rosette strain gages are installed on 15 numbers of locations of the plate. For the x -direction, the linear and quadratic least-square estimate match very well the finite element solution. Comparing the two maximum displacement values, the quadratic least squares estimate is approximately 5 percent higher than the finite element method. The linear least-square estimate is approximately 7 percent lower than the finite element method. The cubic least-square estimate matches very well the finite element method the error is less than 0.1 percent. In the y -direction along the line $x = 0.266$, Figure 49 shows a least- squares displacement estimate that is not quite as accurate as the finite element solution. However, the same general shape of the deformed plate is present in the estimate, the maximum displacement difference is 12 percent for linear, 15 percent for quadratic and approximately less than 2 percent for a cubic least-square estimate.

In Figure 50, loads of 0.2 N are applied at both of the free corners of plate ($(x=0.28, y=-0.1)$ and $(x=0.28, y=0.1)$) in the positive z direction. For the x -direction, the cubic and quadratic least-square estimate match very well the finite element solution. Comparing the two maximum displacement values, the cubic least squares estimate is

approximately the same as the finite element method. The quadratic least-square estimate is approximately 1 percent lower than the finite element method in the free end of the plate. The linear least-square estimate match well the finite element method where the error between the maximum displacements is 0.1 percent. In the y-direction along the line $x = 0.266$, Figure 51 again shows the correct deformed shape. The maximum displacement difference is 0.3 percent for linear, 4 percent for quadratic and approximately 7 percent for a cubic least-square estimate.

In Figure 52, a load of 0.2 N is applied to one of the free corners of plate ($x=0.28, y=-0.1$) in the positive z-direction, and a load of 0.2 N is applied in the other free corner in the negative z-direction. For the x-direction, the cubic least-square estimate matches very well the finite element solution the error is less than 2 percent. Figure 54 shows if we increase the number of the strain gages, the error decreases, the cubic least-square estimate match very well the finite element solution, the error is less than 1 percent. In the y-direction along the line $x = 0.266$, Figure 53 shows a least-squares displacement estimate that is quite as accurate as the finite element solution for cubic approximation; however, for linear and quadratic approximation the same general shape of the deformed plate is present in the estimate.

In order to verify the shape estimation approaches, numerical calculations and experiment results were generated from a cantilevered laminated composite plate with five glued strain gages. Figure 39 shows the setup used for this plate. The dimensions of this plate and the material data are given in Table XIV.

Figure 55 and 56 show the comparison between the least square method and the experiment result for laminate plate along $y = -0.1105$ and $x = 0.2473$ respectively. These Figures shows that the estimation method can predicted accurately the shape of the composite structures.

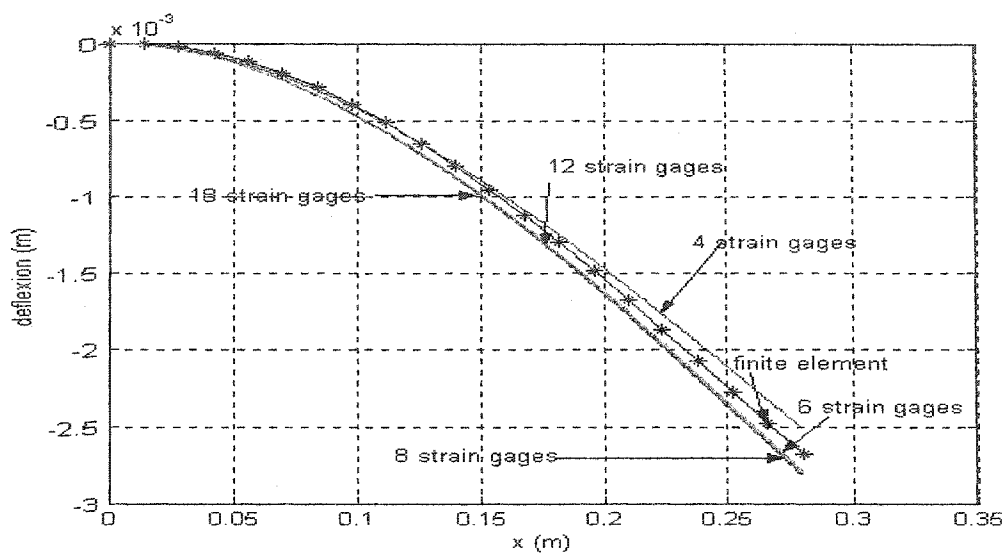


Figure 43 Optimization of the number of strain gages (linear estimation)

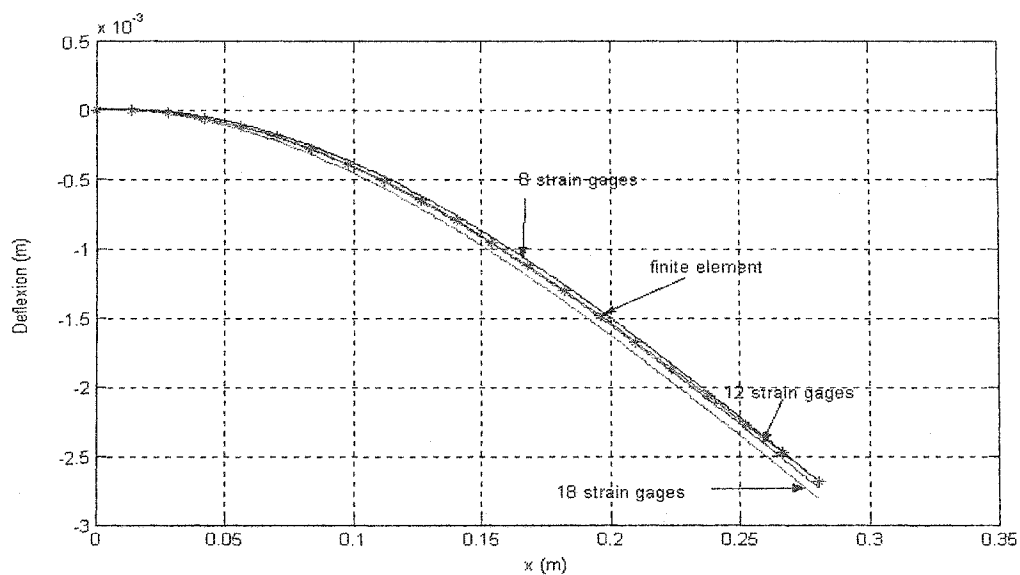


Figure 44 Optimization of the number of strain gages (quadratic estimation)

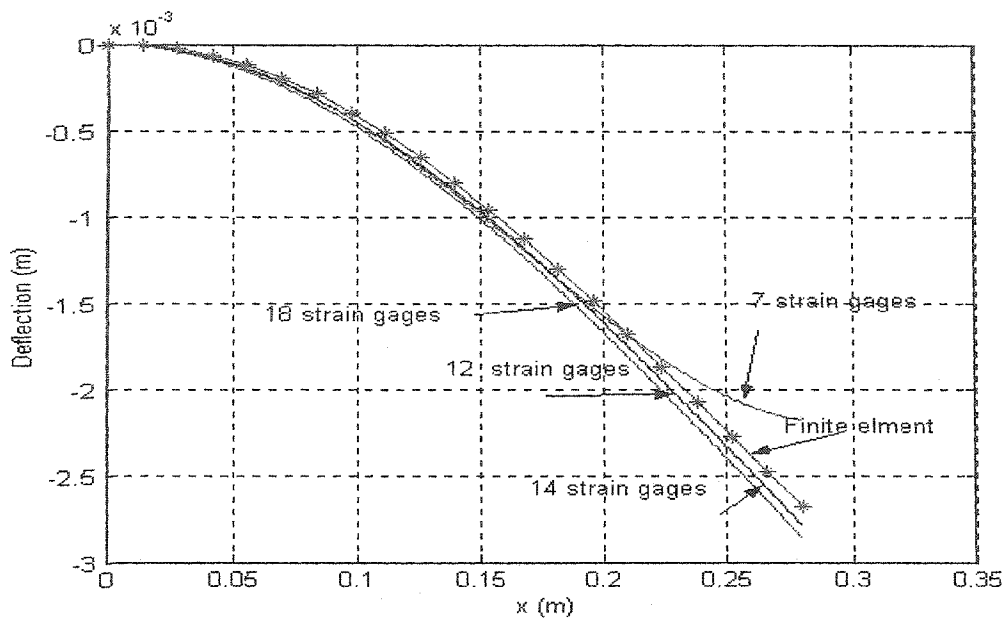


Figure 45 Optimization of the number of strain gages (cubic estimation)

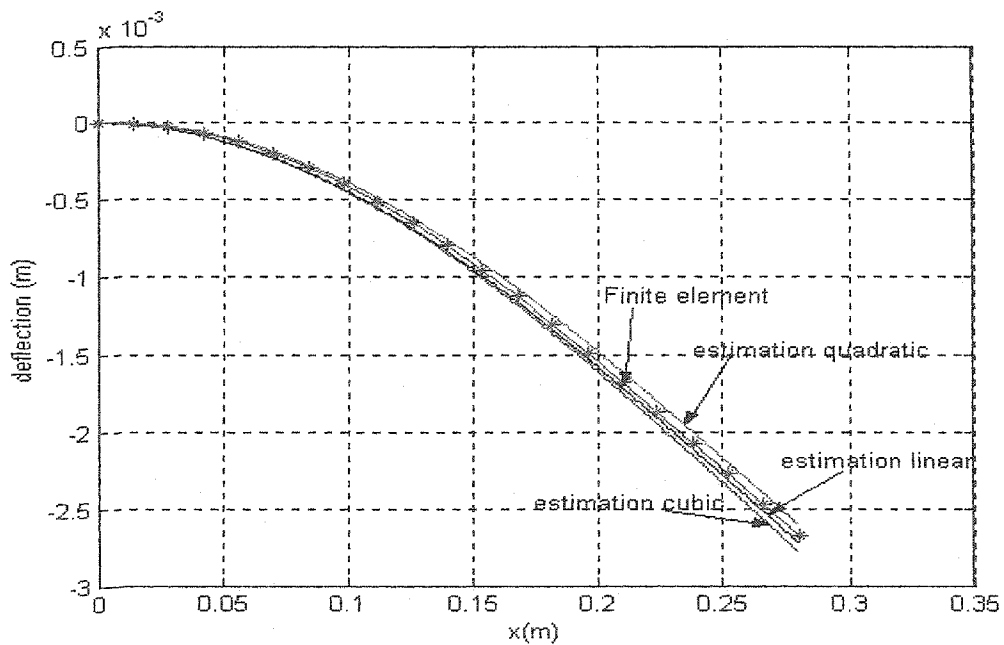


Figure 46 Deformation at line $y = -0.1$ for 12 strain gages

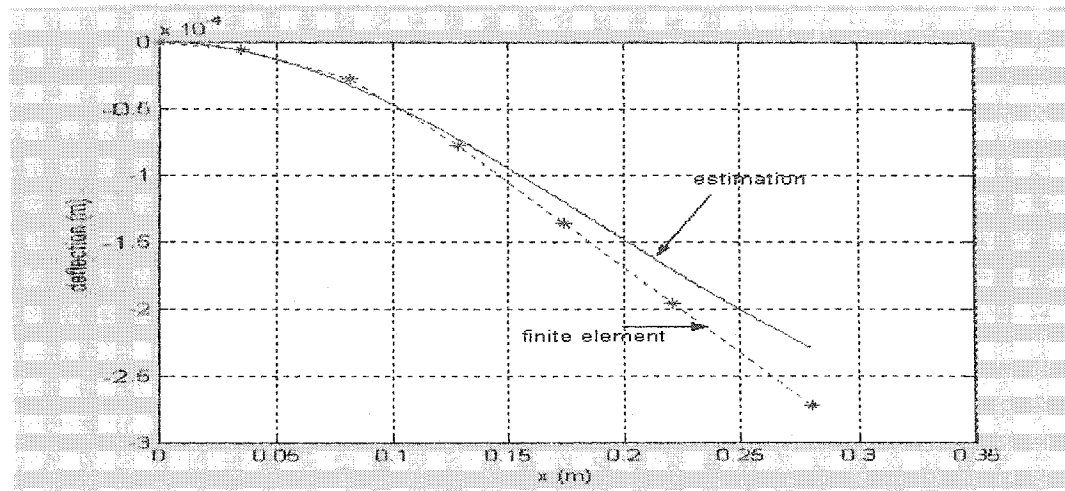


Figure 47 Deflection for a plate with piezoelectric

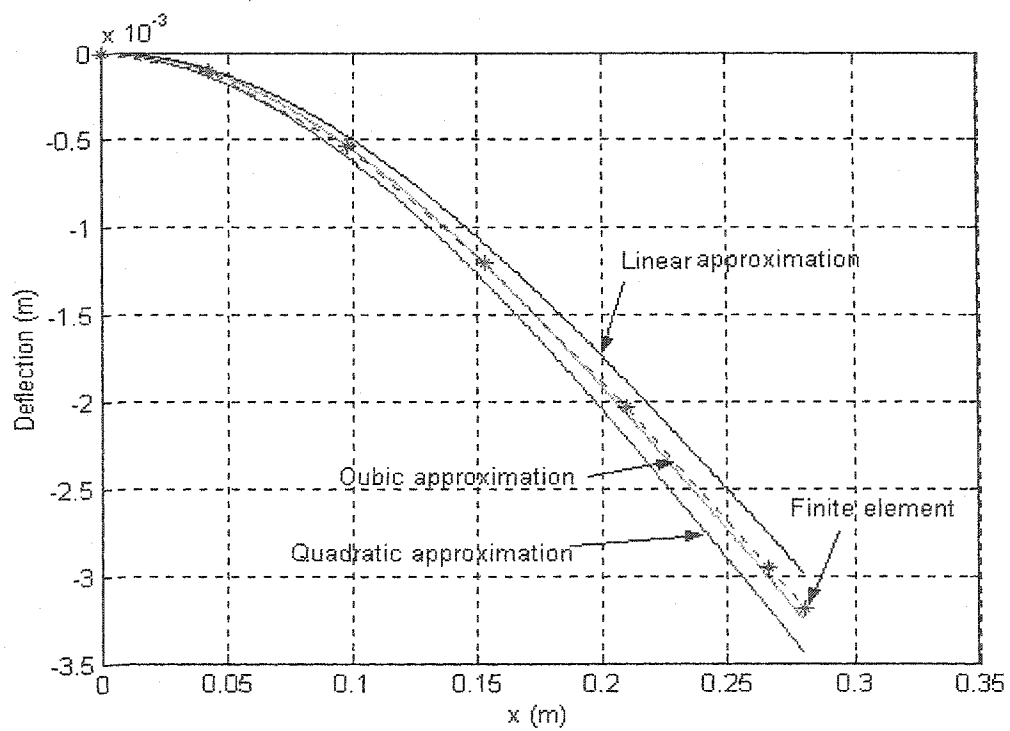


Figure 48 Deformation at line $y = 0.06$ and load at one of the free crones

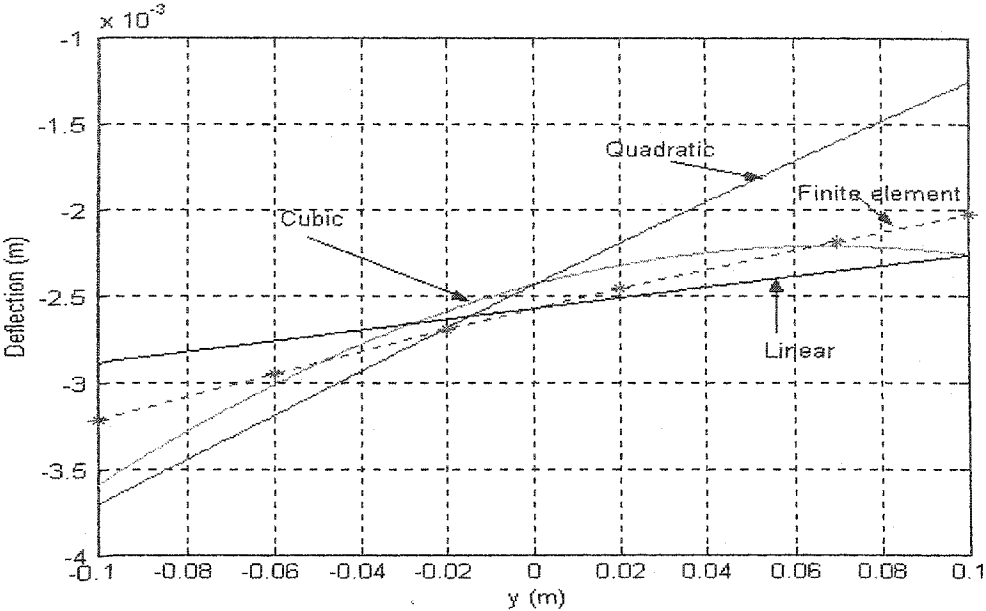


Figure 49 Deformation at line $x = 0.266$ and load at one of the free corners

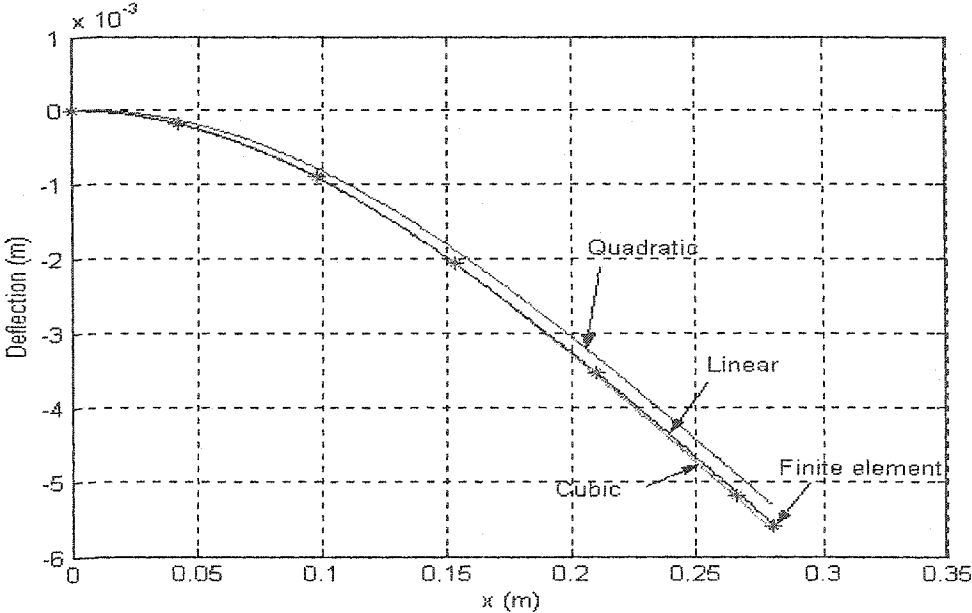


Figure 50 Deformation at line $y = 0.06$ and load at both of the free corners

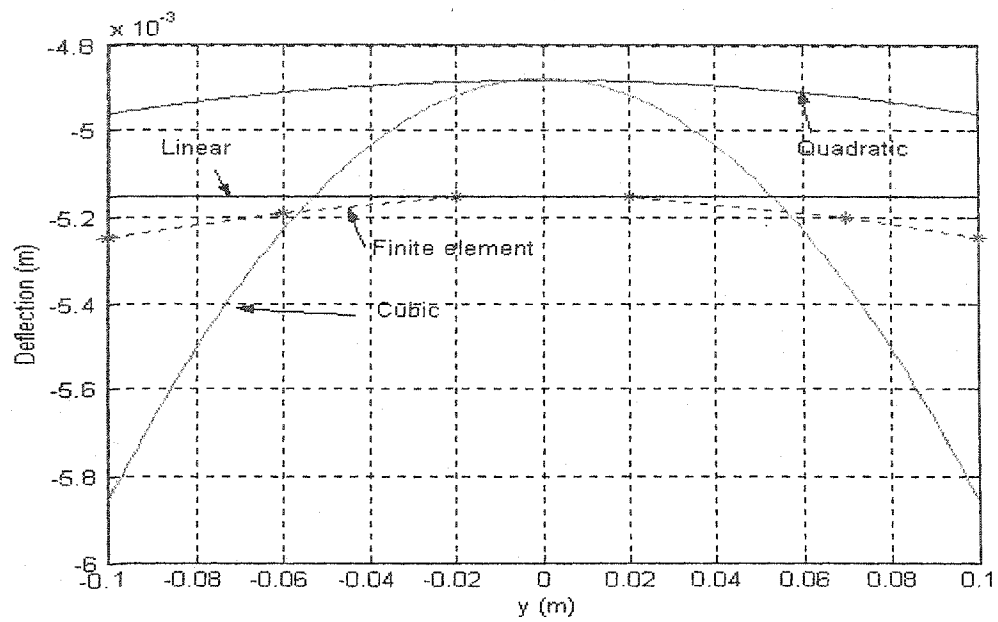


Figure 51 Deformation at line $y = 0.266$ and load at both of the free corners

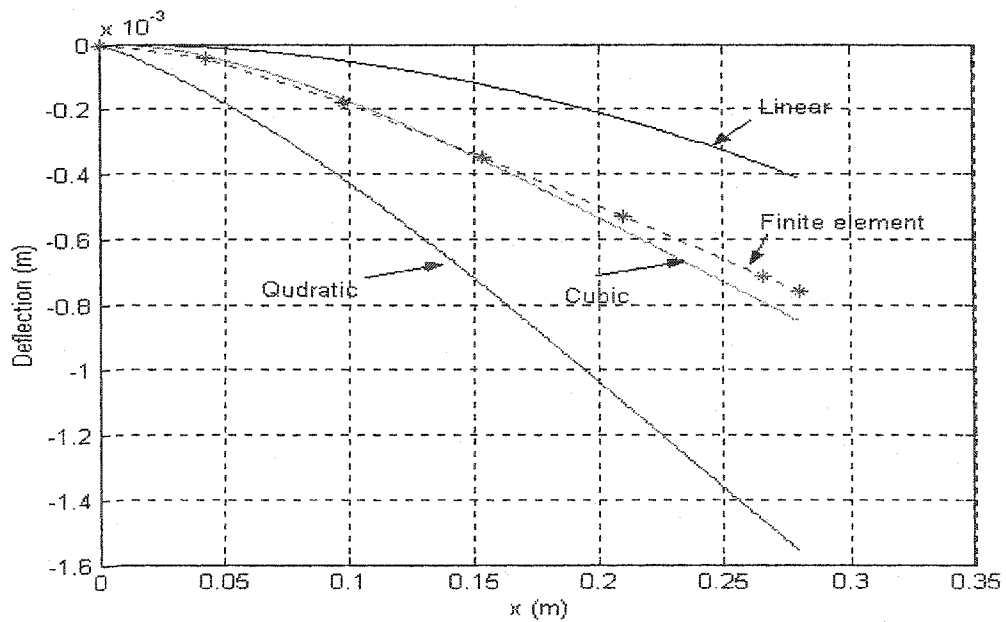


Figure 52 Deformation at line $y = 0.06$ and opposite load at the free corners

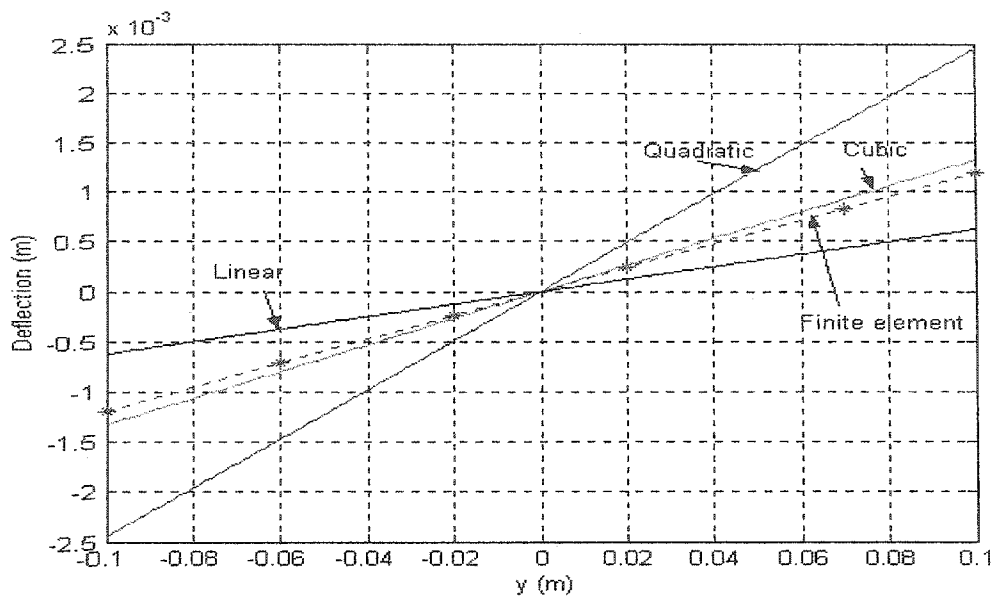


Figure 53 Deformation at line $x = 0.226$ and opposite load at the free corners

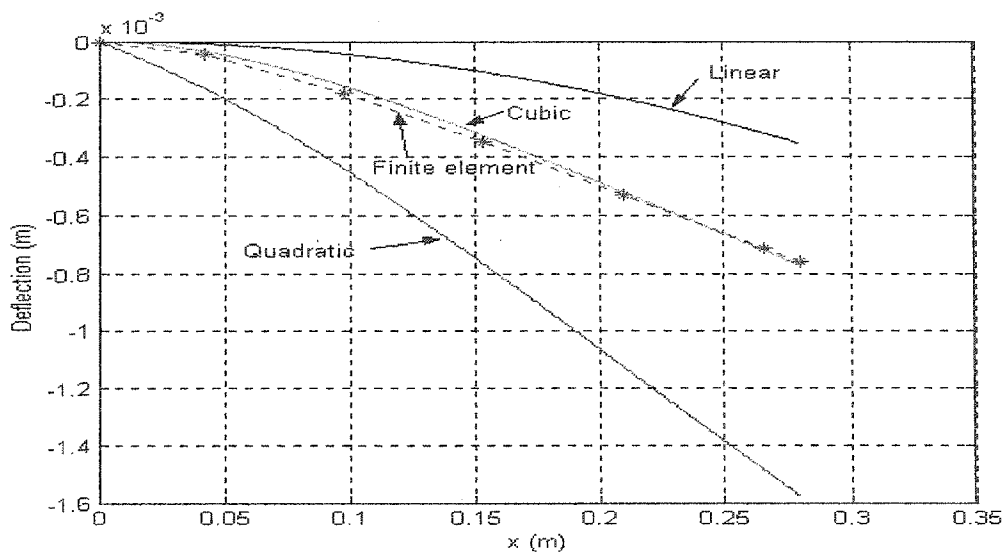


Figure 54 For 31 strain and opposite load at the free corners

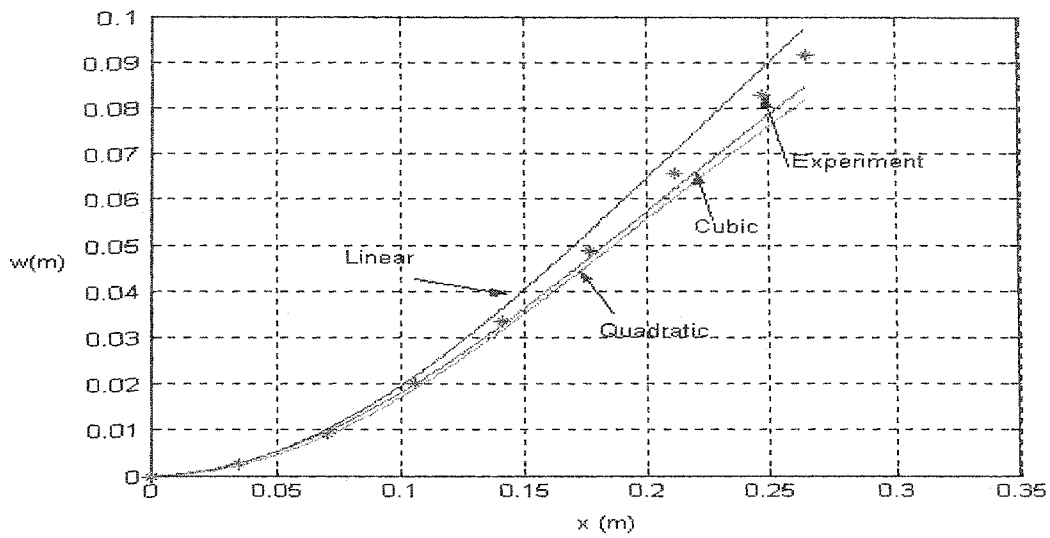


Figure 55 Deformation for 5 strain gages along the line $y = -0.1105$

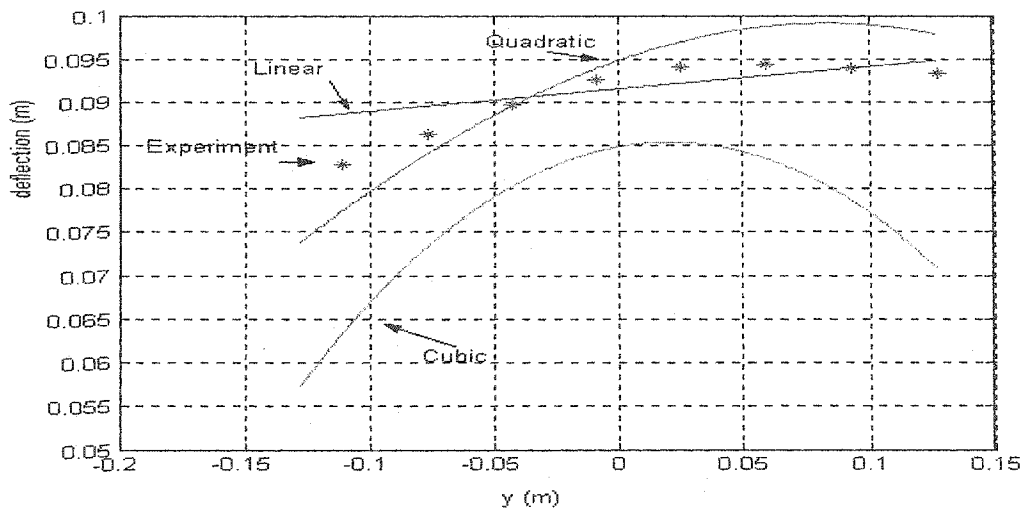


Figure 56 Deformation for 5 strain gages along the line $x = 0.2473$

5.5.2 Circular plate

In order to verify the proposed shape estimation method, experiments results and numerical calculations were generated to compare with the estimation method to the circular plate with distributed eight piezoceramics bonded on the surface of the plate. The schematic of this plate is shown in Figure 22 while the dimensions and the material properties are given in TableXII.

The piezoelectric actuator patches were modeled using solid5 piezoelectric elements and the aluminium circular plate by shell63 structural elements of a commercial finite element code (ANSYS). The static response of the structure was determined by applying a constant voltage to the five piezoelectric actuators.

The various sets of strain information obtained from ANSYS were used to determine the optimum strain gage locations necessary to produce the most accurate estimation of the plate deformation. Figure 42 shows the strain sensors locations on the circular plate. Eight locations of strain gages in the quarter of plate are investigated after several trial and error optimization studies were performed. After that, two load cases and two boundary conditions were investigated. Case one applied concentrated displacement in the centre of plate and clamped in the radius as shown in Figure 41. Case two apply voltage 150V to the piezoelectric actuators and the circular plate is clamped at the inner Figure 40.

Now, the strain field is recovered only from eight strains gage. The reason is simple, because in the practical cases, one cannot install too many strain gages. This field was accessible from any element location on the plate. The finite element also produced out-of-plane displacements for the element locations.

In Figure 57, a voltage of 100V is applied at each piezoelectric. The estimated shape obtained by the proposed method is compared with the finite element method. The shape

estimation error is approximately 1 percent compared with the finite element method. Good agreements are obtained.

In Figure 58, the deformed shape from the shape estimated method and the finite element are presented for all circular plate structure in three dimensions. Good agreements are obtained for most of points.

In Figure 59, we consider that 8 strain sensors are bonded as Figure 42 and a displacement is applied at the centre of plate and the plate is supported in radius. The estimate shape of the circular plate along the radius r with $\theta=0$ using the proposed method and experiment results. The shape estimation error is approximately less than 4 percent compared with experiment results.

Figure 60 present the comparison between the least square method and the experiment result. 150 volt was applied to four piezoelectric. The maximum error is less than 1.5 percent.

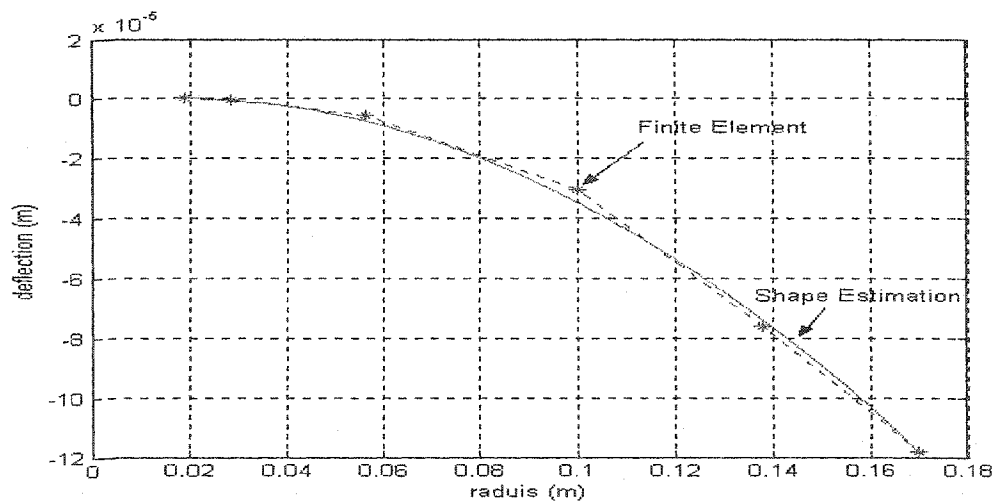


Figure 57 For applied voltage 100V at eight actuator and eight strain gages

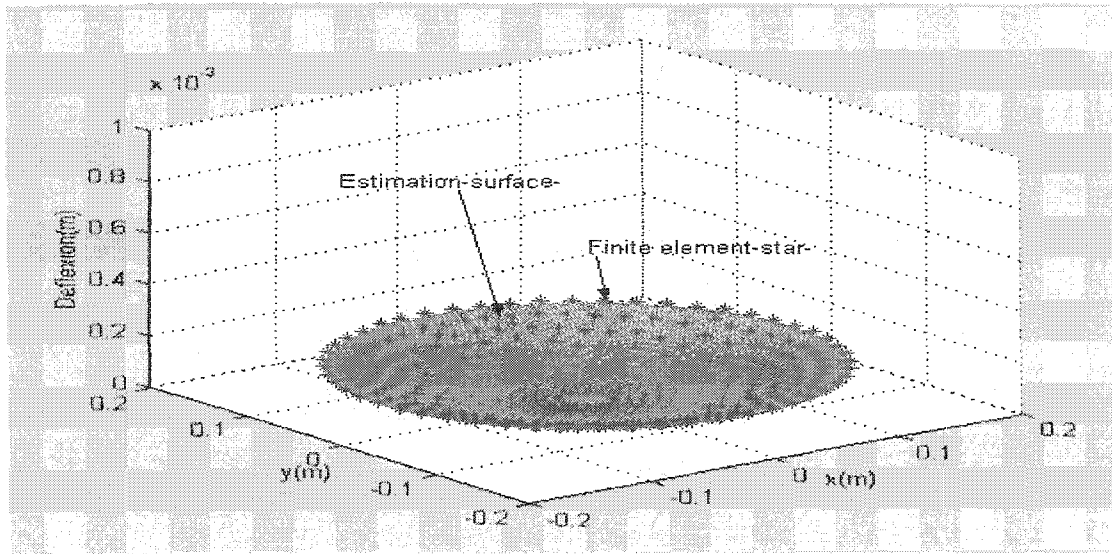


Figure 58 Deformation for applied voltage in 3D

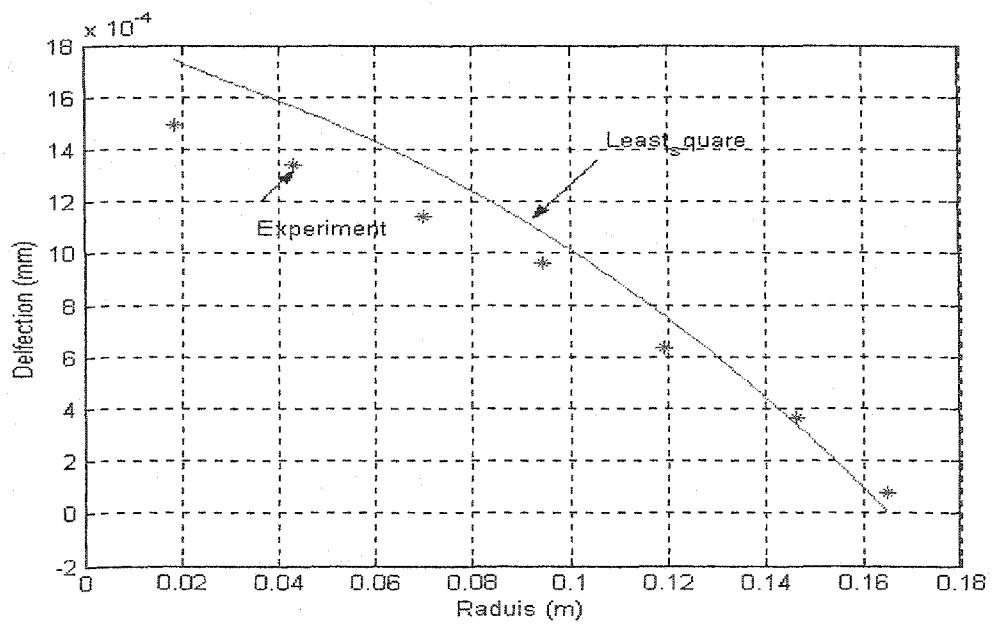


Figure 59 Deflection of simple supported circular plate

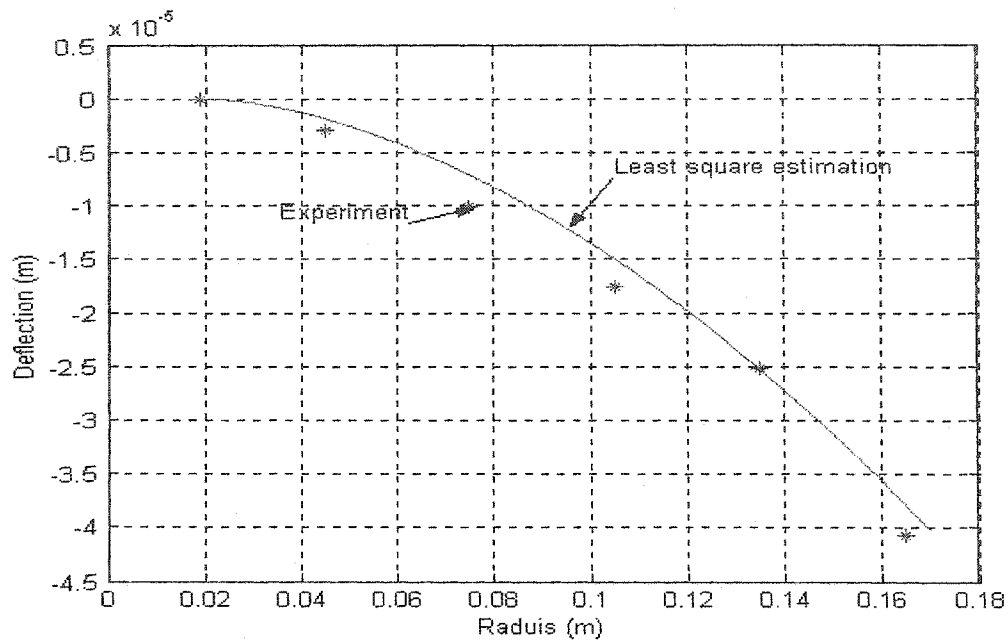


Figure 60 Deformation for applied voltage 150V at four actuator

5.6 Summary

An algorithm has been developed to determine deflection of structures under arbitrary conditions and boundary conditions. The model utilizes only strain information from a set of number of strain gage sensors mounted on the structures. The rosette strain gages are installed on the limited number of locations of the studied structure. The location of the strains gages sensors was chosen after several trial-and-error optimization studies were performed. The studies involved finding not only the best locations for strain sensors, but also the optimum number of the strain gages sensors as well. For a rectangular plate the strain field is represented by a two-dimensional bi-polynomial function, while for a circular plate, the strain field is calculated using polar components of stress in terms of Airy's stress function. The coefficients of each function are

determined based on the relationship of strain, displacement, and strain compatibility. The strain field is constructed by least squares smoothing procedure. This shape estimation method is verified by the numerical method, finite element and experimental results. Relatively good agreements between the results of these three approaches are observed.

CONCLUSION

Advanced intelligent structures with integrated actuators and sensors are becoming increasingly important in high-performance space structures and mechanical systems. In the first part of this thesis, an integrated distributed piezoelectric actuator/ sensor design for flexible structures (aluminum and laminate beams, plates and shells) was developed and the static and dynamic analysis and characteristics of the system were studied and evaluated.

In order to evaluate the dynamic and static performance of the structure, two major packages, ANSYS by Swanson, Inc. and ABAQUS by HKS, Inc. were used and the capabilities of the piezoelectric elements were reviewed. It was shown that the piezoelectric elements provided by the commercial FEA code gave results comparable to those obtained from proven analytical method and experimental results.

The contributions due to the piezoelectric elements have been discussed in detail. A general model describing the structural dynamics when piezoelectric actuators and sensors are bonded to aluminum beams was developed and verified experimentally. The Euler - Bernoulli hypothesis was used to obtain values for natural frequencies, vibration mode shapes and to analyze the steady-state behavior of this structure. A cantilever beam of aluminum bonded with eight actuators was tested and the experimental results were presented and compared to finite element analysis and other analytical results. Relatively good agreement between the results of these three approaches was observed.

For composite structures, an analytical method for modeling the mechanical-electrical response of fiber-reinforced laminated composite structures containing distributed piezoceramics under static as well as dynamic mechanical or electrical loading was presented. The first order shear deformation beam theory was used for the analysis to ensure accurate bending solutions. The assumed-modes method and finite element analysis results were also presented and compared to the analytical model. Experimental

results obtained from Sung (1992) using T300/976 composite and PZT G1195 piezoelectric ceramics were used to verify the theoretical and the computer simulations. In general, the predictions obtained from finite element analysis (FEA), the assumed-mode method and the analytical results correlated with experimental results. Finally, the effects of the number and location of the actuators on the control system were also investigated. The investigation showed that in designing smart structures with distributed piezoelectric actuators, the number and the location of the actuators must be given careful consideration.

For axisymmetric structures, an analytical approach was developed for modeling a circular plate structure with integrated distributed piezoelectric actuators, under static as well as dynamic mechanical or electrical loading. Also, the mathematical solution based on the Kirchhoff plate model for free vibration was introduced. Examining static as well as dynamic analysis of a circular plate containing eight bonded actuators established the validity of the theory. The equations governing the dynamics of the plate, relating the strains in the piezoelectric elements to the strain induced in the system, were derived for a circular plate using partial differential equations. Numerical simulation results were obtained using the finite element approach. In addition, a modeling approach based on the Rayleigh-Ritz assumed mode shape method was presented. The sub-structuring analysis in ANSYS was used to extract the mass and stiffness matrices and load vector of the system to apply active control measures. Experiments using a thin aluminum circular plate structure with distributed piezoelectric ceramics PZT BM532 were also conducted to validate the analytical model and the computer simulations. Relatively good agreements between the results of these three approaches was observed. Finally, the results showed that the model can very accurately predict natural frequencies and mode shapes of a circular plate structure.

The second part of this thesis focused on the shape estimation method. An algorithm was developed to determine deflection of structures under arbitrary loading and boundary conditions. The model only utilizes strain information from a set number of strain gauge

sensors mounted on the structures. Strain and displacement data acquired from a finite element model provided a means of determining the optimum measurement locations to produce accurate displacement estimates. Deploying a set of strain sensors placed on a cantilever aluminum plate (Figure 37), cantilever laminate plate (Figure 38) and circular plate (Figure 42) was investigated. It was found that highly accurate estimates of displacements could be obtained for arbitrary loading. The maximum difference between experiment results and cubic least-squares estimation did not exceed 7 percent for different load scenario. For a circular plate, the error is less than 3 percent. Note that for a rectangular plate, the strain field is represented by a two-dimensional bi-polynomial function, while for a circular plate, the strain field is calculated using polar components of stress in terms of Airy's stress function. The coefficients of each function were determined based on the relationship of strain, displacement, and strain compatibility. The strain field was constructed by the least squares smoothing procedure.

Suggestions for future work

The following studies would be appropriate for the continuation of this research to improve active control systems and to extend them to more complex smart structures.

- Implementation of digital and analog controllers for these structures.
- Extending modeling and shape estimation to other flexible structures such as inflatable membrane structures.
- Modeling inflated structures with bonded piezoelectric patches. Developing of testing procedures for inflated structures.
- Investigating the feasibility of using piezoelectric materials to attenuate vibration in inflated structures.

- Developing a new method to reduce the number of sensors embedded in structures and to obtain the desired shape accuracy. Application of this method to reflector structures.
- Modeling other smart actuators and sensors such as shape memory alloys and fiber optics.

APPENDIX 1

CONTRIBUTIONS TO RESEARCH AND DEVELOPMENT

Sekouri, E. M., Ngo, A. D., and Hu, Y. R. (2003) Modeling of laminated composite structures with piezoelectric actuators. *Journal of Science and Engineering of Applied Composite Materials* (in Print) (Ph.D. work).

Sekouri, E. M., Hu, Y. R., and Ngo, A. D. (2003) Modeling of annular plate with piezoelectric actuators for active vibration controls. Accepted to *Mechatronics The Science of Intelligent Machines An International Journal* (Ph.D. work).

Sekouri, E. M., Hu, Y. R., and Ngo, A. D. (2003) Strain-based shape estimation for circular plate with piezoelectric. Submitted to *Advances in Structural Engineering Journal (ASE Journal)* (Ph.D. work).

Sekouri, E. M., Ngo, A. D., and Hu, Y. R. (2003) Shape estimation of composite and flexible structures under arbitrary loads . Submitted to *Journal of Science and Engineering of Applied Composite Materials* (Ph.D. work).

Sekouri, E. M., Ngo, A. D., and Hu, Y. R. (2003) Strain-based shape estimation for plate structures. *Proceedings of the Forth Canadian International Conference on Composites* (Ph.D. work).

Sekouri, E. M., Hu, Y. R., and Ngo, A. D. (2003) Strain-based shape estimation for flexible structures. *Proceedings of SPIE, International Symposium on smart structures and materials*. Vol.5049-66 (Ph.D. work).

Sekouri, E. M., Ngo, A. D., and Hu, Y. R. (2002) Modeling of laminated composite structures with piezoelectric actuators. *Proceedings of The Fourth Joint Canada-Japan Workshop on Composites*. Pp. 463-470 (Ph.D. work).

Sekouri, E. M., Hu, Y. R., and Ngo, A. D (2002) Modeling of annular plate with piezoelectricactuators for active vibration control. *Proceedings of ASME International Mechanical Engineering Congress & Exhibition , Aerospace Division (Publication) AD*. v67 p341-350 (Ph.D. work).

Sekouri, E. M, and Hu, Y. R. (2001) Modeling of flexible structures with piezoelectric actuators using finite element approaches. *Proceedings of 1st Canada-US workshop on Smart materials and Structures*.

Sekouri, E.M, and Ngo, A.D. (2001) Curvature and twisting effect on the cross-section of fibers in twisted fiber yarns. *Proceedings of The Third Canadian International Conference on Composites*

Yazdani, A., Sekouri, E.M. and Hu, Y.R., (2001) On the finite element modeling of smart structures. Proceedings of ASME Adaptive Structures and Material Systems Symposium.

BIBLIOGRAPHY

- Agrawal, B. N. and Treanor, K. E. (1999). Shape control of a beam using piezoelectric actuators. SMS, f 8, 729-740.
- Allik, H. and Hughes, T. J. R. (1970). Finite element method for piezoelectric vibration. IJNME, 2, 151-157.
- Almeida, S. F. M. (1999). Shape control of laminated plates with piezoelectric actuators including stress-stiffening effects. AIAA, 37, Technical notes, 1017-1019.
- Ambrosino, G. Celentano, G. and Verde, L. (1993). Active sound reduction in an aircraft by means of piezoelectric sensors and actuators. Recent Advances in Active Control of Sound and Vibration, Virginia Tech., 23-27.
- Ambrosino, G., Celentano, G. and Verde, L. (1992). Modeling and control of a spacecraft with maneuverable flexible beam. Aerospace Control 92 - Ottobrunn Germany, September.
- Ashley, S. (1995). Smart skis and others adaptive structures, Mechanical Engineering, 11:76-81.
- Bailey, T., Hubbard, J. E. (1985). Distributed piezoelectric-polymer active vibration of a cantilever beam. Journal of Guidance, Control, and Dynamics, 8(5): 605-611.
- Banks, H. T., Smith, R. C. and Wang, Y. (1995). The Modeling of Piezoceramic Patch Interactions with Shells Plates and Beams. Quarterly of Applied Mathematics, 53(2), 353-381.
- Barrett, R. (1994). Active plate and missile wing development using directionally attached piezoelectric elements. AIAA Journal; 32(3): 601-609.
- Bartley-Cho, D. J., Wang, P. D. and Kudva, J. N. (Apr. 2001). Shape Estimation of Deforming Structures. AIAA/ASME/ASCE/AHS/ASC Structures, Structural Dynamics, and Materials Conference and Exhibit, 42nd, Seattle, WA, pp.16-19.
- Batra, R. C. and Liang, X. Q. (1996). Shape control of vibrating simply supported rectangular plates. AIAA, 34, 116-122.
- Belvin, W. K., Edighoffer, H. H. and Herstrom, C. L. (1989). Quasistatic Shape Adjustment of a 15-meter Diameter Space Antenna. Journal of Spacecraft, 26(3): 129-136.

Benjeddou, A. (2000). Advances in piezoelectric finite element modeling of adaptive structural elements: a survey. *CS*, 76, 347-363.

Birman, V., Saravanos, D. A. and Hopkins, D. A. (1994). Sensory Composite Beams for Delamination Detection in Thermal Environments. *Adaptive Structures and Composite Materials: Analysis and Application*, Edited by E. Garcia, H. Cudney, and A. Dasgupta, ASME International Mechanical Engineering Congress and Exposition, Chicago, Illinois, Nov. 6-11, 351-358.

Birman, V., Saravanos, D. A. and Hopkins, D.A. (1994). Sensory Composite Beams for Delamination Detection in Thermal Environments. *Adaptive Structures and Composite Materials: Analysis and Application*, Edited by E. Garcia, H. Cudney, and A. Dasgupta, ASME International Mechanical Engineering Congress and Exposition, Chicago, Illinois, Nov. 6-11, 351-358.

Carpenter, M. J. (1997). Using energy methods to derive beam finite element incorporating piezoelectric materials. *JIMSS*, 8, 26-40.

Celentano, G. and Setola, R. (1999). The modeling of a flexible beam with piezoelectric plates for active vibration control, *JSV*, bf 223, 483-492.

Celentano, G., Ciniglio, U., Scala, S. and Setola, R. (1996). Robust Vibration Control of flexible structure by using piezoelectric devices, *Internoise 96*, Liverpool, 30 July-2 August.

Chan, K. H. and Hagood, N. W. (1994). Modeling of Nonlinear Piezoceramics for Structural Actuation. *Proc. of the SPIE Conference on Smart Structures and Materials: Smart Structures and Intelligent Systems*, Feb. 14-16, Orlando, Florida, 195-25.

Chandrashekhara, K. and Agarwal, A. N. (1993). Active vibration control of laminated composite plates using piezoelectric devices: A finite element approach. *JIMSS*, 4, 496-508.

Chee, C. Y. K., Tong, L. and Steven, G. P. (1998). A review on the modeling of piezoelectric sensors and actuators incorporated in intelligent structures. *JIMSS*, 9, 3-19.

Choe, K. and Baruh, H. (1990). Actuator placement in structural control. *AIAA Guidance*, 15, 40-47.

Crawley, E. F. and Lazarus, K. B. (1991). Induced strain actuation of isotropic and anisotropic plates. *AIAA*, 29, 944-951.

Crawley, E. F. (1989). Induced Strain Actuation of Isotropic and Anisotropic Plates. *AIAA Journal*, vol. 29, no. 6, 944-951.

- Crawley, E. F. and Anderson, E. H. (1990). Detailed models of piezoceramic actuation of beams. *JIMSS*, 1, 4-25.
- Crawley, E. F. and DeLuis, J. (1987). Use of piezoelectric actuators as elements of intelligent structures, *AIAA*, 25, 1373-1385.
- Dally, W. and Riley, F. (1991). *Experimental Stress Analysis*, Third Edition.
- Davis, M. A., Kersey, A. D., Sirkis, J. and Frieble, E. J. (1994). Fiber Optic Bragg Grating Array For Shape and vibration Mode Shape Sensing. *SPIE Vol.2191*, Paper #10, Orlando.
- Dimitriads, E. Fuller C. R. and Rogers CA. (1991). Piezoelectric actuators for distributed vibration excitation of thin plates. In: *ASME J. Appl. Mech.*, 113:100-107.
- Donthireddy, P. and Chandrashekhara, K. (1996). Modeling and Shape Control of Composite Beams with Embedded Piezoelectric Actuators. *Composite Structures* 35, 237- 244.
- Fanson, J. L. and Chen, J. C. (1986). Structural control by the use of piezoelectric active members. *Proceedings of NASA/DOD Control-Structures Interaction Conference*, NASA CP-2447, Part II.
- Haerting, G. H. (1986). Piezoelectric and Electrooptic Ceramics, Chapter 3 of *Ceramic Materials for Electronics*. ed: Buchanan, R. C., Marcel Dekker, Inc., New York.
- Heyliger, P. R and Ramirez, G. (2000). Free Vibration of laminated Circular Piezoelectric Plates and Discs. *Journal of Sound and Vibration* 229(4), 935-956.
- Heyliger, P. R., Ramirez, G. (1999). Free vibration of laminated piezoelectric plates and discs. *Journal of Sound and Vibration*, 229:935-956.
- Khorrani, F. (1994). Adaptive control of flexible-link manipulators with piezoelectric ceramic sensors and actuators. *Proceeding of IFAC Symposium on Robot Control, SYROCO'94*, pp.523-528.
- Kim, S. J. and Jones, J. D. (1995). Influence of piezo-actuator thickness on the active vibration control of a cantilever beam. *Journal of Intelligent Material Systems and Structures*, 6, 610-623.
- Kirby, G. C., Lim, T. W., Weber, R., Bosse, A. B., Povich, C. and Fisher, S. (1997). Strain-Based Shape Estimation Algorithms for a Cantilever Beam. *SPIE Vol.3041*, pp.788-798.

- Kirby, G. C., Lim, T. W., Weber, R., Bosse, A. B., Povich, C. and Fisher, S. (1997). Strain-Based Shape Estimation Algorithms for a Cantilever Beam. SPIE Vol.3041, pp.788-798.
- Kirby, G. C., Lindner, D. K., Davis, M. A. and Kersey, A. D. (1995). Optimal Sensor Layout For Shape Estimation From Strain Sensors. SPIE Vol.2444, pp.367-376.
- Kirchhoff (1850). *Über das Gleichgewicht und die Bewegung einer elastischen Scheibe*.h. J. 40(5) pp51-58.
- Konis, D. B., Kollar, L.P. and Springer, G.S. (1994). Shape Control of Composite Plates and Shells with Embedded Actuators, I. Voltage Specified. J. Composite Mater. 28, 415-458.
- Lalande, F., Chaudhry, Z. and Rogers, C. A. (1994). Impedance modeling of In-Phase Actuation of Actuators Bonded on Ring Structures, Adaptive Structures and Composite Materials: Analysis and Application, Edited by E. Garcia, H. Cudney, and A. Dasgupta, ASME International Mechanical Engineering Congress and Exposition, Chicago, Illinois, Nov. 6-11, 193-200.
- Lancaster, P. and Salkauskas, K. (1986). *Curve and Surface Fitting*, Academic Press, London.
- Leissa, A. (1993). *Vibration of Plates*.
- Lin, R. R. (1990). *Active Vibration Control of Rotor bearing Systems Utilizing Piezoelectric Pushers*. Ph.D. Dissertation, Texas A and M University.
- Mitsugi, J., Yasaka, T., Miura, K. (1990). Shape Control of Tension Truss Antenna. AIAA Journal, 28(2): 316-322.
- Miura, K., Natori, M. C. (1991). Aerospace Research Status on Adaptive Structures in Japan. 2nd Joint Japan-US Conference on Adaptive Structures, Nagoya, 3-14.
- Natori, M., Murohashi, S., Takahara, K. and Kuwao, F. Control of Truss Structures Using Member Actuators with Latch Mechanism. The Winter Annual meeting of the ASME, San Francisco, CA: 69-75.
- Palazzo, A. B., Lin, R. P., Kascak, A. F., Montague, J., Alexandre, R. M. (1989). Piezoelectric Pushers for Active Control of Rotating Machinery. ASME Journal of Vibration, Acoustics, Stress and Reliability in Design, 111:298-305.
- Poisson, S. D.(1829). *Mémoires de l'Académie Royale des Sciences de l'Institut de France, l'équilibre et le mouvement des corps élastiques. série 2, tome VIII p.357.*

Preumont, A., Sparavier, M., Dufour, J. P.(1990). Application of piezoelectric actuators to the active damping of a truss structures. Proceedings of the 31st AIAA/ASME/ASCE/AHS/ASC Structures, Structural Dynamics, and Materials Conference pp. 1907-1913.

Reddy, J. N.(1997). Mechanics of Laminated Composite Plates, Theory and Analysis, CRC Press, Inc.

Samanta, B., Ray, M. C., Bhattacharyya, R. (1996). Finite element model for active control of intelligent structures. AIAA journal; 34:1885-1893.

Saravanos, D. A. Lin, Y. J. Choi, B. B. and Hopkins, D. A. (1994). On Smart Composite Structures For Active Tip Clearance Control. Adaptive Structures and Composite Materials: Analysis and Application, Edited by E. Garcia, H. Cudney, and A. Dasgupta, ASME International Mechanical Engineering Congress and Exposition, Chicago, Illinois, Nov. 6-11, 145-153.

Shahinpour, M. (1996). Intelligent materials and structures revisited. SPIE Proceedings on smart structures and materials: smart materials technology and biomimetics, 2716, 238-250.

Shakeri, C. Noori, M. N. and Hou, Z. (1996). Smart Materials and Structures; A Review. Proceedings of the Fourth Materials Engineering Conference, Washington, D.C., November 10-14, 863-876.

Southwell, R. V. (1992). On the free transverse vibrations of uniform circular disc clamped at its center; and on the effects of rotation. Proceedings of the Royal Society. 101: 133-153.

Sung Kyu Ha, Charles Keilers, and Fu-Kuo Chang (1992). Finite Element Analysis of Composite Structures Containing Distributed Piezoceramic Sensors and Actuators. AIAA Journal, Vol.30, no. 3.

Swanson, Inc. (2000). ANSYS User's Manual. Version 5.7. Houston, PA Swanson. Inc.

Tabata, M., Yamamoto, K., Inoue, T., Noda, T., Miura, K. (1991). Shape Adjustment of a flexible Space Antenna Reflector. 2nd Joint Japan-US Conference on Adaptive Structures, Nagoya, 393-405.

Timoshenko, S. P. and Goodier, J. N. Theory of Elasticity. McGraw-Hill, New York.

Tylikowski, A. (2001). Control of Circular Plate Vibrations via Piezoelectric Actuators Shunted with a Capacitive Circuit. Thin-Walled Structures 39, 83-94.

- Tzou, H. S. Active Vibration Control of Flexible Structures via Converse Piezoelectricity, *Developments in Mechanics*. 14-c:1201-1206.
- Tzou, H. S., Gadre, M. (1989). Theoretical analysis of a multi-layered thin shell coupled with piezoelectric shell actuators for distributed vibration controls, *JSV*; 32:433-450.
- Tzou, H. S., Bao, Y. and Ye, R. (1994). A Theory on Nonlinear Piezothermoelastic Shell Laminates. *Proc. of the SPIE Conference on Smart Structures and Materials: Smart Structures and Intelligent Systems*, Feb. 14-16, Orlando, Florida, 206-214.
- Iyengar, K.T.S.R. and Raman, P. V. (1978). Free Vibration of Circular Plates of Arbitrary Thickness. *Journal of the Acoustical Society of America* 64, 1088-1092.
- Jiarang, F. and Jianqiao, Y. (1990). Exact Solutions for Axisymmetric Vibration of Laminated Circular Plates, *ASCE Journal of Engineering Mechanics* 116, 920-927.
- Jones, R. T., Berkoff, T. A., Bellemore, D. G., Early, D. A., Sirkis, J. S., Putnam, M. A., Friebele, E. J. and Kersey, A. D. (1996). Cantilever Plate Deformation Monitoring Using Wavelength Division Multiplexed Fiber Bragg Grating Sensors. *SPIE Vol.2718*, pp.258-268.
- Umland, J. W., Chen, G. S. (1990). Active member vibration control for 4 meter primary reflector support structure, *Proceedings of the 33rd AIAA/ASME/ASCE/AHS/ASC Structures, Structural Dynamics, and Materials Conference*, pp.393-401.
- Van Neikerk, J. L., Tongue, B. H., Packard A. K. (1995). Active control of circular plate to reduce transient transmission noise. *Journal of Sound and Vibration*, 183:643-662.
- Vogel, S. M., Skinner, D. W. (1965). Natural frequencies of transversely vibrating uniform annular plates. *Journal of Applied Mechanics*. 32: 926-931.
- Wang, K.W., Lai, J.S. and Yu, W.K. (1994). Structural Vibration Control Via Piezoelectric Materials with Real-Time Semi-Active Electrical Networks, *Adaptive Structures and Composite Materials: Analysis and Application*, Edited by E. Garcia, H. Cudney, and A. Dasgupta, *ASME International Mechanical Engineering Congress and Exposition*, Chicago, Illinois, Nov. 6-11, 219-226.
- Wang, Q., Quek, S. T., Sun, C. T., Liu, X. (2001). Analysis of piezoelectric coupled circular plate", *Smart Materials and Structures*, 10:229-239.
- Yousefi-Koma, A. (1997). Active vibration control of smart structures using piezoelements. Ph.D. thesis, Department of Mechanical and Aerospace Engineering, Carleton University.

Yang, S. M. and Lee, Y. J. (1994). Modal analysis of stepped beams with piezoelectric materials, JSV, 176, 289-300.